Palynology and foraminiferal geochemistry of the Lower Pleistocene Olduvai Subchron (ca. 1.8 Ma) in DSDP Hole 603C, western North Atlantic

Eva Iman Fischer, B.Sc.

Earth Sciences

Submitted in partial fulfillment
of the requirements for the degree of

M.Sc. in Earth Sciences

Faculty of Mathematics and Science, Brock University
St. Catharines, Ontario

DEDICATION

This thesis is dedicated to the memory of my father Prof. Klaus Peter Fischer
without whom I would not have the courage to pursue my dreams,
no matter where they take me.

Abstract

Marine palynology and benthic and planktonic foraminiferal geochemistry are combined to reveal long- and short-term (Milankovitch-scale) paleoceanographic changes across the upper half of the Olduvai Subchron (ca. 1.86–1.77 Ma, lower Pleistocene) in DSDP Hole 603C from the lower New Jersey continental rise. Planktonic foraminiferal Mg/Ca ratios reveal annual sea-surface temperatures between 14.5° and 25°C, whereas modern values vary between 16° and 20°C. Despite evidence of downslope transport in much of the studied interval, dinoflagellate cyst and acritarch assemblages appear to reflect fluctuating temperate to subtropical water masses. These assemblages comprise both neritic and oceanic species, and are marked by a transition upsection from warm conditions, dominated by *Lingulodinium machaerophorum*, *Polysphaeridium zoharyi* and *Cymatiosphaera*? *invaginata*, to cooler conditions dominated by *Filisphaera filifera*. Combining dinoflagellate cyst proxies with planktonic foraminiferal geochemistry allows downslope transport events to be recognized during glacial episodes, and events dominated by intensified bottom-water circulation during interglacial episodes. Sixty-two *in-situ* dinoflagellate cyst and acritarch taxa were recorded including several not previously described.

ACKNOWLEDGEMENTS

The development and completion of this thesis would not have been possible without the input and support of numerous individuals. I'm very grateful to my supervisor Prof. Martin J. Head for the opportunity to undertake this research, and for his guidance and support in this project. He was never too busy for questions or discussions.

I would further like to express my thanks to Dr Jeroen Groeneveld, from the Alfred Wegener Institute in Germany, for the comprehensive analysis of the foraminifera. I would also like to thank Prof. Francine M. G. McCarthy for her good advice and help, and Dr. Stijn De Schepper (formerly Bremen University, now Bergen University), whose e-mails and advice about statistics were extremely helpful.

Special thanks are extended to graduate students from the Department of Earth Sciences: Lisa, Holly, Heather, Melissa, Bill, Matt and Colin. We've listened to each other complain about our thesis, our supervisors and our undergrads and I will always remember you for that. To my former office mate Manuel Paez Reyes (Smithsonian Institute in Panama): I can't imagine sharing the office for so long with any other guy. You were willing to confirm my findings and you didn't mind having long discussions about palynology despite the fact that you know so much more than I ever will. To Jan Hennissen, PhD student at the University of Toronto, I'm passing the torch of DSDP Hole 603C to you. Processing was a lot more fun when you were there, for that alone I thank you.

Special thanks to Mike Lozon (cartographer) for his advice on Corel Draw, his program connections and his awesome printers, Pete Barclay for always providing ink for the printer as well as HF and waste bottles, and to Diane Gadoury (administrative assistant) for being willing to shoot the breeze and always knowing what to do.

Finally, special thanks are extended to the Integrated Ocean Drilling Program for providing the samples. This research was supported by an NSERC Discovery Grant awarded to Prof. M. J. Head.

Table of contents

Table of Figures

List of Tables

List of Plates

List of Abbreviations

AABW: Antarctic Bottom Water

AAIW: Antarctic Intermediate Water

ACC: Antarctic Circumpolar Current

BR: Bermuda Rise

BBOR: Blake-Bahama Outer Ridge

CA: Correspondence analysis

CCA: Canonical correspondence analysis

CCD: Carbonate Compensation Depth

CLSW: Coastal Labrador Sea Water

DCA: Detrended correspondence analysis

DSDP: Deep Sea Drilling Project

DSOW: Denmark Strait Overflow Water

DWBC: Deep Western Boundary Current

GSSP: Global boundary-stratotype section and point

HOR: Hatteras Outer Ridge

IODP: Integrated Ocean Drilling Program

ISOW: Iceland-Scotland Overflow Water

LSW: Labrador Sea Water

mbsf: metres below sea-floor

MIS: marine isotope stage

NADW: North Atlantic Deep Water

NRG: Northern Recirculation Gyre

ODP: Ocean Drilling Program

SAIW: Subarctic Intermediate Water

SAMW: Subantarctic Mode Water

SST: Sea-surface temperature

ULSW: Upper Labrador Sea Water

WBUC: Western Boundary Undercurrent

WG: Worthington Gyre

Chapter 1 – Introduction

The period marking the transition across the former Pliocene–Pleistocene boundary (Aquire and Passini, 1985) at 1.8 Ma (Lourens et al., 2004) is often overlooked in terms of paleoclimate studies. Much recent work has targeted the Pliocene extending to and around its upper boundary at 2.6 Ma (Head et al., 2008a; Gibbard et al., 2010; Gibbard and Head, 2010), and the mid-Pleistocene Transition at around 1.2–0.5 Ma (Head et al., 2008b); far fewer studies are aimed at the intervening interval. The present study examines deposits from the mid-latitude western North Atlantic around 1.8 Ma. Deep Sea Drilling Project (DSDP) Hole 603C, located on the lower slope of the New Jersey continental rise (35°29.78'N; 70°01.86'W, at 4643 m water depth; Figure 1), was drilled as part of DSDP Leg 93 in 1983 (van Hinte et al., 1987). Excellent core recovery and sedimentation rates estimated at 10 cm per kyr facilitated the recognition of a detailed and essentially uninterrupted paleomagnetic record extending from the early mid-Pleistocene back to the latest Miocene (Canninga et al., 1987; Moullade, 1987).

Preliminary analyses of the dinoflagellate cysts (hereafter "dinocysts") in Hole 603C at low sampling resolution (57 samples for the entire Lower Pleistocene through Upper Miocene interval) has already been undertaken (Head and Norris, 2003; M. J. Head, unpublished data). That preliminary study showed intriguing fluctuations in abundance among the dinocysts and acritarchs within the Olduvai Subchron. The present study aims to explore these assemblage fluctuations at Milankovitch-scale resolution and thereby improve our understanding of the paleoceanography, paleoclimate, and taphonomic processes in operation. This has been accomplished by analyzing a total of 48 samples both for marine palynology (principally dinocysts and acritarchs) and planktonic and benthic foraminiferal geochemistry (Mg/Ca and oxygen isotopes) using the same-sample methodology of De Schepper et al. (2009). Samples were processed at Brock University, and the foraminifers picked, identified, and sent to Bremen University for geochemical analysis (by Dr. Jeroen Groeneveld). Palynological analyses were conducted by the author at Brock University, and both palynological and geochemical results were integrated and interpreted by the author. This is the most detailed investigation yet

undertaken that combines marine palynology, foraminiferal Mg/Ca, and oxygen isotopes for this time interval.

The first part of this thesis introduces the geological context of DSDP Hole 603C, and details the past and present oceanographic conditions for the site, as determined by previous studies of isotopes, carbonate dissolution estimates, planktonic foraminiferal ecology, sediment composition and color, as well as palynological analysis. The second part presents in detail the methodology used for the palynological and foraminiferal analyses. Geochemical and palynological results, including statistical analyses of palynological taxa, are presented in the third part of this thesis. The sedimentation rates estimated by Canninga et al. (1987) for the studied interval are mainly the result of correlation coefficients calculated between the polarity transitions measured for Hole 603C using the geomagnetic polarity time scale. These sedimentation rates serve to constrain the ages of the top and base of the studies interval. The use of benthic foraminiferal geochemistry in this study provides an additional layer of temporal constraint, which will also be explained with the results. The fourth, and final, part presents an overview of the paleoenvironmental conditions inferred from DSDP Hole 603C around the upper portion of the Olduvai Subchron based on the proxies studied here, and discusses how these conditions fit within the context of the New Jersey Shelf and rise at the time.

The goals of this thesis are to (1) obtain a multiproxy record of palaeoceanographic conditions at DSDP Site 603 around the upper part of the Olduvai Subchron using a combined palynological and planktonic geochemical approach; (2) use this approach to further understanding of the ecology and stratigraphic ranges of dinocyst and acritarch species for the examined interval; and (3) astronomically tune the studied section by comparing the benthic foraminiferal isotopic record of the present study with the global benthic $\delta^{18}O$ stack of Lisiecki and Raymo (2005).

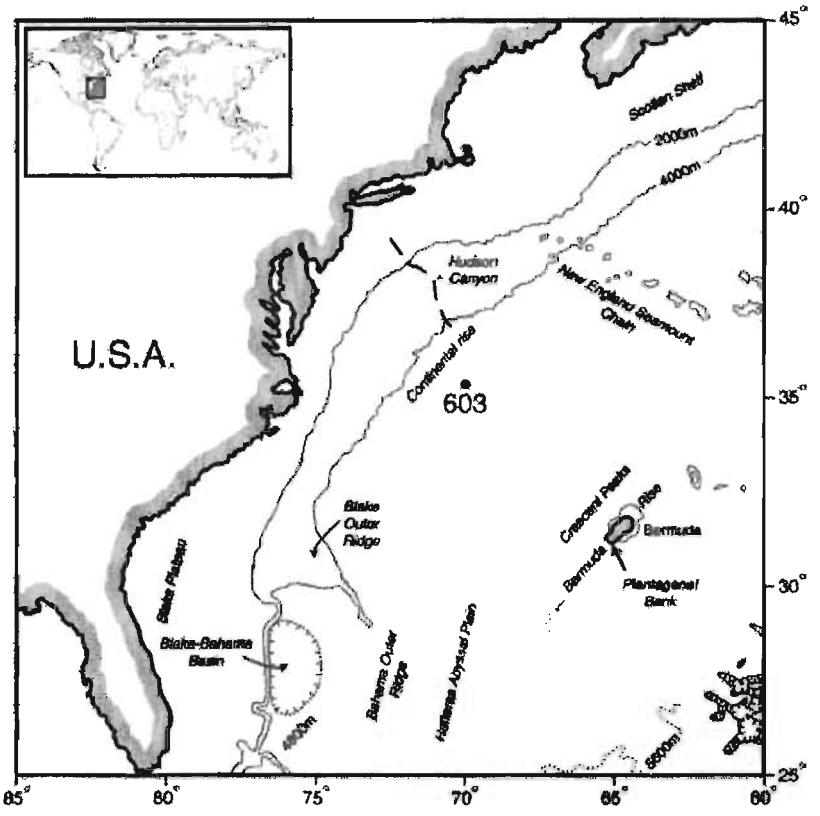

Figure 1. Location of DSDP Site 603, western North Atlantic with respect to the Blake–Bahama Outer Ridge (BBOR), Bermuda Rise (BR), and other geographical features (from Head and Norris, 2003, fig. 1)

Chapter 2 – Present oceanographic setting of DSDP Site 603

DSDP Site 603 is presently situated directly in the path of the warm-water Gulf Stream. The Gulf Stream follows a distinct north-eastern direction, continuing from the Florida Current (Gyory et al., 2009) which originates in the Gulf of Mexico. Cold currents emerging from the northern North Atlantic and Arctic Ocean, most notably the Labrador Current and East Greenland Current, flow southward along the continental margin of Newfoundland, over the Grand Banks, and then southwestwards to Cape Hatteras, where they are redirected by the north-eastern flowing Gulf Stream (Figure 2)

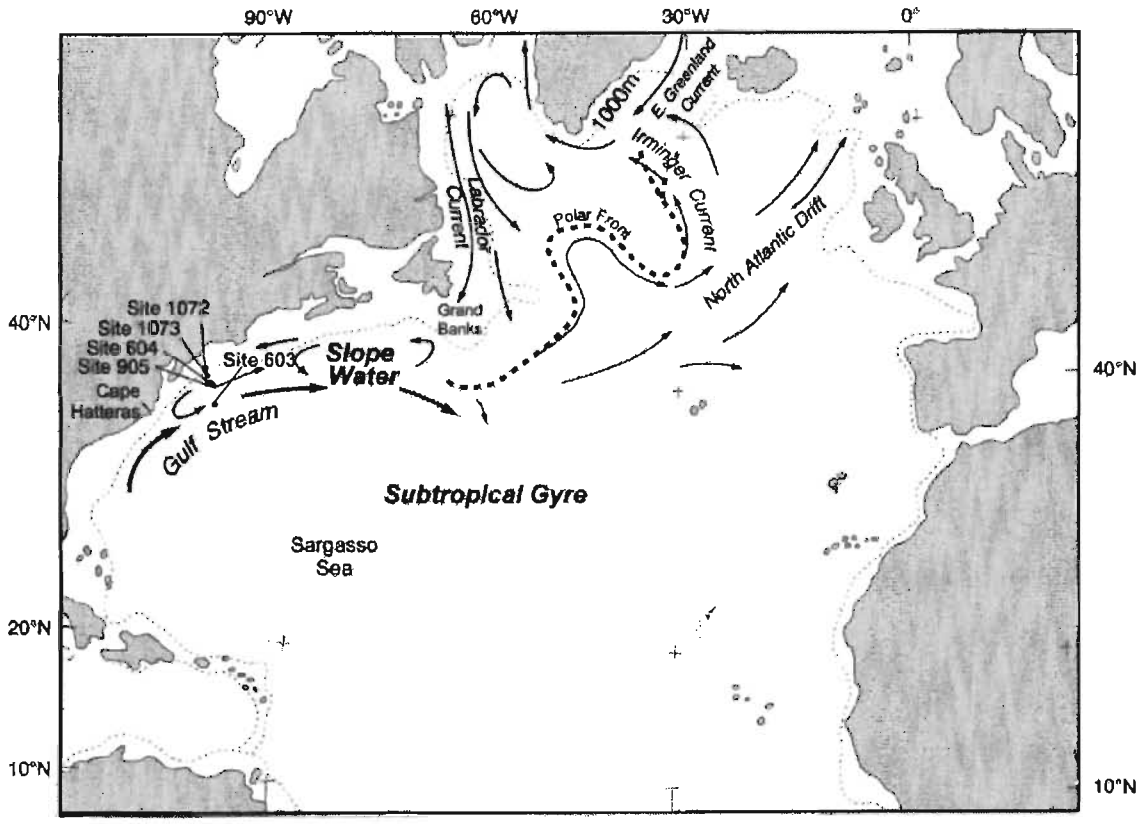

Figure 2. Location of DSDP Site 603 with regards to modern local surface currents. Also shown are the positions of Ocean Drilling Program sites from the New Jersey continental shelf and Iberian peninsula (modified from McCarthy et al., 2000a, text-fig. 1).

Other modern currents in the mid-latitude North Atlantic include the cool-water Canaries Current and the warm-water Northern Equatorial Current (Figure 2). Furthermore, a narrow triangular region between the Gulf Stream and Cape Hatteras is presently occupied by a cool, less saline cyclonic recirculation gyre called the Slope Water, for which the temperature and salinity rarely exceed respectively 23°C and 36 psu. The term Slope Water was coined by Iselin (1936) and further defined by Csanady and Hamilton (1988) to acknowledge that this narrow band of ocean between the Gulf Stream and the continental shelf from Cape Hatteras to the Grand Banks differs significantly from its neighbours. This cool, low-salinity cyclonic recirculating gyre integrates freshwater runoff from land and advection along constant density surfaces (isopycnals) from the Sargasso Sea thermocline and Coastal Labrador Sea Water (CLSW). The advection from the Saragasso Sea is responsible for increased nutrient levels in the Slope Water

(Csanady and Hamilton, 1988). The combination of these components accounts for the unique properties of this water mass, which occupies only the top few hundred metres of this area. McCarthy et al. (2000a) estimated that the palynological facies observed on the New Jersey continental margin for the past 1.4 myr reflects the inflow of relatively cool and low salinity CLSW (oceanic water) in addition to a fluvial influx into the Slope Water (estuarine-type water). The contrasting properties of the warm Gulf Stream and the cool Slope Water are clearly reflected by the sea-surface conditions (temperature and salinity) found on the eastern coast of North America today. The loose isotherms and the dispersed salinity curves between the Florida peninsula and Cape Hatteras reflect the strong influence of the continuously warm Gulf Stream, whereas the closely spaced isotherms and salinity curves from Cape Hatteras to the Grand Banks are a clear indication of the rapidly cooling conditions due to the intrusion of the cool northern-sourced waters into the area of Slope Water (Figure 3).

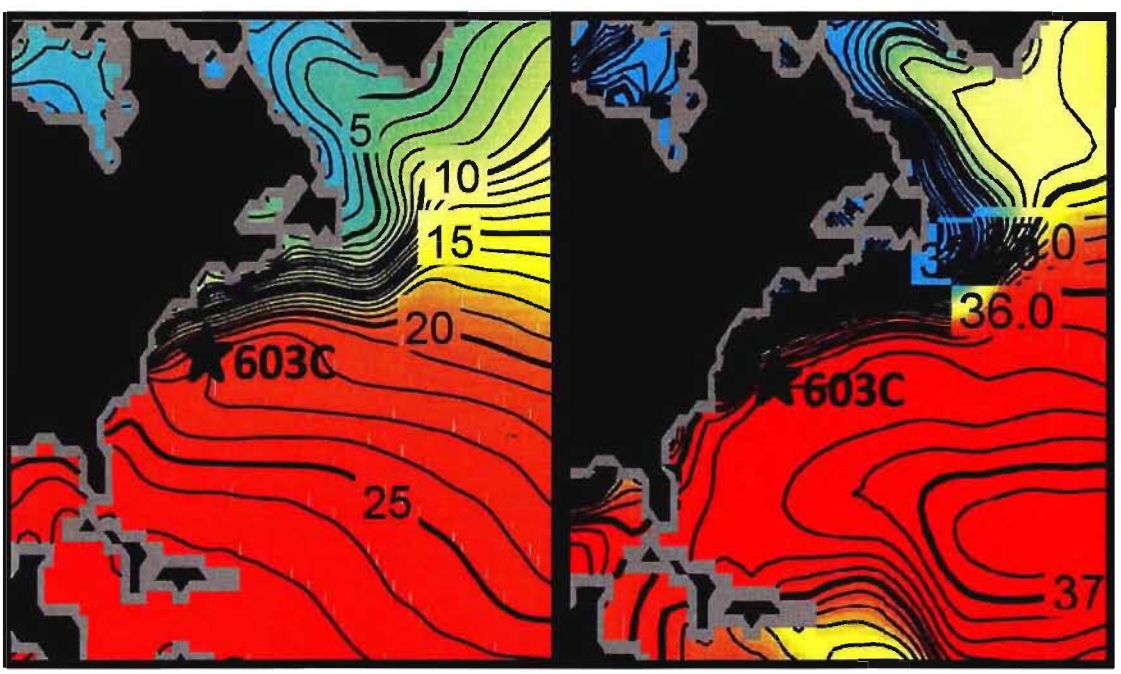

Figure 3. Modern annual sea-surface temperatures and sea-surface salinities in the western North Atlantic showing the contrast between the cool Slope Water (from the north) and the warm Gulf Stream (from the south), in the eastern North Atlantic (modified from Locarnini et al., 2006 and Antonov et al., 2006).

The production of cold North Atlantic Deep Water (NADW) in the northern North Atlantic and its approximately southwestward to southward flow is the most commonly cited deep-water influence on this region, and its passage in the deep waters off the coast of the North America can be confirmed by the low temperatures on a 4500 m isotherm map (Figure 4, left). This deep water current travels southward towards Antarctica, at first at the bottom of the water column and then above the northward flowing Antarctic Bottom Water (AABW) (Figure 5).

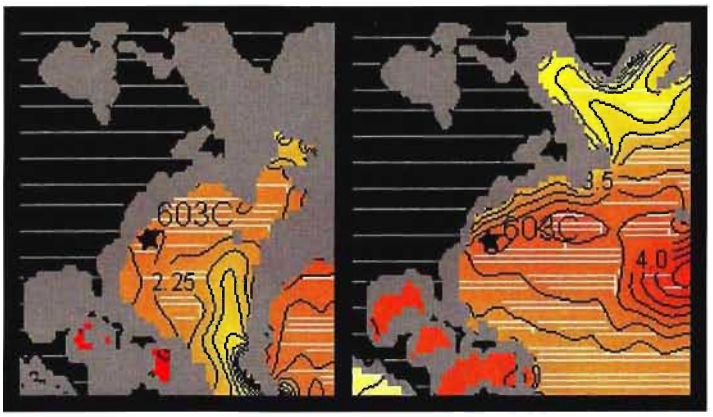

Figure 4. Local annual deep-sea temperatures in the eastern North Atlantic. Depth 4000 m on the left, 2500 m on the right (modified from Locarnini et al., 2006)

The AABW is the densest water mass in the world ocean (Orsi et al., 1999), and as such usually occupies the lowest depths. After mixing with the Antarctic Circumpolar Current, the AABW has a typical salinity of 34.7 psu and a temperature of 0.3°C. The strong NADW and associated currents, which will be described in detail subsequently, inhibit the circulation of the AABW in the North Atlantic, and the contrasting nutrient levels between the AABW (high) and the NADW (low) (Lynch-Stieglitz et al., 2007) allow for their differentiation at depth. In the western North Atlantic the strong AABW signature extends as far north as Bermuda (Talley, 2002) where it is believed to upwell into the NADW layer above it. The main factors that control the depth of flow of the NADW and the AABW are salinity, which allows the NADW to sink as far as it does, and temperature, which does the same for the AABW (Weaver et al. 1999). By the 24th parallel, the temperature of the AABW has been elevated enough to allow it to integrate into the overlying NADW.

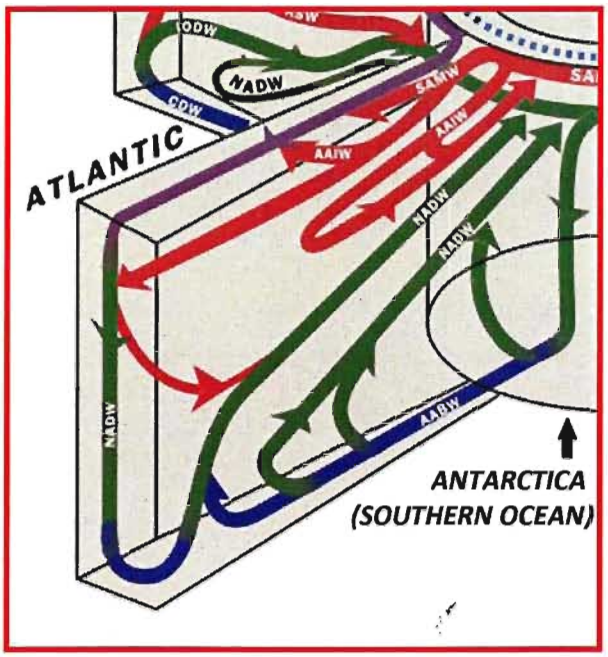

Figure 5. Principal surface (purple), intermediate (red), deep (green) and near-bottom (blue) water currents of the Atlantic Ocean. NADW (North Atlantic Deep Water), AABW (Antarctic Bottom Water), AAIW (Antarctic Intermediate Water), SAMW (Subantarctic Mode Water) (modified from Chapman, 1999, fig. 2).

Intermediate currents have been found to interact with surface waters of the North Atlantic. This intermediate depth water level is occupied by a number of cool-water currents flowing northward and southward, as also indicated by the slightly higher temperature displayed on the 2000 m isotherm map (Figure 4, right), notably the Antarctic Intermediate Water (AAIW), the Western Boundary Undercurrent (WBUC), the Deep Western Boundary Current (DWBC), and the Sub-Arctic Intermediate Water (SAIW).

The AAIW forms at the Antarctic Convergence, north of the Antarctic Circumpolar Current (Talley, 2002) in the latitudinal belt between 50° and 60°S and can be traced by its relatively low salinity (33 psu) and low temperature (4°C) as far north as latitude 35°N in the North Atlantic. North of this latitude, in the Gulf Stream region, the AAIW appears to be modified by mixing with other intermediate, more saline, water masses (van Aken, 2007). Its impact on the region of Site 603 is therefore not direct.

The Subarctic Intermediate Water (SAIW) originates from the North Western Atlantic and comprises cold, relatively fresh water. After its formation as winter mode water north of the polar front (van Aken, 2007), part of the SAIW subducts and re-circulates in the northern cyclonic gyre while another part subducts below the North Atlantic Current and flows towards the eastern Atlantic margin. The impact of the SAIW on the region targeted in this study can therefore be estimated as limited.

The WBUC drives the Denmark Strait Overflow Water and the North East Atlantic Deep Water around a counterclockwise gyre in the Irminger basin (between Greenland and Iceland) and the Labrador basin (Fagel et al., 1997, fig. 1). As such, it is an important component of the NADW circulation north of the Grand Banks. Bulfinch and Ledbetter (1984) hypothesized that the WBUC flows along the eastern continental slope and rise of North America at a depth between 1000 and 5000 m.

Henry Stommel was the first to theorize, fifty years ago, that recently ventilated waters of high-latitude origin, such as the NADW, must be transported equatorward at depth along western-intensified boundary currents (Stommel, 1958; Hogg and Huang, 1995; Lozier, 2010). Following this hypothesis, deep western boundary currents (DWBC) have been detected in all three meridional oceans (Atlantic, Indian and Pacific) and were found to be interconnected across the different hemispheres and basins, to form a continuous stream of deep waters spreading through the abyss. The Atlantic DWBC contains most of the water masses beneath the surface-water Gulf Stream, thus transporting the NADW to the equatorial Atlantic (Bower and Hunt, 2000). Following its arrival at the equator, the DWBC is subject to mixing with the northward flowing Antarctic Waters, thus changing the characteristics used to constrain and name them and losing their identity. In summary, a total of four intermediate and deep water masses of northern origin (the ISOW, the DSOW, the LSW and the ULSW) are recognized by Bower and Hunt (2000) as being transported by the DWBC, comprising the NADW, ranging in depth from 700 to 4000 m.

The two main components of the WBUC, the Denmark Strait Overflow Water (DSOW) and the North East Atlantic Deep Water, also known as the Iceland–Scotland Overflow

Water (ISOW), make up the two deepest and coldest water masses (2500–4000m, 2°–3°C).

The Labrador Sea Water (LSW) lies above the overflow waters, in the depth range of 1500–2000 m (3°–4°C). LSW is considered the final stage in the modification of mode waters from the North Atlantic sub-polar gyre, which takes place in the Labrador Sea (van Aken, 2000). This water is formed by deep convection in winter within the centre of the cyclonic circulation in the Labrador Sea, when the relatively fresh surface layer entrains convectively the underlying Atlantic water. The cool temperatures observed at 2000 m depth (Figure 4, right) confirm the origins of this water.

Finally, the Upper Labrador Sea Water (ULSW) represents the lightest component of the NADW and is found between 700 and 1500 m (4°–6°C). The ULSW is believed, by Bower and Hunt (2000), to form along the western boundary of the Labrador Sea.

The position where the DWBC crosses under the Gulf Stream, near 36°N, is located close to the southernmost extension of the intrusion of the surface Slope Water, between the Gulf Stream and the continental slope of North America. At this location most of the ULSW is redirected eastwards between the Northern Recirculation Gyre and the Worthington Gyre (Pickart and Simethie, 1993), with a narrow band continuing southwards directly against the continental slope. In contrast, most of the deeper overflow waters follow the topography more closely, crossing under the Gulf Stream and continuing equatorward, with only limited recirculation. The circulation patterns of deep waters illustrated in Bower and Hunt (2000, fig. 1) show a less pronounced southward intrusion of cold northern water at depth than the cold surface slope water illustrated by McCarthy et al. (2000a, text-fig. 1) (Figure 6, contrasting Bower and Hunt with McCarthy et al., 2000a). Regardless of whether intrusion is principally at depth or at the surface, it is noteworthy that the area of Site 603 seems to be a region of convergence between the northern (Slope Water and Northern Recirculation) and southern (Worthington and Subtropical) gyres of the middle North Atlantic.

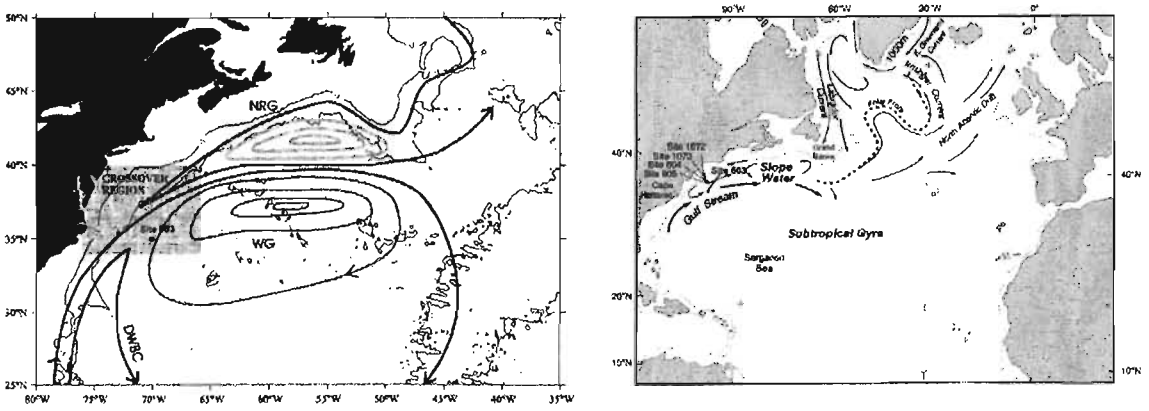

Figure 6. Contrasting deep-water circulation patterns (from Bower and Hunt, 2000, fig. 1) and sea-surface circulation patterns (from McCarthy et al. 2000a, text-fig. 1) in the eastern North Atlantic. The cool Northern Recirculation Gyre (NRG) intrudes only until 35°N, whereas the cool surface Slope Water intrudes until 30°N. DWBC = Deep Western Boundary Current; WG = Worthington Gyre.

The palynological and geochemical analyses of the present study should therefore reflect a fluctuating interplay between alternating cool (northern sourced) and warm (Gulf Stream related) surface waters, and down-slope transport and bottom-current redistribution. There might also be an influence of cool, estuarine-type water originating from the region of the Gulf of St. Lawrence.

Chapter 3 – Paleoceanographic conditions at DSDP Site 603, western North Atlantic, around 1.8 Ma – a review.

3.1 History of the Pliocene–Pleistocene boundary

Charles Lyell, in 1839, introduced the term "Pleistocene" for the epoch of the youngest marine fauna that pre-dated his "Recent" (later to become Holocene) epoch, in line with Desnoyers' (1825) concept of a Quaternary interval as the most recent part of geological history (Nikiforova, 1997). The first step towards fixing the position of the boundary between the Pliocene and the Pleistocene was the organization of a special temporary commission at the XVIII International Geological Congress in London, in 1948. The commission, while stating that the bases of the Quaternary and Pleistocene were coeval, outlined three criteria for the placement of the boundary: (1) the boundary should be

based on a faunal change in a section of marine deposits; (2) the boundary should be located in the classic territory of Quaternary deposits of Italy, the area in which these principles can best be applied; and (3) the boundary should be placed at a horizon demonstrating the first indication of a deteriorating climate in the Italian deposits, as evidenced by the first appearance of (unspecified) 'northern guests' in the Mediterranean Sea (King and Oakley, 1949).

Two species identified as 'northern guests' were the mollusk *Arctica islandica* and the boreal benthic foraminifer *Hyalinea baltica*. The presence of *Hyalinea baltica* in the Vrica section, and both species in other correlated sections in Italy (Rio et al., 1996), in combination with established magnetostratigraphy, prompted the first formal definition of the Plio–Pleistocene boundary. This was effected by designation of a global stratotype section and point (GSSP) at Vrica in Calabria, southern Italy (Aguirre and Passini, 1985). This boundary has since been dated by astronomical tuning at 1.806 Ma (Lourens et al., 2004). The Plio–Pleistocene boundary, and base of the Quaternary, are presently defined by a GSSP at Monte San Nicola in Sicily (Gibbard and Head, 2009a, 2010; Gibbard et al., 2010), which is astronomically dated at 2.58 Ma (Gibbard and Head, 2009b). The Vrica GSSP, representing the old Plio–Pleistocene boundary, nonetheless remains available to define the base of the Calabrian Stage (the lowest stage of the Pleistocene Series). It is relevant here because the present study spans the moment in time represented by the Vrica GSSP.

The original evidence for establishing the Plio–Pleistocene boundary at the Vrica section was questioned soon after its formalization in 1985, and progressively over the 24 years of its existence. For example, additional cold-tolerant migrants into the Mediterranean, such as the planktonic foraminifer *Neogloboquadrina atlantica*, are now known to have arrived in the Mediterranean earlier (2.5–2.7 Ma) than previously thought (Suc et al., 1997; Head et al., 2008a; Gibbard and Head, 2010). Another important stratigraphic event associated with the former Plio–Pleistocene boundary, the so called 'wolf-event' in Europe synonymous with the appearance and massive expansion of *Canis etruscus* (an

extinct member of the genus *Canis*, which includes dogs, wolves, coyotes and jackals), has also been found earlier in the Pleistocene (Sardella and Palombo, 2007).

Nonetheless, global events do occur at around 1.8 Ma (the old Plio–Pleistocene boundary), including important continental early human dispersal (Ashley et al., 2010), increased aridity over a large proportion of the African continent (deMenocal, 2004), and intensification of the Walker Circulation in the Pacific (Ravelo et al., 2004).

3.2 Terrestrial evidence

Early human dispersal around, or slightly before, 1.8 Ma has surprisingly not been attributed to climate, but rather to human biological evolution or cultural or social advances (van der Made, 2010), surmised by the absence of a specific special climatic or faunal event at the time. However, cumulative stress of the changing climate leading to episodes of increased aridity in North Africa and Southwest Asia might have had an impact as well.

The ca. 1.8 Ma timing of increased aridity, measured for the African continent from cores in the Arabian (Ocean Drilling Program – ODP Site 721/722) and Mediterranean (ODP Site 967) seas, as well as for the Atlantic Ocean (ODP Site 659), falls within the error bars of the significant breakpoints for trends measured at these sites (Trauth et al. 2009). This timing is believed by Trauth et al. (2009) to coincide with a 400-kyr eccentricity maximum and thus a period of precessional-forced extreme climate variability (short alternating periods of extreme wetness and aridity) The increased dust fluxes recorded at these sites are rather evidence for the alternating wet and arid cycle in the Saharo-Arabian desert belt, prior to 1.8 Ma, and the subsequent dispersal of the dust due to increased monsoon dynamics at ca. 1.8 Ma.

The more complete records for European mammals come from the Villafranchian fauna, which traditionally comprises the Italian and French records but have in recent decades been augmented by records around continental Europe. Extensive paleomagnetic

investigations by Rook and Matínez-Navarro (2010) have allowed the correlation of the late Villafranchian faunas to the geomagnetic polarity time scale. The Middle/Late Villafranchian transition is placed between the Reunion and Olduvai subchrons. Major events and dispersals for the early Late Villafranchian include the widespread extension of the fossil bovid *Leptobos etruscus*, the first appearance of two derived forms of deer (*Eucladoceros dicranios-ctenoides* and *Pseudodama nestii*), a member of the goat-antelope subfamily *Capinae* (*Procamptoceras brivatense*), as well as the first appearance of two extinct carnivore species, the large hyaena (*Pachycrocuta brevirostris*) and a jaguar (*Panthera gombaszoegensis*). *Pachycrocuta brevirostris* is considered to be the largest true hyaena ever recorded (Turner et al., 2008) and the only significant hyaena still operating in Europe during the early–middle Quaternary. Rook and Martínez-Navarro (2010) proposed naming the timing of its appearance as the 'Pahycrocuta brevitostis event', in line with the now defunct 'wolf-event' because of the significant and widespread impact of this carnivore in the Early Pleistocene faunal assemblages from the Iberian Peninsula to eastern China and Indonesia. Hyaenas are absent today from Europe, existing rather in Africa, the Middle East, Afghanistan, Pakistan and western India. Their presence in Europe at the time is possibly attributable to the spread of open habitats, where the probability of finding large carcasses was higher (Ferretti, 2007). This situation does not exist in modern-day continental Europe.

3.3 Marine evidence

3.3.1 Pacific Ocean

Within the marine realm, the development of strong Walker Circulation is cited by Ravelo et al. (2004) as a cause for an increase in the latitudinal sea-surface temperature (SST) gradient in the Pacific between 2.0 and 1.5 Ma; and some authors (Trauth et al., 2007) even narrow this interval to around the former Plio-Pleistocene boundary (1.9–1.7 Ma). In fact, intensification of the Walker Circulation has been linked to a reduction in NADW formation (Trauth et al., 2007 and references therein). Unlike the unidirectional flow of warm water northwards in the North Atlantic, warm equatorial water from the Pacific is exported both towards the north and the south. Pierrehumbert (2000) concludes that this bias of Pacific heat transport reflects the need to supply the South Atlantic (through the Antarctic Circumpolar Current – ACC) with heat, which is then carried northwards. A change in the heat "distribution", as would have occurred with the development of the Walker Circulation at the time, would have increased the heat transport to the South Atlantic via the ACC, and thus into the North Atlantic and possibly reducing the strength of NADW formation itself.

3.3.2 Atlantic Ocean

Henrich et al. (2002) found that starting at 1.9 Ma preservation of the planktonic foraminiferal species *Neogloboquandrina atlantica* and *Neogloboquandrina pachyderma* began to alternate between good and poor in the regions of the southern Labrador and Norwegian–Greenland seas. The good preservation values were interpreted by the authors as evidence of the first intrusion of the Proto-Norwegian Current into a narrow corridor in the southeastern Norwegian–Greenland Sea. For the southern Norwegian–Greenland Sea, a comparative study between alkenone unsaturation index (representing near–surface ocean temperatures) and benthic $\delta^{18}O$ records demonstrated, inter alia, an

event of pronounced cooling (i.e. cooling greater than two standard deviations from the running mean of both records) at ca. 1.70 Ma in marine isotope stage (MIS) 60 (Lawrence et al., 2009).

Further south, in the central part of the North Atlantic, specifically at the BBOR and the northeastern BR (Figure 1), anomalous hematite was deposited between 1.8 and 1.6 Ma (Giosan et al., 2002). A simultaneous increase in Upper Carboniferous spores in these sediments indicates that, like a previous event of hematite deposition at around 2.6 Ma, the provinence of this hematite is most likely the Permo-Carboniferous red beds of the Maritime provinces of Canada (mainly exposed in the Gulf of St. Lawrence, on Prince Edward Island and on the eastern part of New Brunswick). Giosan et al. (2002) hypothesized that this increase in hematite content and Carboniferous spores, accompanied by increased sedimentation rates, may be explained by an intensification of fluvial activity through the St. Lawrence valley due to unknown causes, such as augmentation by glacial meltwater, and rearrangements within the St. Lawrence drainage basin related to glacial or tectonic movement.

Deposits along the coast of eastern North America provide limited further evidence of environmental change at around 1.8 Ma, based on studies of the pollen, bivalve mollusks, ostracodes, gastropods and dinocysts from the Atlantic Coastal Plain and Chesapeake Bay, although fluctuating sea-levels have left these records partially incomplete.

3.3.3 Onshore eastern USA

The James City Formation, in eastern North Carolina, and the lower Waccamaw Formation, in northeastern South Carolina, to which it is considered correlative (Krantz, 1990), belong to the Windyn Substage and the Colerainian Stage (Blackwelder, 1981). Paleomagnetic evidence (Cronin et al., 1984) and the occurrence of the planktonic foraminifera *Globorotalia truncatulinoides* and *Globigerinoides obliquus obliquus* (Akers, 1972) constrain the lower Waccamaw Formation, and thus the James City Formation, between 1.9 and 1.7 Ma. Ward et al. (1991) proposed that the James City and

Waccamaw shelly quartz sands were deposited in a shelf sea that extended across the outer coastal plain of North and South Carolina. Mollusk assemblages from these two formations are indicative of subtropical marine climates (Blackwelder, 1981) and the abundance of *Globigerinoides* spp. in the Waccamaw Formation was used to propose the presence of relatively warm surface waters (Cronin et al., 1984). Temperatures during the deposition of the James City Formation, specifically, have been estimated by Krantz (1990) using mollusk-isotope records at between 18.9 and 20.7°C. These warm-temperate values are shown to differ significantly from previous marginally subtropical temperature estimates using ostracode assemblages, with maximum values of 25–27.5°C (Hazel, 1988). The details of this divergence will be covered in more detail in the geochemical section.

Other bivalve and gastropod studies of the James City Formation qualify the fauna as paratropical (Petuch, 2004). Petuch's definition of paratropical environments, faunistically defined with gastropods and bivalve mollusks, typically lacks well developed carbonate environments and associated coral reefs and mangrove forests typically found in tropical lagoonal environments, but contains some cool-tolerant, eurythermal offshoots of tropical coral families.

This paratropical climate seemed to continue north along the eastern North American coast, at least until the Gelasian Omar Formation in Delaware, as indicated by pollen analysis (Groot and Jordan, 1999). Assemblages include pollen of inundation-resistant trees and shrubs from both warm and cooler environments. The genus *Podocarpus*, distributed primarily in the southern hemisphere but also found in the Caribbean (Kelch, 1997), *Taxodium* (bald cypress), with a modern USA distribution from southern Delaware to southern Florida, and west to southwestern Texas (United States Forest Service, 1990), and *Cyrilla* (Ironwood), which occurs in warm parts of America (Allaby, 2006), are mixed with more temperate species such as *Liquidambar* (sweetgum) and *Nyssa* (tupelo) in the older of two samples analysed for the Omar Formation. Reduced frequencies of *Liquidambar* and *Nyssa* pollen, as well as the presence of *Sequoia* (redwood) type pollen, in a slightly younger sample of the Omar Formation might attest

to diminishing water levels. Groot and Jordan (1999) interpreted these two samples as warm-temperate.

3.4 DSDP Site 603

Sedimentological, seismic, paleontological, and geochemical studies conducted at Site 603 all yield results of relevance to the studied interval. Of particular interest are studies of benthic foraminiferal biostratigraphy (Blanc-Vernet and Moullade, 1987), oxygen and carbon isotopes of planktonic foraminifera (Ganssen, 1987), and planktonic foraminiferal biostratigraphy (Ma'alouleh and Moullade, 1987). Integrated stratigraphic, sedimentological, and physiographic studies of Site 603 and its surroundings have illuminated its depositional environment (Wise and van Hinte et al., 1987; Wise and van Hinte, 1987).

Evidence from benthic foraminiferal assemblages, despite low numbers of specimens, suggests that Site 603 was situated in a transition zone, under the simultaneous influence of both the AABW and NADW during the Neogene and Quaternary (Blanc-Vernet and Moullade, 1987). These results are noteworthy, especially considering that the AABW today does not significantly affect bottom sediments north of Bermuda (Talley, 2002). However, if the NADW formation was reduced due to intensification of the Walker Circulation, as mentioned by Trauth et al. (2007), then the AABW would extend further north than at present. All the taxa found in Hole 603C are known to live at great depths in present-day oceans.

Given the low abundance of benthic foraminifera (Blanc-Vernet and Moullade, 1987), only planktonic foraminiferal species were used for oxygen and carbon isotope analysis in Hole 603C, these being *Globigerinoides ruber* and *G. obliquus* (Ganssen, 1987). Ganssen (1987) found that the oxygen isotope record revealed a significant pattern of changing climatic and oceanographic conditions. Specifically, three intervals were identified from the earliest Pliocene to ca. 1.5 Ma. Unfortunately, large sampling intervals only allowed for a partial documentation of the younger samples (between 3.0

and 1.5 Ma). However, a gradual decrease in the carbon isotope values in these younger samples led Ganssen (1987) to propose a slow continuous increase in the surface-water CO_2 budget at the site. Considering that photosynthesis discriminates against ^{13}C (Ravelo and Hillare-Marcel, 2007), a decrease in the $\delta^{13}C$ values would reflect a similar decrease in the photosynthesis activity in the surface waters and thus the CO_2 budget.

Three paleoclimatic events were also detected using planktonic biostratigraphy (Ma'alouleh and Moullade, 1987): two prior to, and one close to, the present study interval. Ma'alouleh and Moullade (1987) linked the net increase in numbers of planktonic foraminifera per gram, located near the former Plio-Pleistocene boundary, to a warming event but indicated that there was no corresponding response at the species level.

Mesozoic to late Cenozoic depositional environments for Hole 603C were also addressed by Wise and van Hinte (1987) using seismic horizons and sedimentology. They advanced the following hypothesis concerning the location of the passage of the WBUC, the lowest layer of the NADW: under the influence of a strengthening WBUC, turbiditic silts and clays were deposited rapidly starting from the middle Miocene to form muddy contourites in 'antidune-like' sediment waves. These grew with no appreciable break until the early–middle Quaternary to form the lower continental rise hills of the Hatteras Outer Ridge (HOR) (Figure 7). The crest of the HOR was considered by Wise and van Hinte (1987) to have grown where the turbidity currents were intercepted by the WBUC. The main current has since shifted towards the continent and now runs in the valley located above the site, preventing deposition since the early–middle Quaternary. At around the time of the present study interval, Site 603 would therefore have undergone changes in the strength and/or location of the WBUC as it flowed along the bottom of the continental slope of eastern North America, and this will have influenced the palynological assemblages.

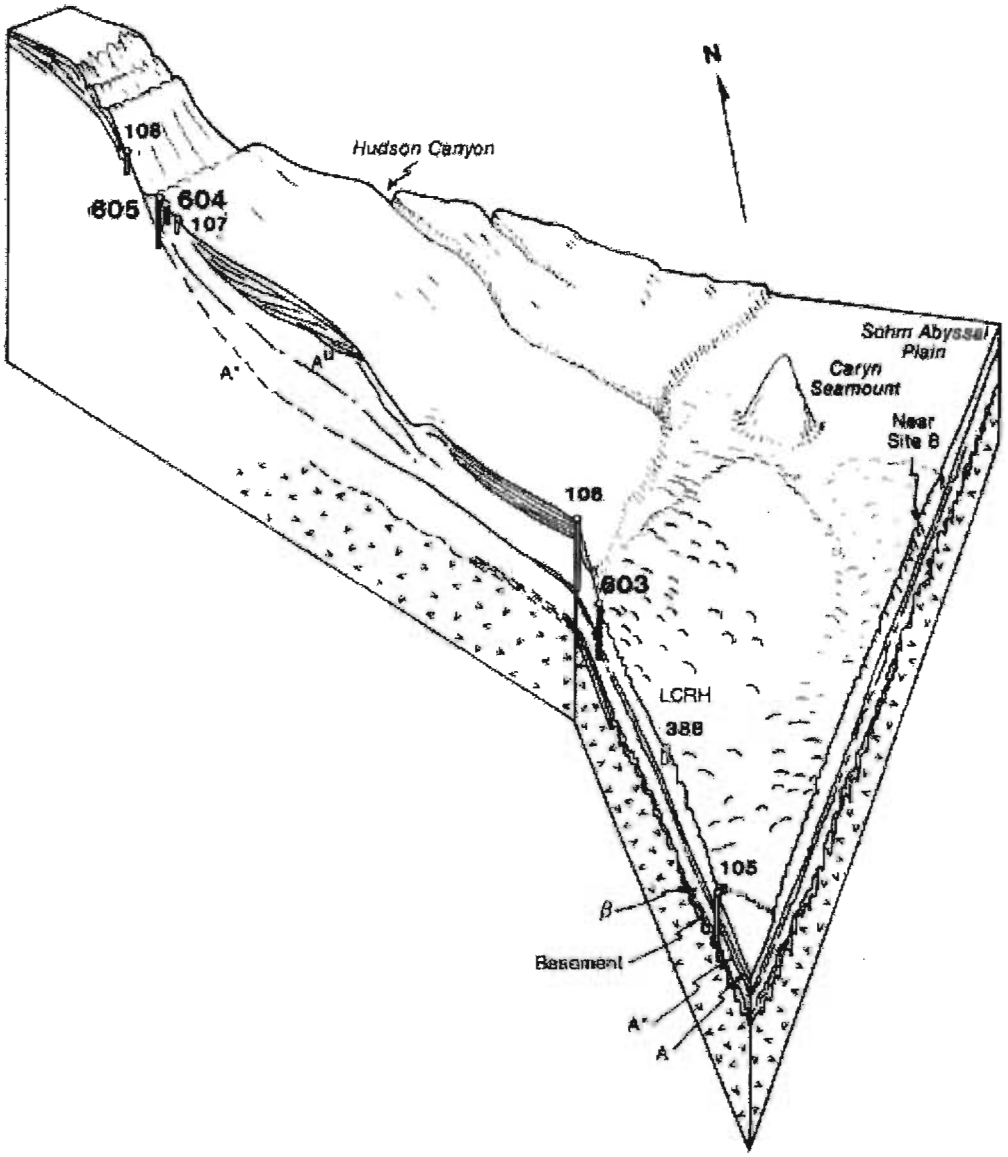

Figure 7. Sketch of the slope and continental rise in the Leg 93 study area showing Sites 603, 604 and 605. Other drill sites and principal seismic reflection horizons are also shown (from Wise and van Hinte, 1987; fig. 35). LCRH = Lower Continental Rise Hills.

Chapter 4 – Material

Forty-eight samples were taken from DSDP Hole 603C, between 11.8 and 29.975 metres below sea-floor (mbsf), representing an average sample spacing of about 37 cm along this 18.175 m cored interval. Sample 4-5; 49–51 cm at 27.69 mbsf was missing from the sample set received from the Integrated Ocean Drilling Program (IODP) core repository

in Bremen, explaining the sampling gap at this level. The average weight of the samples processed was 23.5 g.

The samples used in this study are from lithological Subunit IA of Hole 603C, which is characterized as nannofossil-bearing clay/claystone (Wise and van Hinte, 1987). This is one of four subunits belonging to lithological Unit I, and ranges from the sediment/water interface (Pleistocene) down to 419.8 m (Lower Pliocene/Upper Miocene) in Hole 603C. The following details for the samples used in this study come from the original description from van Hinte et al. (1987). The samples are greenish gray to dark greenish gray hemipelagic clays with differing but significant amounts (usually 5–30%) of calcareous nannofossils. These sediments are also slightly to moderately bioturbated. The hemipelagic nature of the sediments is demonstrated, in addition to clay, by rare quartz (1.5%), rare to common mica (usually 3–5%), and trace amounts of feldspar, in addition to trace amounts of heavy metals, glauconite, palagonite and opaque minerals. Also present are pyrite, siderite, plant debris, fish scales, and nannofossils. Pyritization observed in the present study conforms to the description of van Hinte et al (1987) as occurring as small veins, replacement material on certain specimens of foraminifera, and burrows and dissiminated grains. The middle Miocene to Pleistocene sediments from Unit I are a rather monotonous succession, with faint banding being the most significant sedimentary structure recognized. The cause of this banding was most likely due to slight changes in the biogenic carbonate, quartz silt and organic matter content, and perhaps clay mineralogy (van Hinte et al., 1987). However, bioturbation (mostly horizontal *Planolites*-type burrows) has commonly disrupted the banding or completely churned the sediment, consequently the banding is poorly preserved. Sample details are presented in Table 8.

Chapter 5 – Methodology

5.1 Processing

Samples were processed in two phases: 1) wet sieving of the raw sediment at 125 μm to obtain foraminifera for geochemistry, and 2) palynological processing of the dried and weighed <125 μm filtrate to concentrate the dinocysts, acritarchs, and other palynomorphs. The foraminiferal processing protocol was developed by Dr Stijn De Schepper at the University of Cambridge (De Schepper, 2006; De Schepper et al., 2009), synthesized by Jan Hennissen (University of Toronto), and summarized below. Only one or two elements were modified from the original protocol. The dinocyst processing protocol follows standard procedures and is also described below.

5.1.1 Benthic and planktonic foraminifera

About 20 cc from each of the 48 samples were disaggregated in water and passed through a 125 μm metal sieve to separate the larger foraminifera from the smaller fraction (including palynomorphs). The initial weights as well as the weights for the <125 μm fraction (subsequently dried filtrate) and >125 μm fraction are provided in Table 9. The detailed elements of the foraminiferal processing protocol are supplied in APPENDIX 1 – Methodology.

Isotopic and elemental analysis required collecting 25 to 35 (40 if possible) specimens of the planktonic species *Globigerina bulloides*. For benthic foraminifera, five specimens were sufficient owing to the relative stability of bottom waters and the fact that benthic foraminifera do not migrate through the water column. Two benthic species were targeted: *Cibicidoides wuellerstorfi* and *Uvigerina peregrina*.

The picked foraminifera were sent in labeled foraminiferal containers to Dr. Jeroen Groeneveld at the Alfred Wegener Institute for Polar and Marine Research (AWI) in Bremerhaven, Germany, who verified the species identifications and then had them analyzed.

The analysis of stable isotopes ($\delta^{18}O$ and $\delta^{13}C$) was performed on an inductively coupled plasma mass spectrometer (ICP-MS), whereas the analysis for elemental data (in this case Mg/Ca ratios) used inductively coupled plasma optical emission spectrometry (ICP-OES). The difference between the two is that the mass spectrometer measures the masses of different isotopes or elements, whereas the optical emission spectrometer measures the specific wavelength emitted by each element when it reaches the plasma. The precise methodology followed for both the elemental data and the stable isotopes is described in De Schepper et al. (2009). The cleaning process for the Mg/Ca analysis was adopted from the method described in the appendix of Barker et al. (2003) with one main difference. After the samples had been lightly crushed between two glass plates and clay particles and organic matter thence removed, any additional remaining silicate particles are then free to be removed as well. In the methodology of Barker et al. (2003) the remaining non-carbonate particles are removed under the microscope using a fine brush. For the Hole 603C samples, non-carbonates are separated using a centrifuge. After crushing, the sample is dissolved in HCl and then spun in a centrifuge; the dissolved carbonate solution is then transferred into a clean tube while the remaining non-dissolved non-carbonate particles are concentrated at the bottom of the tube. No oxidation or alkali were applied to the samples. Other elements that were also measured and compared to the calcium content are: strontium (Sr), manganese (Mn), iron (Fe), lithium (Li), beryllium (Be), zinc (Zn) and aluminum (Al). Of thoses elements only a few have been used historically to determine paleoenvironmental conditions using planktonic foraminifera. The present study will briefly touch upon the additional information that the Sr/Ca and Li/Ca ratios can tell us about the local hydrological conditions at the time.

5.1.2 Marine palynomorphs

Below is a brief description of the method used at Brock University to concentrate palynomorphs from the filtrate obtained by sieving the disaggregated sediment sample at >125 μm. The filtrate was collected and allowed to settle in a 1L beaker, and dried and weighed prior to palynological processing. A more detailed account of the palynomorph processing technique is given in APPENDIX 1 – Methodology. Acid treatments were conducted in an HF-rated fume hood.

The palynological processing technique used in this study employs the least amount of chemical and mechanical treatments possible. The dried filtrate was digested using both cold HCl (20% conc.) and cold 48% HF. The resulting organic residue was then sieved at 10 μm using Nitex filter cloth to concentrate the palynomorphs and retain the *Lycopodium clavatum* spores, as these are necessary to estimate palynomorph concentrations. No ultrasound was used for these samples, as they did not contain large amounts of obscuring amorphous organic material.

The residue was mounted on microscope slides using glycerine jelly. Two microscope slides were made for all but one sample (31A), for which three microscope slides were made. The first of these slides were scanned with a Leica DM 2500 microscope using a 40x objective. Palynomorphs were counted until approximately, and no fewer than, 300 dinocysts had been enumerated for each sample, which were scanned along non-overlapping transects After reaching this number, the rest of the slide was scanned, with the same objective, for rare species. For all samples one slide was sufficient for the 300 dinocyst count. The samples were scanned at random to ensure maximum objectivity. Detailed morphological analysis of dinocyst and acritarch species was performed using a 100x objective. All photographs were taken with a Leica DC 300 digital camera. The following palynomorph categories were counted: in-situ dinocysts, reworked dinocysts, acritarchs and bisaccate pollen. The nomenclature for dinocysts follows Fensome et al.

(2004), De Schepper et al. (2004), and De Schepper and Head (2008), and the acritarch nomenclature that of Head et al. (1989), Head and Westphal (1999), Head and Norris (2003), and De Schepper and Head (2008).

Bisaccate pollen and reworked dinocysts were counted to determine the influence of offshore transport. A high ratio of bisaccate pollen to dinocysts is an indicator of high offshore transport, possibly accompanied by elevated quantities of reworked material. The raw counts of all taxa enumerated are given in APPENDIX 7 – Raw counts

Results for the geochemical analyses performed at AWI, Bremerhaven and palynomorph analyses performed at Brock University are presented in the Results section below.

5.2 Geochemical analysis of benthic and planktonic foraminifera

To estimate the annual sea-surface temperatures for the Mg/Ca ratios extracted from the planktonic foraminiferal species *Globigerina bulloides*, both the Mashiotta et al. (1999) and Elderfield and Ganssen (2000) calibrations give reasonable results.

The Mashiotta et al. (1999) calibration yields the following exponential fit:

$$Mg/Ca = 0.474 \times e^{0.107T}$$

This calibration is based on Mg–temperature relationships established for *G. bulloides* using culturing experiments performed at the University of California Santa Barbara and at the Wrigley Institute for Environmental Studies on Santa Catalina Island, California, USA, as well as two core top samples from the Southern Ocean (Mashiotta et al., 1999). Cores RC11-120 and V22-108, from the Subantarctic Indian Ocean and the Subantarctic Atlantic Ocean, respectively, were the only cores at the time available to extend the calibration curve. The culturing experiments were performed for set temperatures of 16, 22 and 25°C, whereas the core-top samples were targeted for temperatures below 15°C. Mean annual sea-surface temperatures for the two core-top samples were estimated at 11.5 and 9.7°C.

The Elderfield and Ganssen (2000) calibration yields a different exponential fit:

$$Mg/Ca = 0.52 \times e^{0.10T}$$

This calibration used modern core-top samples of eight species of planktonic foraminifera (*Globigerina bulloides*, *Globigerinoides ruber*, *Globigerinoides sacculifer*, *Globigerinella siphonifera*, *Neogloboquadrina pachyderma*, *Globorotalia hirsuta*, *Globorotalia inflata* and *Globorotalia truncatulinoides*) for a latitudinal transect of the North Atlantic Ocean from ~30° to 60°N at about 25°W. The range of annual sea-surface temperatures for this transect varied from about 8° to 22°C.

Experimentation suggests that the Mg/Ca paleothermometry method has an accuracy of ±0.5 to 1° C (Nürnberg and Groeneveld, 2006).

The conversion from planktonic $\delta^{18}O_{calcite}$ to $\delta^{18}O_{seawater}$ was also undertaken using a calibration from Elderfield and Ganssen (2000):

$$\delta^{18}O_{seawater} = \delta^{18}O_{calcite} + 0.27(4.38 - (4.38^2 - 0.4(16.9 - T)^{1/2})) /0.2$$

Since both *U. peregrina* and *C. wuellerstorfi* were picked and analyzed, a conversion factor of +0.43 was applied to the *C. wuellerstorfi* benthic $\delta^{18}O$ values. The conversion factor was taken from Lear et al. (2000) to allow for interspecies comparison.

All other elemental analysis (Li/Ca, Sr/Ca and $\delta^{13}C$) was used without any conversion values or calibrations, as they were analyzed on a purely relative basis

I will attempt to link the information provided by the elemental and isotopic analysis to draw a more complete picture of the information extracted from the palynomorphs, which is described in the Results section. The benthic $\delta^{18}O$ signal will serve to support the age

model constrained by the sedimentation rates and the age determination previously estimated for this interval of Hole 603C.

5.3 Palynological analysis

5.3.1 Palynomorph concentrations

Lycopodium clavatum spore tablets were introduced during processing to enable palynomorph concentrations to be estimated (Stockmar, 1971; Maher, 1981; Mertens et al., 2009). Data for the *Lycopodium* spore tablets (batch number 006720) are as follows: X = 11850 and s = ± 200, where X is the estimated total number of spores in one tablet, and s is the error (one standard deviation) on this estimate. Since two tablets were used in each sample, based on previous counts for this section of DSDP Hole 603C (M.J. Head, unpub. data), the standard deviation needs to be adjusted. The new standard deviation, from Maher (1981), for N = two tablets is:

$$s_2 = s*(N)^{½} = 200*(2)^{½} = 282.84.$$

The error calculated for the concentration of dinocysts per gram dry weight per sample, as estimated from Maher (1981) and Stockmarr (1971) for all but one sample, are listed in Table 10.

5.3.2 Statistical analysis

Using two main statistical packages, MiniTab® and Multivariate Statistical Package (MVSP 3.1; Kovach, 2007), five statistical analyses were performed on data from the present study: Correspondence analysis, Constrained cluster analysis, Detrended correspondence analysis, Canonical correspondence analysis, and Detrended canonical correspondence analysis. Descriptive statistics were also performed on the raw data:

Richness, Evenness and the Shannon index were plotted using MVSP. One feature has become quite clear in terms of statistical analysis: the presence or absence of acritarch species makes an important difference to the results provided by the statistical tools. The question remains of course whether or not to include acritarchs in the statistical analysis since they are not included in the summary count for the dinocyst taxa. Many authors (McCarthy et al., 2000a; Dale and Dale, 2002a; De Schepper et al., 2009) exclude the acritarch species from their statistical analyses, but not all do so (Versteegh, 1995). In order to allow more comparable results, most of the statistical analyses performed here did not include acritarch species.

Correspondence analysis (CA). Correspondence analysis is based on unimodal species response, in which it is assumed that a species' abundance increases as its limiting resources increase, but then decrease when the limiting resources reaches a concentration beyond comfortable levels (Dale and Dale, 2002a), i.e. nutrient poisoning. The 51 taxa of dinocysts and acritarchs listed in Table 11 were used in a simple correspondence analysis. The acritarch species were included in this analysis because in plotting the dinocysts alone group distinctions were not as clear.

Constrained cluster analysis. In methods of agglomerative clustering, or cluster analysis, individual objects are combined into larger groups by agglomerating objects with similar features while maintaining that local similarity is more important than larger differences (Dale and Dale, 2002a). In the context of this study, constrained cluster analysis was used to preserve the sequence of the samples in stratigraphic order. The method of farthest neighbor was chosen because it produced the cleanest diagram.

Detrended correspondence analysis (DCA) Detrended correspondence analysis is a "corrected" version of Correspondence analysis. MVSP allows for the graphic representation of both the species and the samples with regard to greatest species variation, both of which were produced for this study.

Canonical correspondence analysis (CCA) Canonical correspondence analysis is another variant of correspondence analysis that allows the distributions of species or samples to be constrained to linear combinations of pre-assigned environmental variables; in this case there are the dinocyst-based Oceanic/Neritic, Pollen/Dinocyst and Warm/Cool axes as well as the foraminifera-based temperature (Mg/Ca), surface $\delta^{18}O_{seawater}$, and surface $\delta^{13}C$ axes. Detrended CCA can also be carried out considering the same "corrections" as with the DCA.

Richness. The species richness of a sample is simply the sum of the species found in that sample, irrespective of whether included in the 300 count or just acknowledged as present. This is the simplest measure of species diversity (De Schepper, 2006).

Shannon Index. The Shannon index (H') is a measure of biodiversity based on species richness (counted species) and the way in which individuals are divided in just proportion into the species counted (eveness) within a sample (Park, 2007). High values for the Shannon index indicate high species diversity and/or even distribution among the species; low Shannon index values indicate the opposite. The Shannon index is obtained using the following formula:

$$H' = -\sum_{i=1}^{S}(p_i \ln p_i)$$

Where:

S is the number of species in the sample.

p is the proportion of individuals belonging to the i^{th} species.

Evenness. Evenness (J') is a measure of how similar the individual species are in their abundances (Magurrant, 2004). High Evenness values are an indication that most species are equally abundant. The Evenness index is obtained using the following formula:

$$J' = H'/H'_{max} = H'/\ln S$$

Where:

H is the Shannon index.

S is the species richness.

Chapter 6 – Results

6.1 Description of the palynological record

A total of 55 dinocyst and seven acritarch taxa were found in the present study. The raw counts are given in APPENDIX 7 – Raw countswhile an alphabetical list can be found in APPENDIX 3 – List of known acritarch and dinocyst taxa from DSDP Hole 603C. Preservation is moderately good for all 48 samples observed, and all samples were rich enough to allow a 300 dinocyst count. A few samples (46D, 46B, 46A, 44C, 42C and 31A) were visibly richer in terrestrial material and acritarch taxa than others. The assemblages contain species and genera both of oceanic (e.g. *Impagidinium* spp.; Dale et al. 2002) and shelf environments (e.g. *Tectatodinium pellitum*; Head, 1997) as well as from alternating warm (e.g. *Polysphaeridium zoharyi*; Head and Westphal, 1999) and cool (e.g. *Filisphaera filifera*; Head, 1996) conditions.

6.1.1 Common dinocysts

The dinocyst taxa listed in Table 1 are common in the samples from Hole 603C, and counted in nearly every slide.

Table 1. Commonly found dinocyst taxa in the studied interval of DSDP Hole 603C.

Dinocyst taxa	**Figures**
Bitectatodinium raedwaldii	(Plate 1, fig. 3)
Bitectatodinium tepikiense	(Plate 1, figs. 4–6)
Corrudinium harlandii	(Plate 1, figs. 9–12)
Filisphaera filifera	(Plate 2, fig 2)
Filisphaera microornata	(Plate 2, figs. 3–4)
Impagidinium aculeatum	(Plate 2, fig. 10)
Impagidinium pallidum	(Plate 2, fig 12)
Impagidinium paradoxum	(Plate 2, fig. 15)
Impagidinium patulum	(Plate 2, fig. 16)
Impagidinium strialatum	(Plate 2, fig. 18)
Lingulodinium machaerophorum	(Plate 3, fig. 1)
Nematosphaeropsis labyrinthus	(Plate 3, fig. 3)
Operculodinium centrocarpum sensu Wall and Dale (1966)	(Plate 3, fig. 4)
Operculodinium israelianum	(Plate 3, fig. 7)
Cyst of *Pentapharsodinium dalei*	(Plate 1, fig. 15)
Polysphaeridium zoharyi	(Plate 3, fig. 10)
Selenopemphix nephroides	(Plate 3, fig. 13)
Spiniferites/Achomosphaera complex	(Plate 3, figs. 14–15)
Spiniferites ludhamensis	(Plate 3, fig. 14)
Spiniferites cf. *rubinus*	(Plate 3, fig. 15)
Achomosphaera andalousiensis subsp. *andalousiensis*	No figure
Tectatodinium pellitum	(Plate 3, fig. 17)

6.1.2 Rarer dinocysts

The dinocyst taxa listed in Table 2 and Table 3 were usually counted in a few slides only or recorded outside of the counts. The rarer dinocysts can be divided into those abundant enough to help with paleoenvironmental reconstructions for the studied interval of Hole 603C (Table 2) and those that appear only once or twice in the entire interval (Table 3).

Table 2. Less commonly occuring dinocyst taxa in the studied interval of DSDP Hole 603C.

Dinocyst taxa	Figures
Amiculosphaera umbraculum	(Plate 1, figs. 1–2)
Ataxiodinium choane	(Plate 4, figs. 1–2)
Ataxiodinium zevenboomii	(Plate 4, figs. 17 and 21)
Capisocysta lata	(Plate 3, fig. 19)
Corrudinium? labradori	(Plate 1, fig. 13–14)
Dapsilidinium pseudocolligerum	(Plate 1, figs. 19–20)
Dalella chathamense	(Plate 1, figs. 17–18)
Desotodinium wrennii	(Plate 2, fig. 1)
Geonettia waltonensis	(Plate 2, figs. 5–6)
Habibacysta tectata	(Plate 2, figs. 7–8)
Hystrichokolpoma rigaudiae	(Plate 2, fig. 9)
Impagidinium cantabrigiense	(Plate 2, fig. 11)
Impagidinium multiplexum	(Plate 4, fig. 7)
Impagidinium plicatum	(Plate 2, fig. 17)
Impagidinium sphaericum	(Plate 4, fig. 4)
Impagidinium velorum	(Plate 2, figs. 19–20)
Lejeunecysta sp.	No figure
Melitasphaeridium choanophorum	(Plate 3, fig. 2)
Nematosphaeropsis cf. *N. labyrinthus* of Rochon et al. (1999)	(Plate 1, figs. 7–8)
Operculodinium janduchenei	(Plate 3, fig. 8)
Operculodinium? megagranum	(Plate 3, fig. 9)
Operculodinium sp. A of Vink et al. (2000)	(Plate 3, figs. 16 and 20)
Operculodinium tegillatum (possibly reworked)	(Plate 5, figs. 6 and 9)
Cyst of *Protoperidinium stellatum*	(Plate 1, fig. 16)
cf. *Quinquecuspis concreta*	(Plate 3, figs. 11–12)
Tuberculodinium vancampoae	(Plate 3, fig. 18)

Table 3. Scarcely occuring dinocysts in the studied interval of DSDP Hole 603C.

Dinocyst taxa	**Figures**
Impagidinium pacificum	(Plate 2, figs. 13–14)
Operculodinium? *eirikianum* var. *eirikianum*	(Plate 3, fig. 5)
Operculodinium? *eirikianum* var. *crebrum*	(Plate 3, fig. 6)
Operculodinium giganteum	(Plate 5, fig. 5)
Operculodinium psilatum	(Plate 5, fig. 4)

Most dinocyst taxa listed here represent less than one percent of the total assemblage.

6.1.3 Acritarchs

Acritarchs in the studied interval, listed in vary from extremely abundant to scarce.

Table 4. Acritarch taxa found in the studied interval of DSDP Hole 603C.

Acritarch taxa	**Figures**
Acritarch sp. 1 of Head, Norris and Mudie (1989c)?	Not illustrated
Algal cyst type I of Head (1996)	Not illustrated
Cymatiosphaera? *invaginata*	(Plate 5, fig. 1)
Cymatiosphaera cf. *latisepta*	(Plate 5, figs. 2–3)
Lavradosphaera crista	(Plate 5, fig. 7)
Leffingwellia costata	(Plate 4, fig. 3)
Nannobarbophora walldalei	(Plate 5, fig. 10)

6.1.4 New dinocyst taxa and acritarch species

Four dinocyst and three acritarch taxa recorded are apparently new to science. They are listed in Table 5 and treated informally in the present study, but are described in detail in APPENDIX 4 – Taxonomy of new dinoflagellates cysts and acritarchs.

Table 5. New dinocyst and acritarch taxa found in the studied interval of DSDP Hole 603C.

Dinocyst taxa	**Figure**
Impagidinium sp. A	(Plate 4, figs. 18–20)
Impagidinium sp. B	(Plate 4, figs. 12–13 and 16)
Dinocyst A	(Plate 4, figs. 14–15)
Nematosphaeropsis sp. A	(Plate 5, figs. 11–12).
Acritarch taxa	**Figure**
Acritarch sp. A	(Plate 4, figs. 8–9)
Acritarch sp. B	(Plate 4, figs. 10–11)
Acritarch sp. C	(Plate 4, figs. 5–6)

6.2 Dinocyst concentration values

The addition of a *Lycopodium* spike enabled the concentration of dinocysts per gram dry weight to be estimated for each sample. Concentrations were calculated for all but one sample (32D) and are listed in Table 10. The mean concentration was 58,610 cysts/g, the minimum concentration was 4,347 cysts/g and the maximum concentration was 1,919,700 cysts/g. This maximum value, which is significantly higher than the mean concentration, was calculated for sample 32B. Only two *Lycopodium* spores were found in sample 32B, and none were found in sample 32D. The counting of just two *Lycopodium* spores in sample 32B implies that the number of dinocysts overwhelmed the *Lycopodium* spike, although the cysts were rather sparsely represented and it was necessary to scan almost an entire slide to reach the count of 300 specimens. The resulting error is accordingly higher for this sample than for the others.

Sample 32D had no *Lycopodium* spores in either slide. The concentration given for sample 32D in Table 10 is an estimated lower limit for this sample. There was slight loss of sample after the second centrifuge run, although this does not alone explain the complete absence of *Lycopodium* spores from the two slides. It is therefore impossible to place an upper limit on the number of dinocysts in this entire sample. However, considering that for 12 traverses, 321 dinocysts were counted and that there are usually 48 traverses per slide and two slides, the lower limit of the number of dinocysts for this sample can be estimated at 2568. Sieved residue for this sample remains, therefore it is safe to assume that the concentration of dinoflagellates is in fact higher than 2568. No other particularly significant anomalies could be detected for the other samples.

6.3 Extensions of geographic and stratigraphic ranges

Most species recorded in the present study have stratigraphic ranges that pass through the Olduvai Subchron, and geographic distributions that include the western North Atlantic. However, the present study extends the published geographic ranges of five taxa: *Spiniferites ludhamensis*, *Operculodinium eirikianum* var. *crebrum*, *Ataxiodinium zevenboomii*, *Capisocysta lata* and *Nematosphaeropsis* cf. *labyrinthus* of Rochon et al. (1999). Stratigraphic ranges are extended for *N.* cf. *labyrinthus* of Rochon et al. (1999) and the cyst of *Protoperidinium stellatum.*

Spiniferites ludhamensis was formally described, and so far has only been reported from the Antian pollen stage (Gelasian) of the Royal Society borehole at Ludham, Norfolk, U.K. (Head, 1996, 1998). The presence of this species within the Olduval Subchron of Hole 603C (this study) and in the Gilbert Chron of Hole 603C (M.J. Head, unpub. data) extends its geographic range to the western North Atlantic.

Operculodinium eirikianum var. *crebrum* was formally described, and also so far only known, from the Piacenzian of DSDP Hole 610A in the eastern North Atlantic (De Schepper and Head, 2008). Although *O. eirikianum* was recorded in Hole 603C (M.J. Head, unpub. data), *O. eirikianum* var. *crebrum* was identified only in the present study.

A single specimen was found, indicating either that this variety is at the limits of its ecological capacity or that the specimen is reworked. Either way, the geographic distribution of this variety is extended to the western North Atlantic.

Ataxiodinium zevenboomii has been recorded from Pliocene and Quaternary deposits of the eastern North Atlantic (De Schepper and Head, 2009) and the North Sea Basin (Head, 1997 and references therein, Louwye et al., 2004), in Pliocene or Lower Pleistocene deposits of the Gippsland Basin, Australia (McMinn, 1992), and the lower Quaternary of the Bahamas (Head and Westphal, 1999). Its presence in Hole 603C was noted in low abundance by M.J. Head (unpub. data) and represents a geographical extension of its Plio–Pleistocene range into the mid-latitude western North Atlantic.

Capisocysta lata was formally described from the Clino Core of the Bahamas where it was recorded from the Pliocene and lower Pleistocene (Head, 1998; Head and Westphal, 1999); modern specimens can be found in the Carribean, Phosphorescence Bay of Puerto Rico, and from the Óbidos Lagoon of Portugal (Head, 1998 and references therein). It has also been found in the Pliocene and Pleistocene of Eastern England (Head, 1998; Fischer and Head, 2008), and late Pleistocene (Eemian Stage) Baltic Sea deposits from Denmark (Head, 2007). Undifferentiated *Capisocysta* spp. were recorded from Upper Pliocene deposits of the eastern North Atlantic (De Schepper and Head, 2009). The recording of *C. lata* in the present study represents a geographical extension of its range to the mid-latitude western North Atlantic.

The cyst of *Protoperidinium stellatum* is recorded mostly in modern sediments. Previous lowest occurrences were in the Pleistocene of the Bay of Biscay in the eastern Atlantic and lower Pleistocene of the Iberian Abyssal Plain (Rochon et al., 1999 and references therein). The recording of this species in the present study, lower than the Iberian Abyssal Plain record, extends its stratigraphic record to the upper Gelasian of the western North Atlantic. Its lowest occurrence in the Iberian Abyssal Plain (ODP Hole 898A) is in calcareous nannofossil zone NN19B (McCarthy and Mudie 1996), for which the age model was established by Liu et al. (1996). Although the nannofossil biostratigraphic

results from ODP Hole 898A do not correlate well with the magnetostratigraphy, three normal polarities were distinguished and correlated by Liu et al. (1996) of which the Olduvai Subchron was constrained immediately below the lower boundary of NN19B and into NN19A. The lowest occurrence of the cyst of *P. stellatum* at ODP Hole 898A would therefore be located immediately above the upper boundary of the Olduvai Subchron. The lowest occurrence of the species in this study (sample 34C), considering our age model, is firmly within the Olduvai Subchron, and thus lower than the Iberian Abyssal Plain occurrence.

Nematosphaeropsis cf. *labyrinthus* of Rochon et al. (1999) has so far been identified only in Holocene sediments from the continental shelf off Nova Scotia (Rochon et al. 1999). The recording of this species in the present study extends its stratigraphic range into the Lower Pleistocene (upper Gelasian) of the western North Atlantic.

6.4 Main dinocyst groupings (assemblage zones)

Samples from this interval of 603C are divided into four chronological assemblage zones (AZ4: 31A – 32A, AZ3: 32B – 41D, AZ2: 42A – 45C and AZ1: 46A – 46D; Figure 8) when using the method of constrained cluster analysis, which can be clearly recognized in the stratigraphic representations plotted with C2 (Juggins, 2007), and subdivided into additional subgroups.

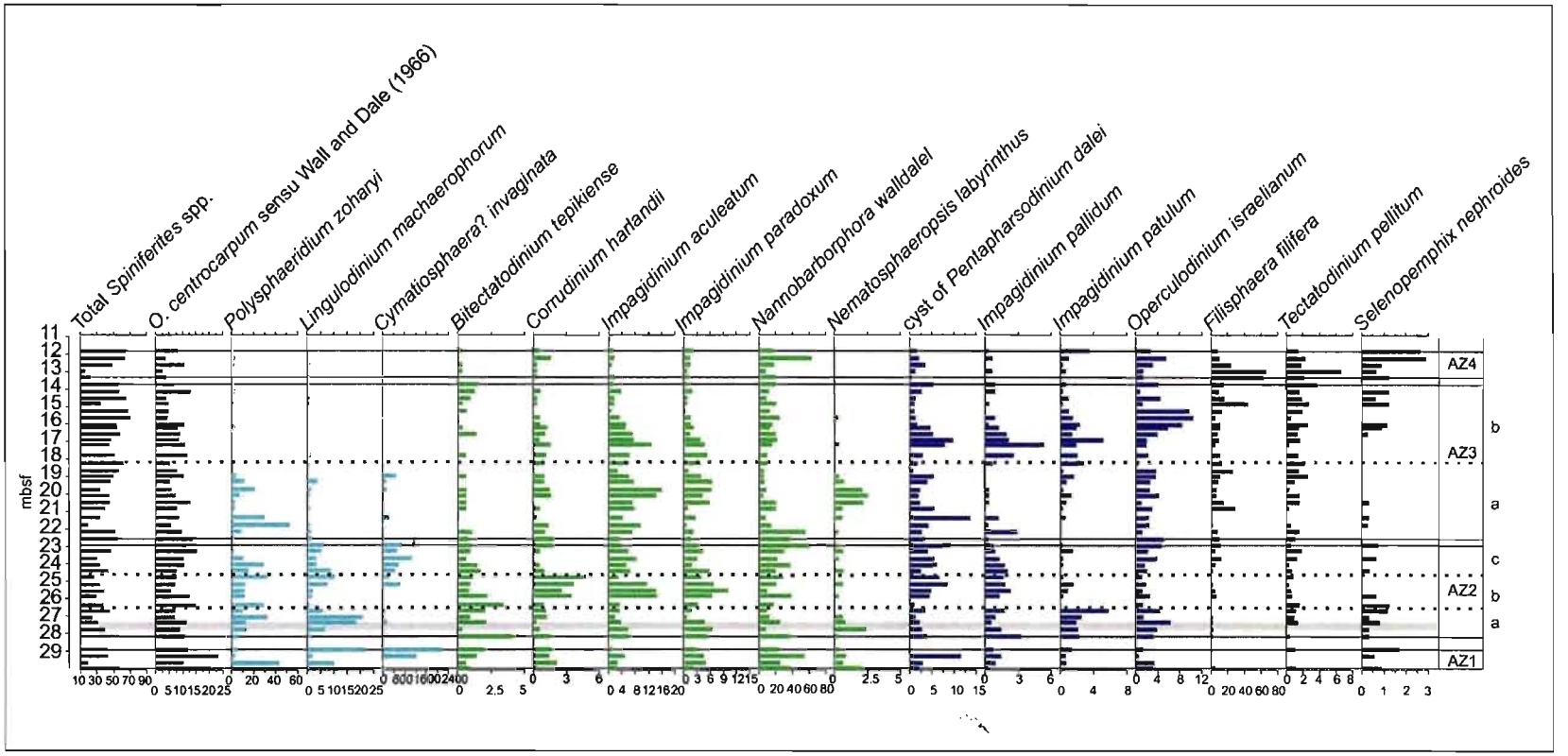

Figure 8. Main dinocyst taxa and acritarch species constraining the Assemblage Zones 1–4 as well as the subzones AZ2a – c and AZ3 a – b. Most dinocyst taxa are in percentages. The acritarch species are in raw counts. The different taxa were color coded based on a visual determination of their first occurrence and/or last occurrence in the studied interval, as well as where they are the most abundant. Taxa abundant throughout are colored in black. Taxa most abundant in the lower part of the interval and mostly absent from the upper part of the interval are colored turquoise. Taxa most abundant in the centre of the interval are colored green. Taxa more abundant towards the upper part of the interval are colored blue. Taxa abundant in the uppermost part of the interval are colored purple.

Assemblage Zone 1 (AZ1: samples 46A–46D) is dominated by *P. zoharyi*, *O. centrocarpum* sensu Wall and Dale (1966) and *Spiniferites* spp., with lower numbers of the cyst of *P. dalei* and *I. paradoxum*. *N. walldalei* and *C.*? *invaginata* are the most abundant acritarch species of this zone. There is a clear antiphase relationship between the decreasing values for *P. zoharyi* and increasing counts for both *C.*? *invaginata* and cysts of *P. dalei*.

Assemblage Zone 2 (AZ2: samples 42A–45C) can be separated into three distinct intervals. *P. zoharyi*, *Spiniferites* spp., *O. centrocarpum* sensu Wall and Dale (1966), *L. machaerophorum*, *B. tepikiense*, *C. harlandii*, *I. aculeatum*, *I. paradoxum*, the cyst of *P. dalei*, *I. patulum* and B. *raedwaldii*, as well as the acritarch species *C.*? *invaginata*, *N. walldalei* and *L. crista*, all contribute during different intervals of AZ2. The first interval (AZ2a) is characterized by increasing values, to varying degrees, of numerous warm-water species (e.g. *I. patulum*, *L. machaerophorum*, *O. israelianum*, *P. zoharyi*) and *B. tepikiense*. The second interval (AZ2b) is characterized by increases in relative abundances of the following species: *C. harlandii*, *I. aculeatum* and *I. paradoxum*. In addition, cysts of *P. dalei* reach peak values in this interval, which continue until the beginning of AZ3. The third interval (AZ2c) corresponds to the second large peak for *C.*? *invaginata*, high relative abundances of *O. centrocarpum* sensu Wall and Dale (1966), and a slight dip for *P. zoharyi*. *N. walldalei* shows its highest values at the transition between AZ2 and AZ3, coeval with the beginning of significant values for *F. filifera*.

Assemblage Zone 3 (AZ3: 32B–41D) can be divided into two intervals. The main dinocyst taxa for this assemblage zone are *P. zoharyi*, *Spiniferites* spp. (and *S. ludhamensis* specifically), *O. centrocarpum* sensu Wall and Dale (1966), *I. aculeatum*, *I. paradoxum*, *N. labyrinthus*, the cyst of *P. dalei*, *I. pallidum*, *I. patulum*, *F. filifera*. *T. pellitum*, *S. nephroides* and *O. israelianum*. The acritarch species are not particularly abundant during this assemblage zone. The last significant peak for the warm-water *P. zoharyi* is located during the first interval (AZ3a). The oceanic species *N. labyrinthus* also shows its most consistent peak during this first interval. The second interval (AZ3b)

is characterized by important increases in *O. israelianum*. Most of the dominant species, such as members of the genus *Impagidinium*, as well as *P. zoharyi* and *L. machaerophorum*, are essentially replaced, or overshadowed, at the top of AZ3b, by the establishment of a new assemblage comprising *F. filifera*, *O. israelianum*, *T. pellitum* and *S. nephroides*.

Assemblage Zone 4 (AZ4: 31A to 32A) has significantly fewer abundant dinocyst and acritarch taxa. Only *F. filifera*, *Spiniferites* spp. *O. centrocarpum* sensu Wall and Dale (1966), *T. pellitum*, *S. nephroides*, *O. israelianum* and *N. walldalei* are abundant in this last assemblage zone. Whereas *F. filifera* is quite abundant at the beginning of AZ4, *Spiniferites* spp. resumes its dominant position at the end of AZ4.

6.5 Paleothermometry and isotopic analysis

6.5.1 Paleothermometry

A visual inspection of the temperature estimates from the Mg/Ca thermometry yielded three main paleo-temperature zones (PTZ1: 46D – 41C, PTZ2: 41C –33B, PTZ3: 33B – 31A, Figure 9), whether using the Elderfield and Gansen (2000) or Mashiotta et al. (1999) calibration. At the upper and lower extremities (PTZ 1 and 3), high maximum values (i.e. 25°C towards the top of the section and 22.5°C towards the bottom) alternate with the lower temperature estimates (14.4°C and 15°C). The more central part of the section (PTZ 2) yields an overall lower mean temperature, and the amplitude is lower as well. In place of the 10°C of amplitude observed towards the top of the section, the central part only shows an amplitude of one or two degrees. Modern annual sea-surface temperatures fall between 16°C and 20°C (Locarnini et al. 2006).

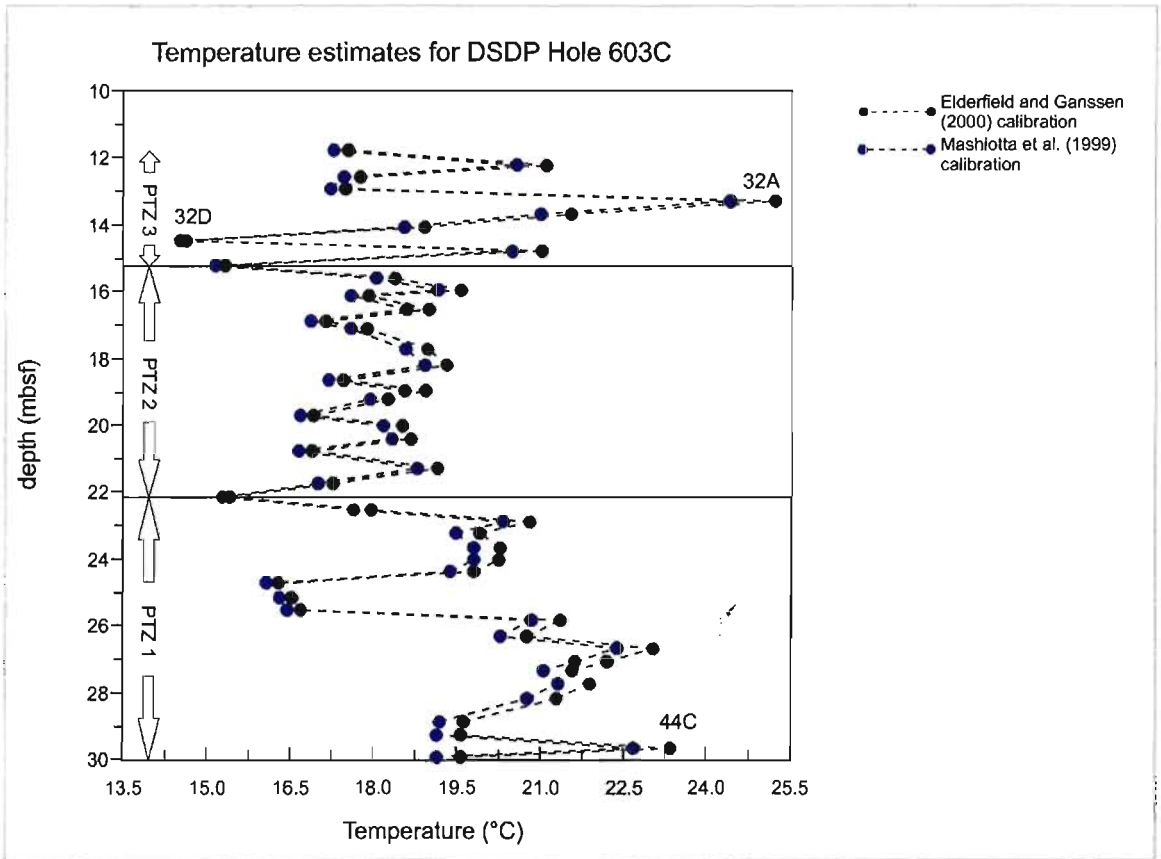

Figure 9. Temperature estimates (°C), using Mg/Ca ratios from planktonic foraminifera for Hole 603C based on the Elderfield and Ganssen (2000) and Mashiotta et al. (1999) calibrations.

6.5.2 Surface $\delta^{18}O$ signal

Since the values for surface $\delta^{18}O_{seawater}$ are controlled partly by the temperature values, the two curves inevitably resemble one another (Figure 10). Some differences, however, can be detected. Where, in the central part of the section (PTZ2), the temperature signal is level, the surface $\delta^{18}O_{seawater}$ signal during this segment dips and then rises. The overall profile provided is therefore an increase from slightly lower values at the beginning of this interval of Hole 603C, followed by a fairly smooth decrease and subsequent increase, as the mean temperature remains level, and finally a major dip in the surface $\delta^{18}O_{seawater}$ signal followed by an equally abrupt peak. These troughs and peaks can be translated into two cool, perhaps glacial, periods, interspaced with a much shorter warm, perhaps interglacial, period, followed finally by a much more unstable period at the top of the interval.

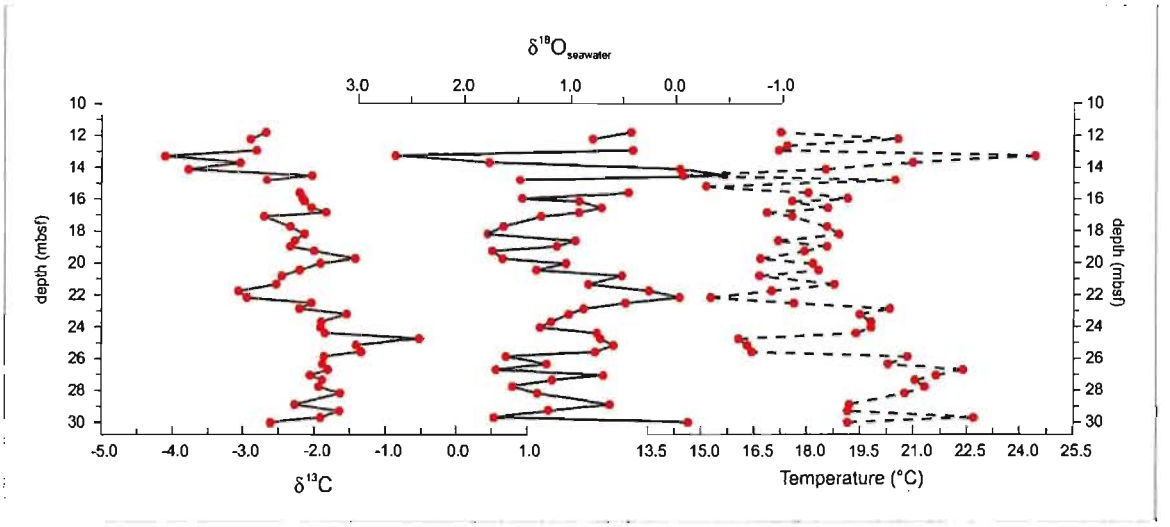

Figure 10. Correlation between temperature (°C) estimates based on the Mashiotta et al. (1999) calibration, surface $\delta^{18}O_{seawater}$, and $\delta^{13}C$ values for DSDP Hole 603C.

6.5.3 Surface $\delta^{13}C$ signal

The surface $\delta^{13}C$ signal is quite different from the temperature and surface $\delta^{18}O_{seawater}$ signals (Figure 10). The trend for this signal is an overall upward decrease: two major peaks and two important troughs alternate along the length of this interval of Hole 603C. The lowest part of the interval has steady values for surface $\delta^{13}C$, followed by a sharp and important increase. The subsequent drop goes below the mean values found prior to the peak. The signal increases again, but does not reach the previous high peak. Finally a slight decrease precedes the most significant drop of the entire section.

6.5.4 Sr/Ca and Li/Ca ratios

The Sr/Ca ratio shows a signal with much less varation. One particularly significant trough can, however, be correlated with the highest value for *P. zoharyi* (sample 41B; Figure 11). Simple stratigraphic plotting of the Li/Ca ratio shows a particularly strong correlation between this signal and the signal for reworked dinocysts (Figure 11) as well as an inverse relation to the O/N signal.

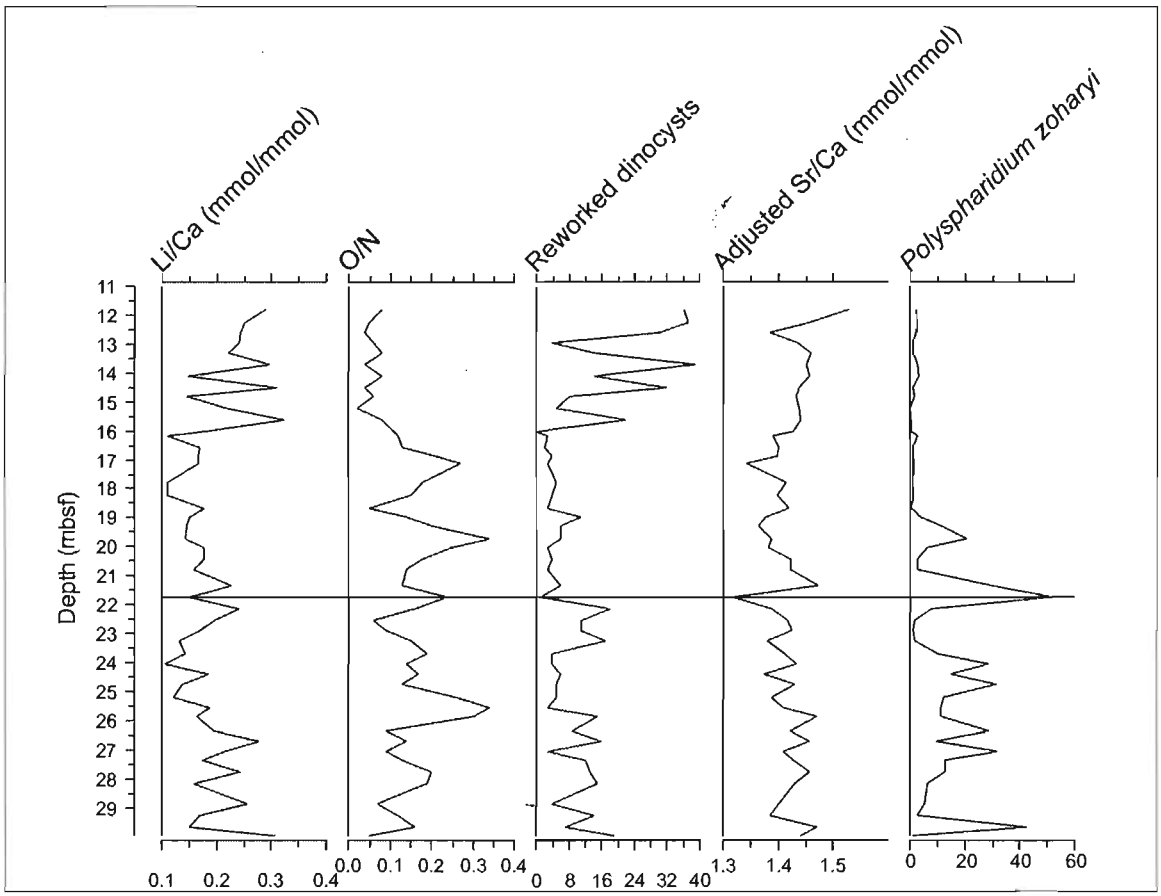

Figure 11. Elemental geochemistry (Li/Ca and Sr/Ca) vs palynomorph data (raw counts of reworked dinocysts, O/N [oceanic/neritic dinocyst] index, and percentage abundance for *P. zoharyi*) to compare specific marine events in DSDP Hole 603C.

Chapter 7 – Discussion

7.1 Age Model for DSDP Hole 603C

The initial goal of comparing the benthic foraminiferal $\delta^{18}O$ data from Hole 603C with the global stack from Lisiecki and Raymo (2005) was greatly hindered by the sparsity of specimens recovered. Only 62.5% of the samples yielded enough benthic foraminifera specimens to produce a measurable benthic $\delta^{18}O$ value (Table 12), not enough to firmly, visually or statistically, correlate the data from this study to the Lisiecki and Raymo stack. The planktonic Mg/Ca and $\delta^{18}O$, as well as the dinoflagellates cyst indices (Figure 12) were also examined for comparison to the Lisiecki and Raymo stack. The fit found between the N/O signal and the Lisiecki and Raymo stack proved to be problematic and will be discussed in more detail subsequently. A tentative fit was also found with the planktonic $\delta^{18}O$ curve.

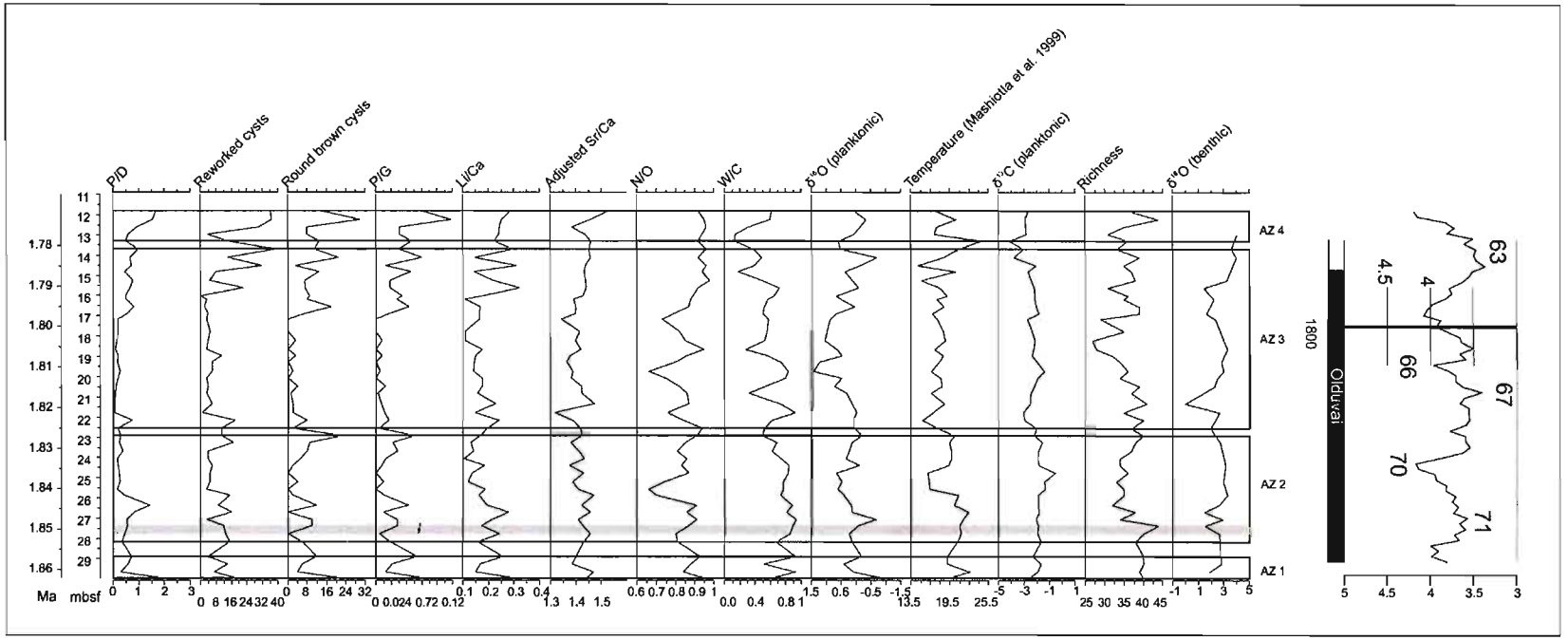

Figure 12. Hole 603C planktonic foraminiferal geochemistry (Li/Ca, Adjusted Sr/Ca, $\delta^{13}C_{planktonic}$, temperature in Celsius and $\delta^{18}O_{planktonic}$) and palynomorph indices (P/D [pollen/dinocyst], reworked cysts, round brown cysts, P/G [protoperidinioid/gonyaulacacoid], N/O [neritic/oceanic], W/C [warm/cool] and richness) compared to the Lisiecki and Raymo (2005) benthic stack, using the sedimentation rate through the Olduvai Subchron and top of the Olduvai Subchron as a tie point for the age model.

The significant but unsurprising lack of benthic data, as previously recorded by Blanc-Vernet and Moullade (1987), requires that the polarity transitions measured and illustrated by Canninga et al. (1987, fig. 6) (Figure 13) be used to constrain the age model for this study. Although the depths of polarity reversals were unfortunately not specifically stated in this publication, their position can be determined quite precisely from published figures(Canninga et al., 1987, figs. 6 and 8), allowing the top and base of the Olduva Subchron to be determined at 13 and 45 mbsf with a visually estimated error of about ±1.5 m. Given that the top and base of the Olduvai Subchron have astronomically calibrated ages of 1.778 and 1.945 Ma respectively (Lourens et al., 2004), and assuming a linear sedimentation rate of (19.2 cm/10^3years), an age model is proposed that places the youngest sample in the present study at 1.771 Ma, and the oldest at 1.866 Ma.

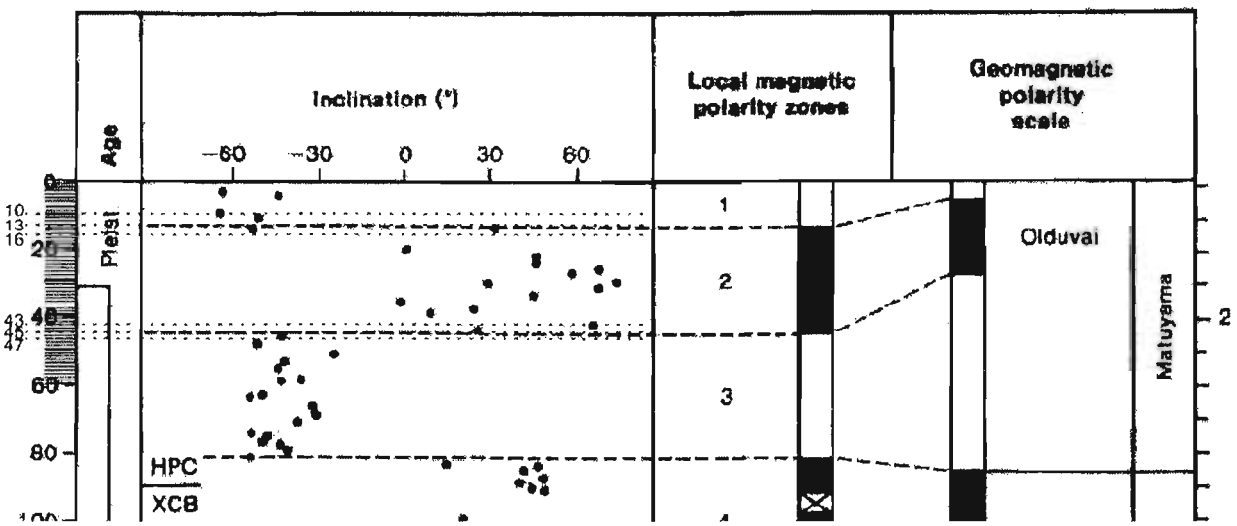

Figure 13. Upper and lower boundaries of the Olduvai Subchron in Hole 603C, as constructed by demagnetisation diagrams and correlated to the Lourens et al. (2004) time scale (modified from Canninga et al., 1987, fig. 6).

7.2 Paleoenvironmental palynological analysis

Several paleoenvironmental indices, based on the actuo- and paleo-environmental tolerances of selected species, have been determined for the recorded assemblages. A brief description of these indices is provided here, along with the results of analyses.

7.2.1 Tropical to subtropical index

Tropical to subtropical samples can be identified according to two criteria (Edwards, 1992), of which only one was strictly applicable to the present study. If the combined percentages of *Impagidinium strialatum*, *Operculodinium israelianum*, *Polysphaeridium zoharyi* and *Tuberculodinium vancampoae* are greater than two percent of the total number of dinocysts in a sample, that sample can be qualified as representing a tropical to subtropical environment. The tropical component is therefore the combined percentages of these four species. All but one sample (35B) from the present study can be qualified as being tropical to sub-tropical by this criterion. However, the abundance of members of the genus *Impagidinium* allows for additional proportional analysis. Values for the tropical to subtropical index as defined by Edwards (1992) are presented in Table 6. Some samples (46C, 44D, 44B, 43B, 42D, 41B, 41A and 36B) clearly have a stronger tropical component than others. These anomalous values are of particular interest. Sample 35B has the lowest value for taxonomic richness.

Table 6. Numerical values for paleoenvironmental palynological analysis methods for DSDP Hole 603C (tropical component and *Impagidinium* index) and temperature range estimates. The winter sea-surface temperature range was derived from the *Impagidinium* index.

Sample code	Depth (mbsf)	Tropical component	*Impagidinium* index	Winter sea-surface temperature range estimate (°C)
31A	11.8	4.6	19.23	6 to 10.5
31B	12.24	8.4	33.33	6 to 10.5
31C	12.62	5.3	30.00	6 to 10.5
31D	12.97	2.2	0.00	0 to 10
32A	13.3	2.5	50.00	10 to 13
32B	13.72	6.5	26.67	6 to 10.5
32C	14.1	4.0	52.00	10 to 13
32D	14.5	5.6	54.55	10 to 13
33A	14.8	3.0	50.00	10 to 13
33B	15.24	9.7	33.33	6 to 10.5
33C	15.62	11.1	48.15	10 to 13
33D	16.005	8.8	57.58	10 to 13
34A	16.175	8.2	47.06	10 to 13
34B	16.56	4.9	60.00	10 to 13
34C	16.895	2.7	38.89	6 to 10.5
34D	17.145	2.8	51.90	10 to 13
35A	17.775	3.4	39.29	6 to 10.5
35B	18.22	1.2	41.30	10 to 13
35C	18.665	4.5	69.23	10 to 13
35D	18.98	7.3	51.35	10 to 13
36A	19.265	14.8	55.10	10 to 13
36B	19.74	24.0	70.89	10 to 13
36C	20.06	12.3	70.00	10 to 13
36D	20.455	4.3	52.17	10 to 13
37A	20.8	5.7	87.50	10 to 13
41A	21.335	32.7	51.61	10 to 13
41B	21.76	55.2	85.71	10 to 13
41C	22.15	10.5	62.00	10 to 13
41D	22.55	7.3	63.64	10 to 13
42A	22.9	5.8	45.45	10 to 13
42B	23.26	5.2	51.11	10 to 13
42C	23.69	14.3	65.85	10 to 13
42D	24.065	30.5	59.38	10 to 13
43A	24.4	16.7	44.19	10 to 13
43B	24.76	32.6	29.41	6 to 10.5
43C	25.19	14.6	54.17	10 to 13
43D	25.56	13.0	50.96	10 to 13
44A	25.875	15.5	64.56	10 to 13
44B	26.36	30.1	47.62	10 to 13
44C	26.7	14.1	24.44	6 to 10.5
44D	27.075	33.0	31.58	6 to 10.5
45A	27.375	19.4	33.33	6 to 10.5
45B	27.775	16.9	35.00	6 to 10.5
45C	28.18	10.0	35.85	6 to 10.5
46A	28.89	7.3	23.81	6 to 10.5
46B	29.28	3.4	41.46	10 to 13
46C	29.68	45.8	30.00	6 to 10.5
46D	29.975	4.0	50.00	10 to 13

7.2.2 *Impagidinium* index

The *Impagidinium* index (II) as described by Edwards (1992) was moderately useful in confirming temperature ranges for DSDP 603C for the time frame considered. This index is considered to be most applicable in temperate, oceanic environments (Edwards et al. 1991). The abundance of specimens of the genus *Impagidinium* in the studied material is suited for the use of this index. Moreover, the *Impagidinium* index is based on species that are oceanic and therefore likely to be broadly in place, in contrast to indices that use neritic species (e.g. *P. zoharyi*, *O. israelianum* and the less common, but nonetheless present, *T. vancampoae*) that in the case of Site 603 have been transported from the shelf. Edwards (1992) developed the *Impagidinium* index using modern material from the eastern coast of North America and oceanic sites in the mid-latitudes between the Mid-Atlantic Ridge and the western European coast. It can only be applied to samples having greater than two percent total *Impagidinium* species, and is as follows:

$$\textit{Impagidinium}\ \text{index} = 100 \quad \frac{(\text{number of specimens of } \textit{I. aculeatum} + \textit{I. strialatum})}{\text{Total } \textit{Impagidinium} \text{ specimens}}$$

In Edwards' study, the total number of *Impagidinium* specimens consisted of *I. aculeatum*, *I. paradoxum*, *I. patulum*, *I. strialatum* and *I. sphaericum*.

An *Impagidinium* index of zero represents winter sea-surface temperatures (WSST) between 0 and 10°C. Temperate samples representing winter sea-surface temperatures between 6 and 10.5°C should have an *Impagidinium* index (II) greater than 0 but less than 40. Samples with an II greater than 40 would have a winter sea-surface temperature between 10 and 13°C.

The main challenges in using this index are when numbers of *Impagidinium* specimens are low and when the provenance of these specimens is in doubt (Edwards et al., 1991). Edwards also indicated that some of the margin parameters require further verification. Regarding the number of *Impagidinium* specimens required for the *Impagidinium* Index to be valid, this remains an open question. And the provenance even of oceanic dinocysts

in an oceanic site is by no means an assurance of local production, although it is fair to assume that some local signal has been preserved, and those cysts that have been transported may reflect the temperature of the currents that transported them to the site.

All but one sample (sample 31D) from DSDP Hole 603C have more than two percent of *Impagidinium* specimens, permitting the *Impagidinium* Index (II) to be applied. The II values and the estimated winter sea-surface temperature ranges estimates are listed in Table 6.

Edwards (1992) suggested that the *Impagidinium* index (II) be used when a sample cannot be classified as tropical to subtropical. Considering the location of Hole 603C, the most likely source of the species used in the tropical to subtropical index is neritic, close to or directly on the continental shelf. The use of II serves as an estimate of oceanic water masses on or beyond the adjacent shelf. Most samples for which the II is above 40, indicating a winter sea-surface temperature between 10 and 13°C, are situated in the middle part of the section, mainly between samples 35C and 44C (Table 6). These high II values correlate with the temperature zone with reduced amplitude variation in the middle of the section (Figure 14). As with the tropical to subtropical index, the anomalous values (i.e. zero value for 31D) are as telling as samples with positive values. In this case, sample 31D was also the sample at which the cool-tolerant neritic species *F. filifera* reached its maximum values.

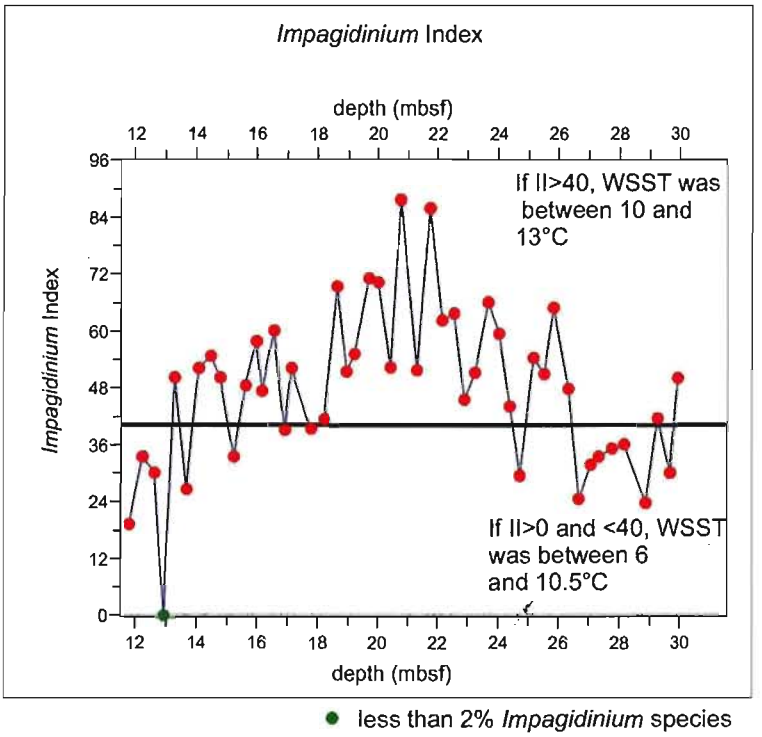

Figure 14. *Impagidinium* Index (II) values plotted for all samples used in the present study of DSDP Hole 603C. WSST (winter sea-surface temperature).

7.2.3 Warm/cold index (W/C)

Spring/summer sea-surface temperature or warm/cold index (W/C). This index gives a simple relative signal based on modern or extinct species understood to have preferential affinities with either warm or cool conditions.

$$W/C = nW/(nW+nC)$$

Where:

n = number of specimens counted.

W = warm-water indicating species.

C = cool-water indicating species.

The selection of warm vs. cool species will vary depending on the species found in each study and as our understanding of the ecological conditions for each species improves,

especially for extinct species. The species used in this study are listed in Table 7. The values determined in using this index offer an estimate of the relative variation in spring or summer sea-surface temperatures over time.

The overall trend for the W/C index is a net decrease over time (Figure 15). It is possible, however, to visually distinguish three clear zones, akin but not simultaneous with the Mg/Ca temperature curve. The main difference between the zones is the amplitude of the signal. The greatest amplitude in the W/C curve is represented by the lowest part of the studied section and most of the upper half, with reduced amplitude in between.

Table 7. Dinocyst taxa from DSDP Hole 603C used to construct both the Warm/Cool and Neritic/Oceanic indices

Warm	**Neritic**
A. zevenboomii	*A. zevenboomii*
B. raedwaldii	*C. lata*
C. lata	*L. machaerophorum*
D. pseudocolligerum	*M. choanophorum*
G. waltonensis	*O. israelianum*
I. aculeatum	*P. zoharyi*
I. paradoxum	*T. pellitum*
I. plicatum	*T. vancampoae*
L. machaerophorum	*Spiniferites* spp.
M. choanophorum	*F. filifera*
O. eirikianum	Cyst of *P. dalei*
O. israelianum	*O. eirikianum*
S. nephroides	*O. centrocarpum* sensu Wall and Dale (1966)
T. pellitum	*C. harlandii*
T. vancampoae	*C.? labradori*
P. zoharyi	*B. tepikiense*
Cool	*B. raedwaldii*
	S. nephroides
B. tepikiense	**Oceanic**
F. filifera	
H. tectata	*A. umbraculum*
I. pallidum	*D. chathamense*
cysts of *P. dalei*	*I. aculeatum*
	I. cantabrigiense
	I. multiplexum
	I. pacificum
	I. pallidum
	I. paradoxum
	I. patulum
	I. plicatum
	I. sphaericum
	I. strialatum
	I. velorum
	N. labyrinthus

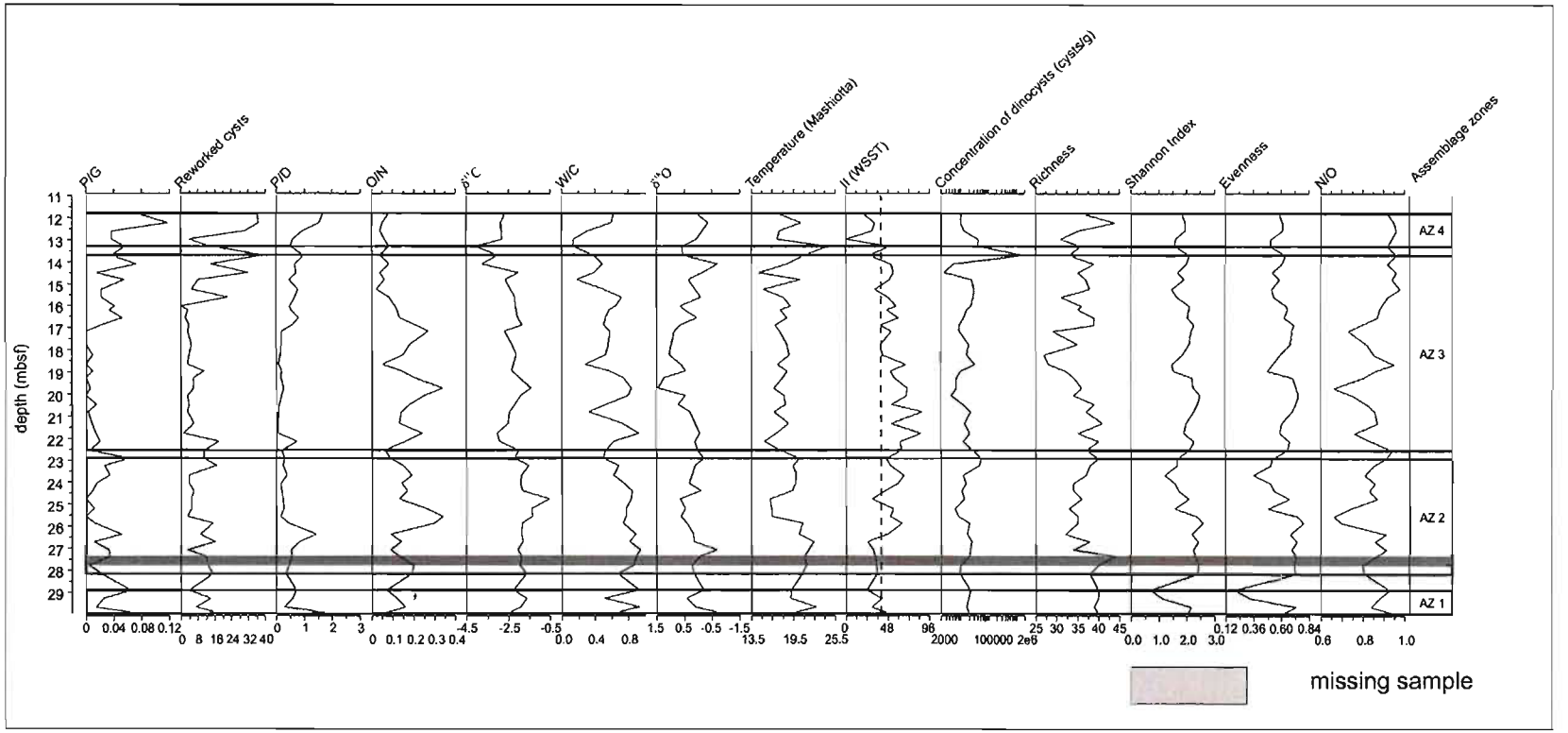

Figure 15. Environmental variables plotted with the four assemblage zones (see Constrained Cluster Analysis, below). P/ G (protoperidinioid/ gonyaulacoid), P/D (pollen/dinocyst), O/N (oceanic/neritic), W/C (warm/cool), N/O (neritic/oceanic), II (*Impagidinium* index) and Reworked cysts are the paleoenvironmental indices related to palynological data from the present study. $\delta^{18}O$, $\delta^{13}C$ and Temperature (Mashiotta, in °C) are drawn from the planktonic foraminifera in the present study

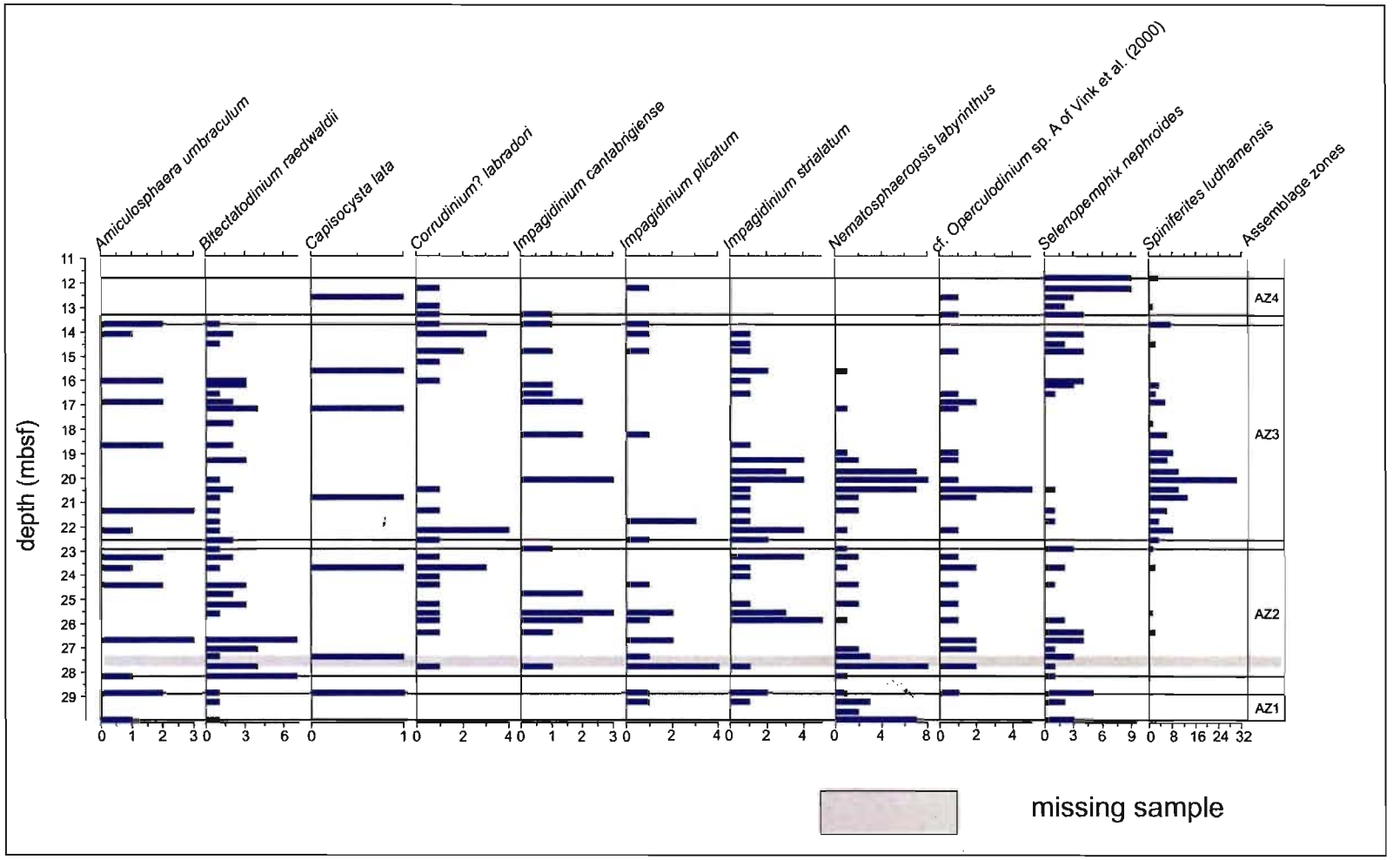

Figure 16. Minor dinocyst species plotted with the four assemblage zones (see Constrained cluster analysis below). The minor dinocyst species are in raw counts

.

7.2.4 Coastal/oceanic or eutrophic/oligotrophic signal

The pollen/dinocyst ratio (P/D) reflects transport from the coast, as most pollen in marine sediments originate from coastal vegetation and fluvial input (with a smaller airborne contribution) (Chmura et al., 1999; McCarthy et al., 2003). They may be transported to oceanic sites by ocean currents and downslope processes (McCarthy and Mudie, 1998). Their abundance typically diminishes with distance from source, and so the P/D ratio is therefore normally used to estimate distance from the coast. It is also true that a decreasing sea level over time will cause the coast to migrate increasingly closer to the site at which the palynomorphs are deposited, and would register a higher influx of pollen or reworked dinocysts. More importantly for oceanic sites, a decreasing sea level also 1) decreases the area of shelf over which clastic sediments (including pollen) can accumulate, causing more input directly into the oceanic realm, and 2) increases the rate of erosion from the shelf (including pollen) and therefore the rate of transport into the oceanic realm (McCarthy et al., 2003). At oceanic sites, bisaccate pollen are more sensitive indicators of terrestrial influence than nonsaccate pollen (and spores) because their air bladders allow them to remain in the water for longer periods (they float) and so travel further. The bisaccate pollen/dinocyst ratio is therefore a useful proxy for coastal influence.

The neritic/oceanic dinoflagellate index is also an estimate of shelfal influence at an oceanic site, and it is subject to similar processes as those affecting the P/D index. Because neritic species reflect nutrient-enriched waters, the N/O index may also register the influence of neritic watermasses at an oceanic site (de Vernal and Marret, 2007), or indeed may serve as an indication of oceanic upwelling in certain areas (Lewis et al., 1990). It might be added that nutrient input may actually be disadvantageous to oceanic (i.e. oligotrophic) dinoflagellates, thus enhancing the sensitivity of the N/O index. Of course, the N/O index is usually strongly influenced by taphonomic processes, and may predominantly serve as an indicator of downslope processes.

The N/O index, as with the warm/cool index, gives a simple relative signal based on the modern or extinct species understood to have neritic (especially protoperidiniacean species, which are heterotrophic) or oceanic (especially *Impagidinium* species, which are oligotrophic) ecological requirements. Species used in this index are listed in Table 7. The index is calculated as follows:

$$N/O = nN/(nN+nO)$$

Where:

n = number of specimens counted.

N = species with a neritic to inner neritic affinity.

O = species with an outer neritic to oceanic affinity.

In the context of this study, the O/N index (inverse value of N/O) is used to contrast with the P/D index, as they are entirely independent of one another. The former index is function of counts internal to the total of dinocysts counted, while the latter is not.

Unsurprisingly the pollen/dinocyst curve and the Reworked Dinocyst curve show similar trends (Figure 15 [See above]). A comparison between the O/N index and the two previous curves shows a definitively negative correlation. Significant pollen and reworked dinocysts values occur in the upper half of the section, after the most important continuous interval of high O/N values. The lower part of the studied section shows alternations between intervals dominated by oligotrophic species and those dominated by pollen and reworked dinocysts.

7.2.5 Protoperidinioid/gonyaulacoid signal

The protoperidinioid/gonyaulacoid (P/G) ratio is ofted used to measure productivity (Versteegh, 1995; De Schepper, 2006). Only two protoperidinioid taxa were actually preserved well enough to be identified in this study (i.e., *S. nephroides* and *Lejeunecysta* spp.), as most round brown cysts were only marginally identifiable. This partial

elimination of the protoperidinioids limits their use as an indicator of productivity. In this study we use the P/G ratio rather as an indicator of oxidation of sediment and possible transport.

$$P/G = nP/(nP+nG)$$

Where:

n = number of specimens counted.

P = protoperidinioid species (including partially preserved round brown cysts, *Lejeunecysta* spp. and *Selenopemphix neproides*).

G = All other species except goniodomaceans (e.g. *Tuberculodinium vancampoae*, *Capisocysta lata*, *Desotodinium wrennii* and *Geonettia waltonensis*).

7.2.6 Relative abundances of specific taxa

Of the dinoflagellate species listed in Table 1, the following 14 taxa represent more than 90% of all assemblages found in this section of DSDP Hole 603C: i) undifferentiated members of the genus *Spiniferites*, ii) *Filisphaera filifera*, iii) *Polysphaeridium zoharyi*, iv) *Operculodinium centrocarpum* sensu Wall and Dale (1966), v) *Lingulodinium machaerophorum*, vi) the cyst of *Pentapharsodinium dalei*, vii) *Operculodinium israelianum*, viii) *Tectatodinium pellitum*, ix) *Corrudinium harlandii*, x) *Bitectatodinium tepikiense*, xi) *Impagidinium aculeatum*, xii) *Impagidinium paradoxum*, xiii) *Impagidinium patulum* and xiv) *Impagidinium pallidum* (Figure 17).

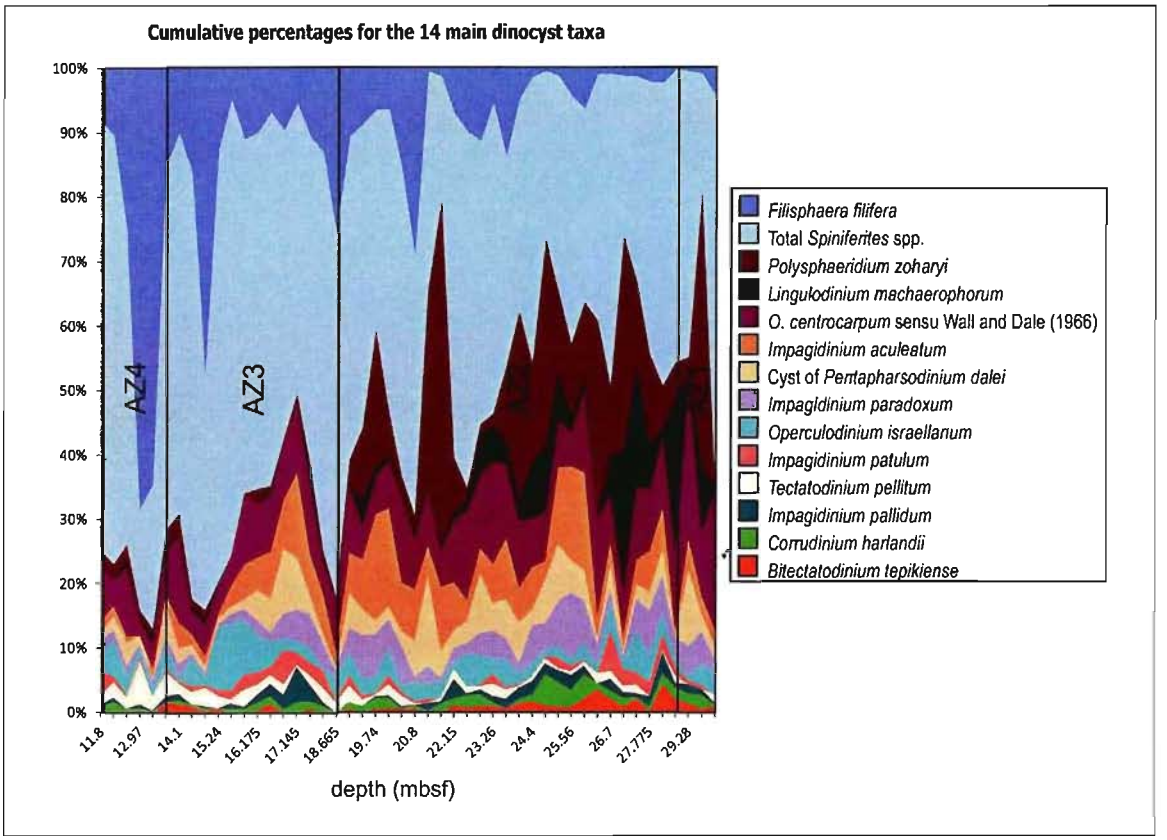

Figure 17. Cumulative percentages for 14 ecologically significant dinocyst taxa and the main assemblage zones.

The simple plotting of those 14 abundant and ecologically revealing species (Figure 18) demonstrates a clear transition from a warm and neritic-species dominated environment to a more oceanic-species strongly influenced environment and finally cool, neritic conditions at the top.

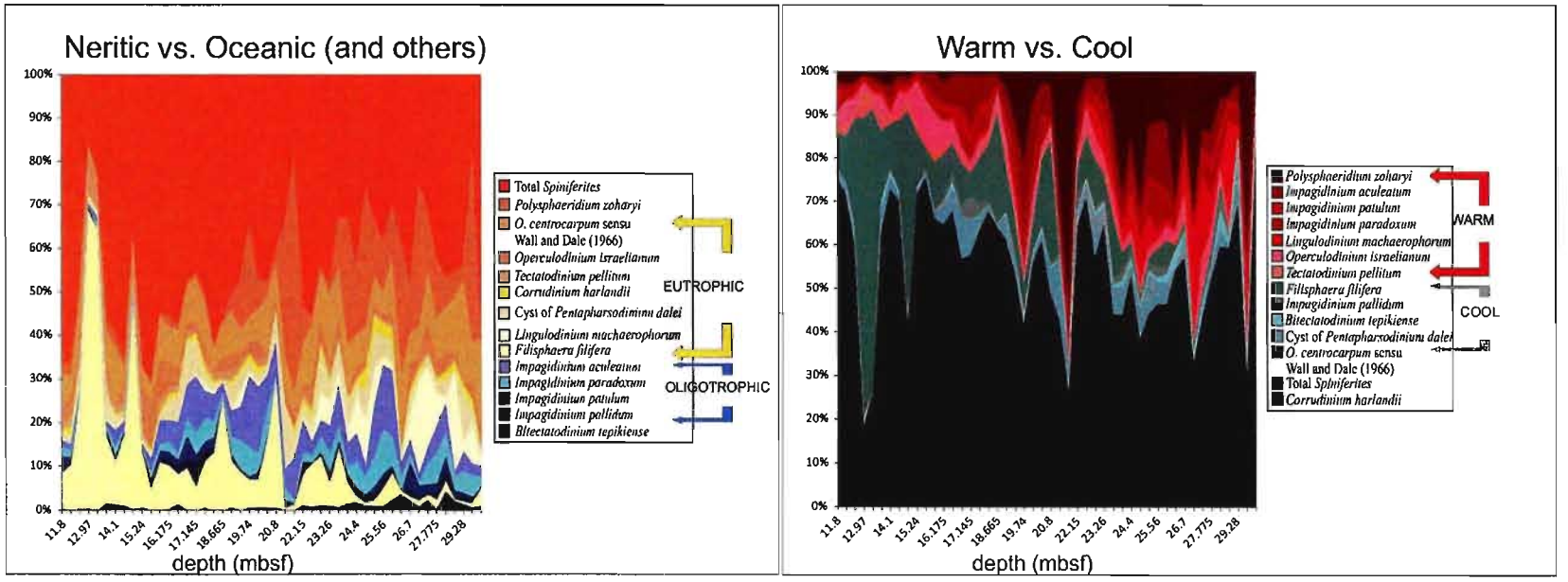

Figure 18. Cumulative percentages of 14 ecologically significant dinocyst taxa, showing alternating warm-cool and eutrophic-oligotrophic (neritic/oceanic) conditions from this study.

Cosmopolitan species such as *Spiniferites* spp. and *O. centrocarpum* sensu Wall and Dale (1966) remain an important component throughout the section. However, a clear negative trend can be seen between the warm-neritic *P. zoharyi*, more abundant in the lower part of the section up to sample 35C, and the cool-neritic *F. filifera*, which is more abundant starting from 36B and reaches its maximum values towards the top of the section. The oceanic component remains present, though not dominant, throughout most of the section, before being completely overshadowed by the neritic species – mainly *F. filifera* – towards the top of the section. The two abundant acritarch species, *N. walldalei* and *C.? invaginata*, help reveal a different set of controlling environmental factors. In the older part of the examined section, peaks of the warm-water *N. walldalei* are linked more closely to peaks of *L. machaerophorum* than to those of *P. zoharyi*. *C.? invaginata*, however, presents a better positive correlation with *L. machaerophorum* and a negative correlation with *P. zoharyi*. More specific details are revealed in the stratigraphic plots of the more abundant species (Figure 19).

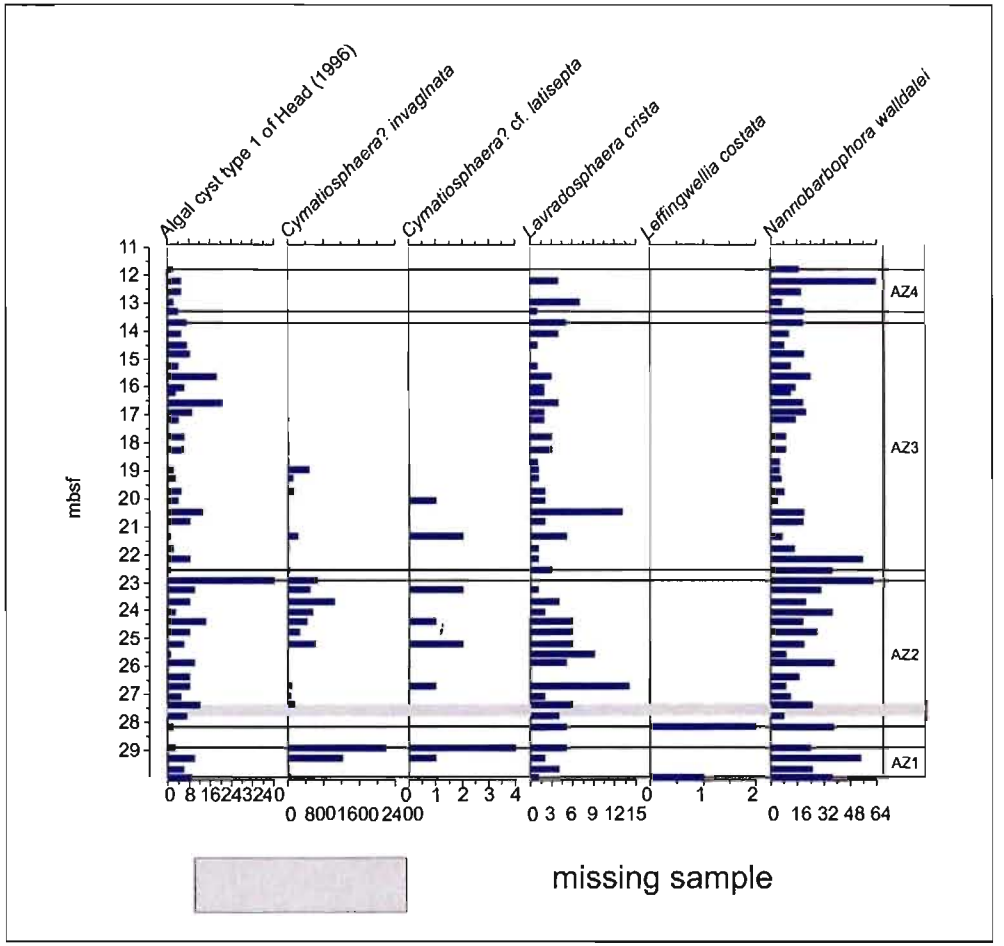

Figure 19. Acritarch taxa recorded in the studied interval of DSDP Hole 603C, plotted with the four assemblage zones (see Constrained cluster analysis, below) according to depth (mbsf). The acritarch taxa are in raw counts. *C.*? *invaginata* is plotted logarithmically .

7.3 Statistical analysis

7.3.1 Correspondence analysis

The 48 samples from Hole 603C can be separated into five groups (Figure 20 and Figure 21), considering the 51 dinocyst and acritarch taxa from Table 1, Table 2, Table 3 and Table 4. Not all taxa listed as present in this study of Hole 603C, in Tables 1 through 5, were used in all the statistical analyses due to their presence only outside of the 300 counts. The scarcity of these taxa (e.g. *O. eirikianum* var. *cerebrum*, *O. giganteum* or *I. velorum*) is difficult to register statistically, so they were left out of the analysis. The groupings defined by the method of correspondence analysis correspond well with results from the relative abundances of taxa and the stratigraphic distribution of the more abundant species, with three main environmental extremes, represented by *F. filifera*, *P. zoharyi* and *C.? invaginata*, clearly separated (Figure 21). However, the fact that the maximum abundance for *C.? invaginata* is ten times greater than the more abundant counts for any other individual species could compound the isolation of *C.? invaginata* with regards to other species.

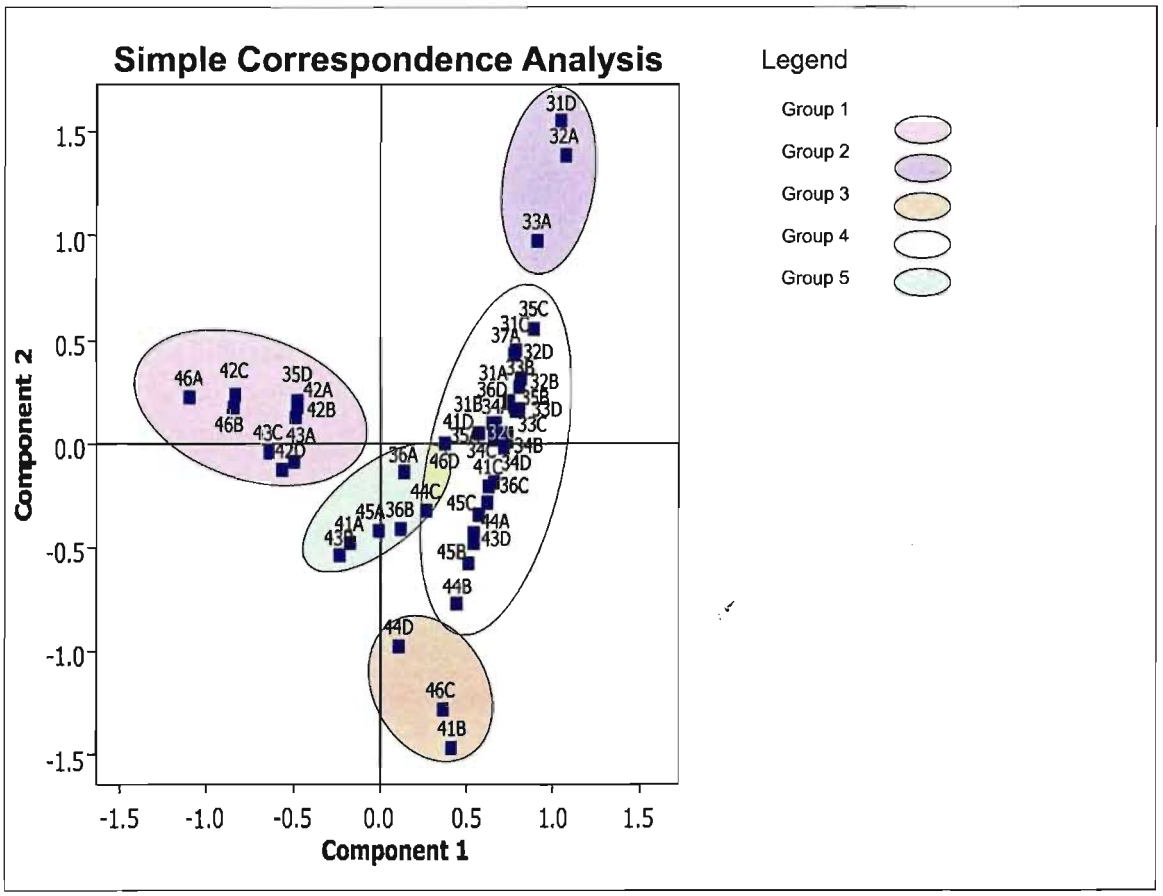

Figure 20. Five main sample groupings obtained using simple correspondence analysis.

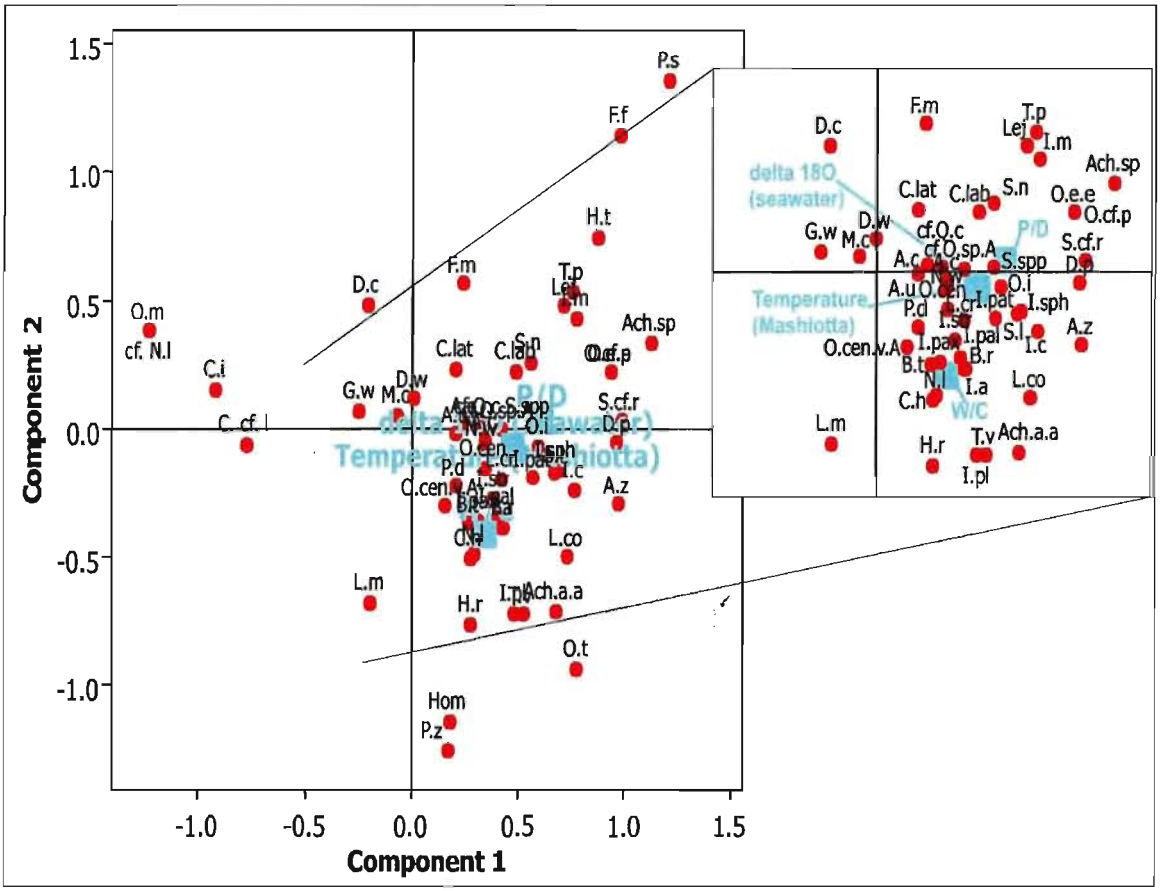

Figure 21 Taxa distribution obtained using simple correspondence analysis (Abbreviations for the dinocyst and acritarch taxa are listed in Table 11).

Group 1 contains nine samples for which the common denominator is high values of *C.*? *invaginata*. Additionally, the pollen/dinocyst ratios for all of the samples, though not the lowest found in the studied section, are still quite low. Most pollen/dinocyst values are below the mean of 0.51. These maximum counts for *C.*? *invaginata* also occur during and just after peak values for surface $\delta^{13}C$. The longest continuous interval dominated by Group 1 would therefore be associated with samples 42A through to 43A.

Group 2 contains three samples and is dominated by high *F. filifera* values. Sample 32A is associated with the lowest value of surface $\delta^{13}C$ recorded for the studied section, whereas samples 31D and 33A are associated with moderately low values. Most samples above sample 33A are coupled with moderately low surface $\delta^{13}C$ values, including these three samples, and indeed the overall trend for surface $\delta^{13}C$ values is a net decrease upsection. However the pollen/dinocyst ratio for these three samples is lower than for the

other surrounding samples of the upper section of Hole 603C. These low pollen/dinocyst ratios indicate that the coastal influence was lower for these three samples, greater than during the peak values of *C.? invaginata*, but lower than for the samples immediately preceding and succeeding these peaks of *F. filifera*.

Group 3, also containing three samples, is dominated by high values of *P. zoharyi*. Sample 41B corresponds to the second most important dip in surface $\delta^{13}C$ and the lowest pollen/dinocyst ratio. Samples 44D and 46C occur at temperature highs. Interestingly, four other samples with comparably high values of *P. zoharyi* (41A = 29.8%, 42D = 28.7%, 43B = 31.5% and 44B = 28.9%) plot in three entirely different groups: 41A and 43B together in Group 5, and 42D and 44B in Groups 1 and 4 respectively. All three samples of Group 3 are coeval with dips in the counts for *B. tepikiense*. Furthermore, none of the acritarch species share any of the peaks, which is all the more significant since acritarchs are counted separately from the dinocysts. The low pollen/dinocyst values are potentially significant as well. *P. zoharyi* is recognized as being an inner neritic species. These peaks, somewhat comparable to counts from more equatorial locations (maximum values at the Clino Core reach 64%; Head and Westphal, 1999), occur, as mentioned earlier, when the pollen/dinocyst ratio is low. Therefore, the source of pollen transported to Site 603 might have been different from the source supplying *P. zoharyi*.

Group 4 contains 27 samples, which is most of the samples analysed for the studied interval. The main common element these samples share is high values for *Spiniferites* spp., presumably since they are not overshadowed by any other major species (e.g. *F. filifera* and *P. zoharyi*). These samples are also well outside of the major peaks for *C.? invaginata*. The longest section following these characteristics covers samples 33B through to 35C.

Group 5, the final 6 samples, sits towards the center of the diagram with moderate to high values of both *P. zoharyi* and *C.? invaginata*. No one particular species predominates over these samples. However, different species are seen to peak at different times during

the intervals represented by Group 5 (e.g. *I. aculeatum*, *I. patulum*, *I. paradoxum*, *C. harlandii* and *N. labyrinthus*).

As can be seen, the plotting of samples in the studied interval does not separate them into particularly distinct groups. The $\delta^{18}O$ benthic stack of Lisiecki and Raymo (2005, fig. 4) for the period around the upper boundary of the Olduvai Subchron shows a series of peaks and dips, suggesting numerous significant changes in the climate conditions around that time. It is therefore not surprising that some samples can be arranged into chronological segments within the groups: samples 31A to 31C within Group 4, 31D and 32A within Group 2, 32B to 41D within Group 4, 42A to 43C within Group 1, and finally 43D to 46D within Group 4.

7.3.2 Constrained cluster analysis

The first four groups isolated with correspondence analysis fit perfectly with the divisions and subdivisions produced by constrained cluster analysis using complete linkage (or farthest neighbour) in Figure 22. The last group (Group 5: Samples 43D to 46D) is much more subdivided using cluster analysis than with correspondence analysis. The data based on geochemistry as well as dinocyst assemblage zones reveal a progressively changing environment with no periods of repetition.

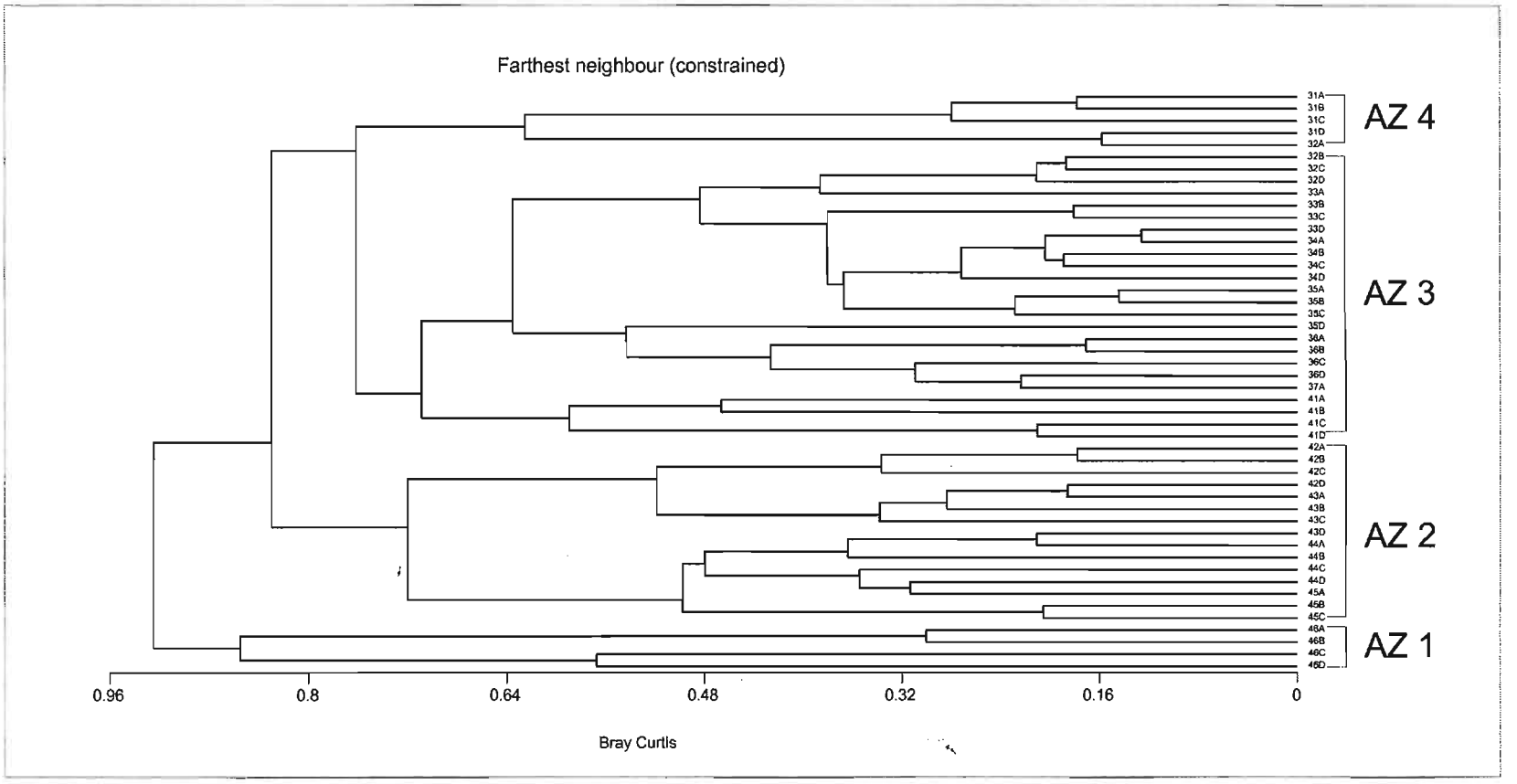

Figure 22. Four main sample assemblage zones delineated with constrained cluster analysis using complete linkage (dinocyst taxa only).

7.3.3 Detrended correspondence analysis.

DCA plotting of the species separates them mainly according to temperature tolerance, with *F. filifera* (representing cooler conditions) at one end of Axis 1 and *P. zoharyi* (the most tropical species found in the studied interval of Hole 603C) at the other end of the axis (double-pointing arrow on Figure 23). These two species can therefore be considered as representing the two thermal extremes for conditions in Hole 603C. Only the cyst of *P. stellatum* plots further away from *P. zoharyi*.

The dispersion along Axis 2 is less clearly identifiable. *L. machaerophorum* and *I. aculeatum* are the two most abundantly occurring species plotting at opposite ends of Axis 2, suggesting that perhaps nutritional conditions are the driving force behind the dispersion. However, the most negative values for *S. ludhamensis* along Axis 2 are the most telling. Most values for *S. ludhamensis* are concentrated around the second peak for surface $\delta^{13}C$ values (Figure 15 and Figure 16), while *L. machaerophorum* and the other species that plot at the end of the positive Axis 2 (*D. chathamense* and *H. rigaudiae*) have very low values or are absent from that peak. These contrasts therefore suggest that anomalies in the surface $\delta^{13}C$ values, rather than simply the overall trend, are the main controlling factor along Axis 2.

In conclusion, dispersion of the samples according to DCA is mainly along Axis 1 (Figure 23 and Figure 24), the thermal axis, but some dispersion along Axis 2, reflecting the surface $\delta^{13}C$ values can be discerned.

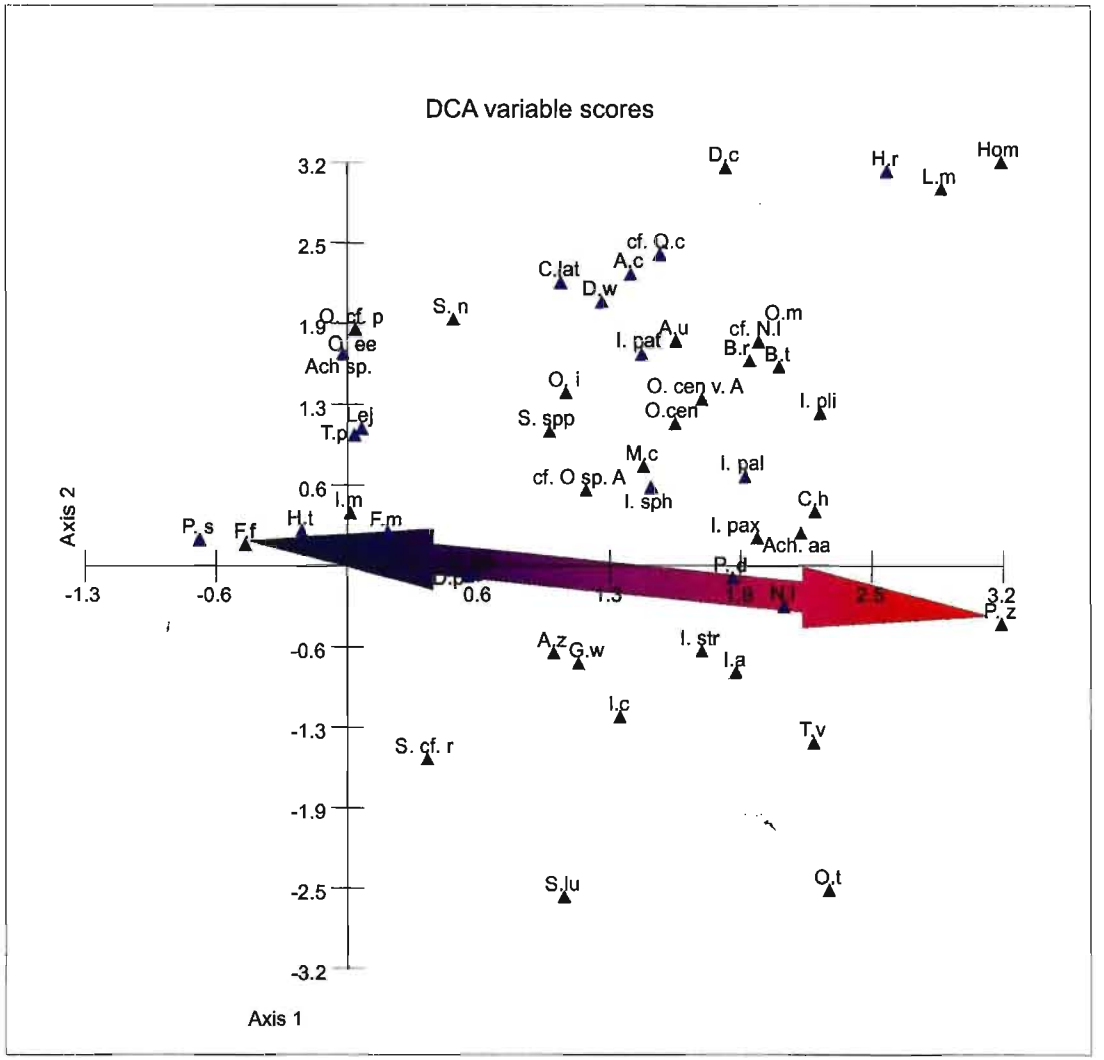

Figure 23. Graphical representation of dinocyst taxa analysed using Detrended correspondence analysis.
The abbreviations for the dinocyst names are in Table 11. The blue and red arrows indicates the main direction of dispersion along axis 1, with cool-tolerant taxa at one end and warmer taxa at the other end.

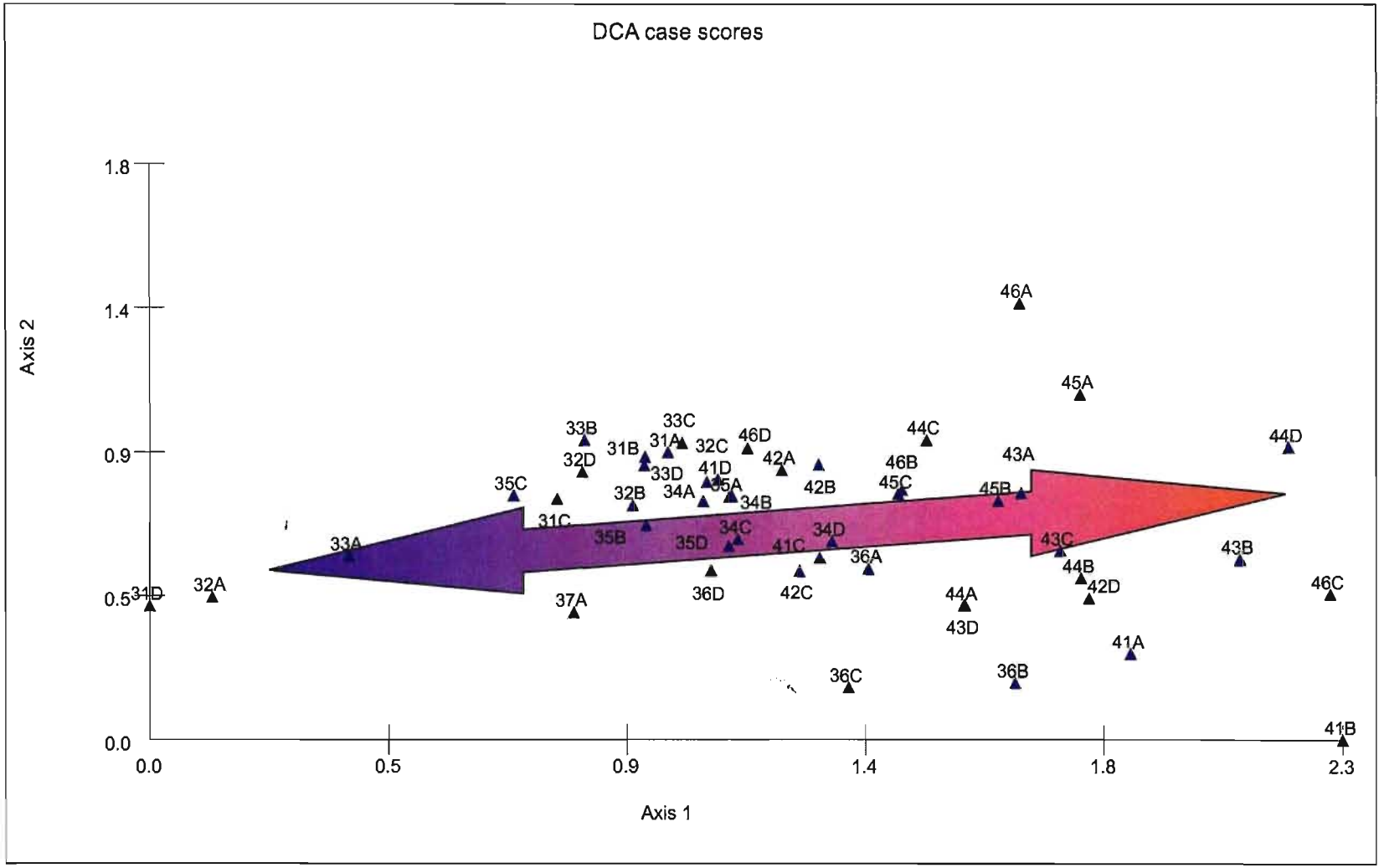

Figure 24. Graphical representation of dinocyst taxa analysed using Detrended Correspondence Analysis.
The blue and red arrows indicate the main direction of dispersion along axis 1, with samples dominated by cool-tolerant taxa, at one end (blue arrow) and samples domimated by warm taxa, at the other end (red arrow).

7.3.4 Canonical correspondence analysis

Graphical representation of sample CCA shows a more diverse dispersion along Axis 1 and 2 than DCA and DCCA (Figure 25) with samples in each quadrant. Considering the first quadrant as positive Axis 1 and 2, and continuing clockwise until quadrant four, a rather clear separation of samples can be made. Dinocyst abundance is determined by comparing the sample CCA (Figure 25) with the dinocyst-only CCA (Figure 26)

Samples 33B to 35D (in yellow) are mostly concentrated in the first quadrant, with some overlap into the second quadrant, migrating between higher and lower O/N values but essentially opposite the temperature (Mg/Ca) axis. This section corresponds to the upper half of AZ3, with major peaks for five dinocyst taxa (the cysts of *P. dalei*, *I. pallidum*, *I. patulum*, *O. israelianum*, and *Spiniferites* spp.) and higher-amplitude WSST between 6–10°C and 10–13°C, and before the O/N index drops significantly. Another small group of samples (36D and 37A, in dark green) are also located in the first quadrant, opposite to the temperature (Mg/Ca) axis. The isolation of these two samples is somewhat peculiar, as the only correlation that can be made is with short, but not very significant, dips in the O/N and W/C signals.

Samples 31A to 32D (orange, fuchsia and grey) plot mostly in the second quadrant, but with some overlap in the first quadrant, along the positive P/D axis and almost opposite to the O/N and surface $\delta^{13}C$ axes. This segment, from 31A to 32D, covers all of AZ4 and overlaps with the top of AZ3. Species that dominate this segment, in addition to the abundant *Spiniferites* spp., are *F. filifera*, *T. pellitum* and *S. nephroides*. The dispersion in this segment is higher than in the previous quadrant with the two *F. filifera*-rich samples plotting well away from the other samples in the quadrant. Temperature (Mg/Ca) estimates vary with great amplitude as well, going from the lowest value estimated for the entire studied interval of Hole 603C (14.5°C) to the highest estimated (24.4°C) within 13 kyr. Elevated P/D and reworked cyst values can also be observed for this segment.

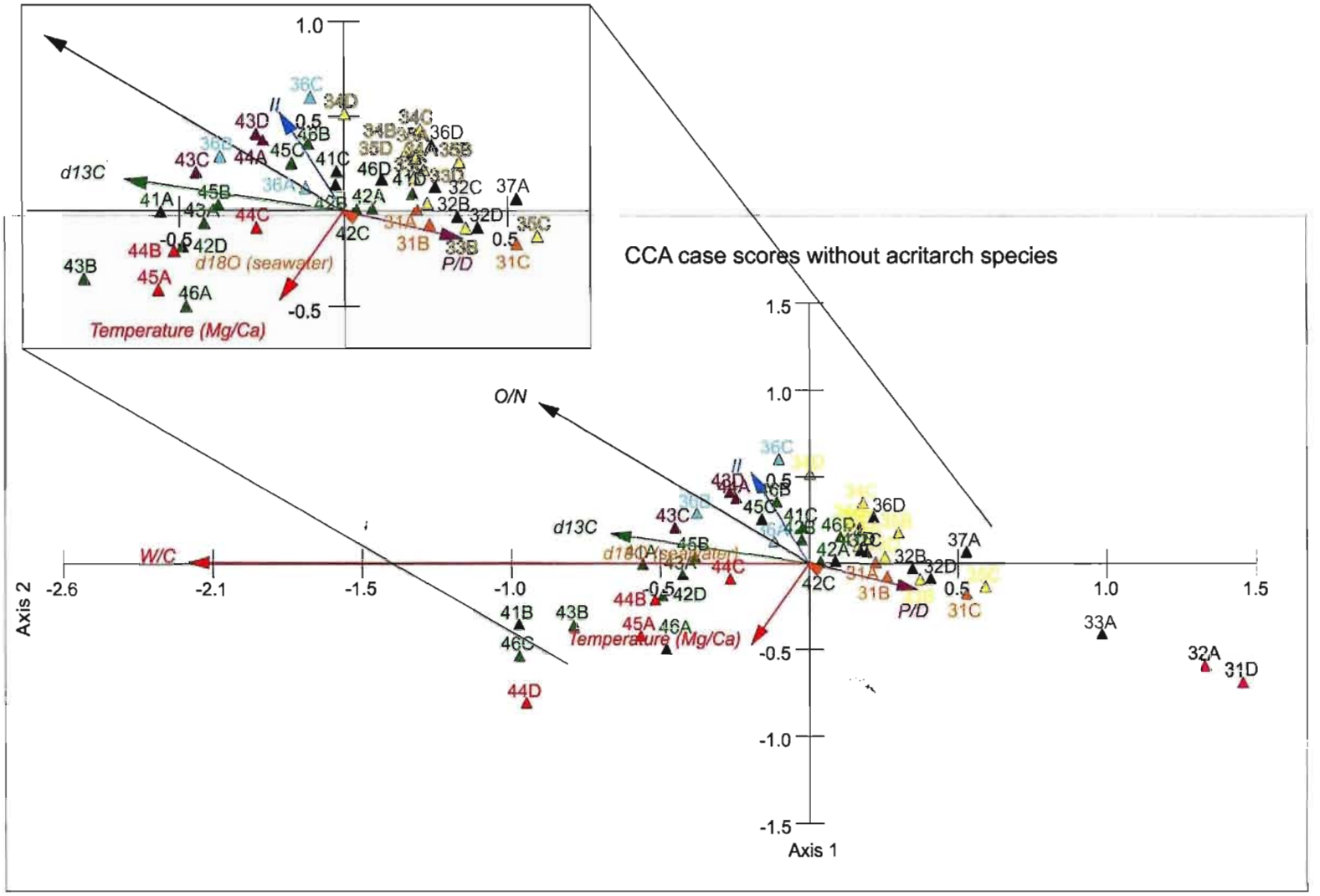

Figure 25. Sample analysis obtained with Canonical Correspondence Analysis (dinocyst taxa only).
O/N (oceanic/neritic), W/C (warm/cool), II (*Impagidinium* index) and P/D (pollen/dinocyst) are paleoenvironmntal indices based on the palynological data from this studied interval. Temperature (Mg/Ca), $\delta^{13}C$ and $\delta^{18}O$ (seawater) are paleoenvironmntal indices based on the planktonic foraminiferal data from this studied interval.

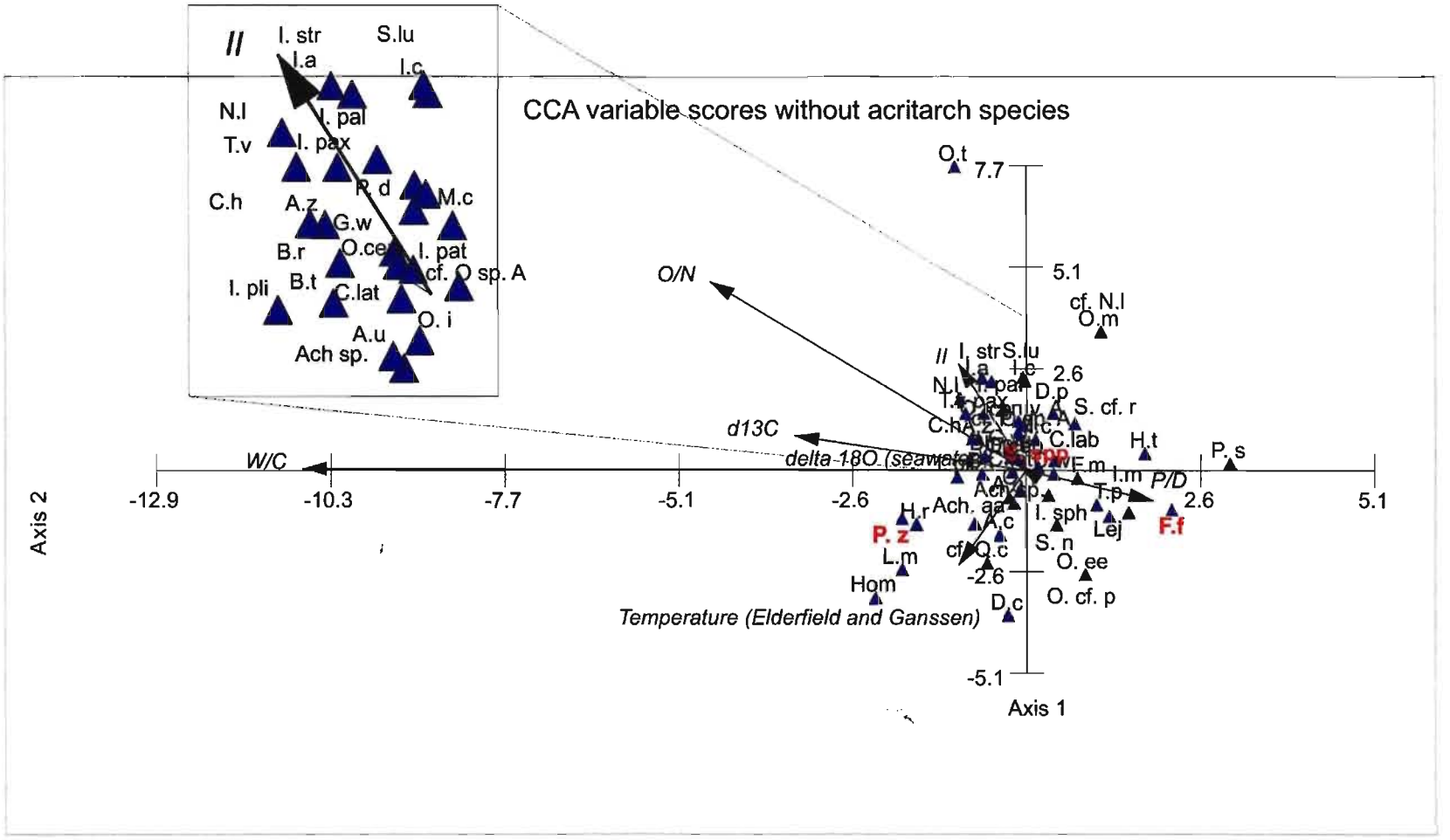

Figure 26. Species analysis obtained with Canonical Correspondence Analysis (dinocyst taxa only).
Abbrviations for the palynological and foraminiferal paleoenvironmental indices are same as in Figure 22. Abbreviations for the dinocyst taxa are listed in Table 11. Colored in red are the three most abundant dinocyst taxa (*P. zoharyi*, *F. filifera* and *Spiniferites* spp.)

Samples from the lower part of the studied interval, from 46D to sample 41A (green), are spread out mostly between the third and fourth quadrants, with some overlap on the first quadrant. There is, however, a small stratigraphic interval between samples 44B and 45A (pink), located in the third quadrant, along the temperature (Mg/Ca) axis which overlaps the position of *P. zoharyi*.

There are two small groups of three consecutive samples (36A to 36C – light blue and 43C to 44A – purple) that plot exclusively in the fourth quadrant, adjacent to the O/N and II indices. The first group of three samples is clustered around the second peak in surface $\delta^{13}C$ values. The second group of three samples is clustered around the first of three major O/N peaks.

CCA was also performed using the new dinocyst and acritarch species despite their lack of significant abundance to determine whether any clear climatic or environmental forcing was in action (Figure 27).

Simply stratigraphically speaking, only Acritarch sp. A and C are abundant enough to reveal any specific pattern of distribution: Acritarch sp. A is coeval with the peak in *C. harlandii* and Acritarch sp. C with the peak in *N. labyrinthus*. In the CCA, Acritarch sp. A plots immediately adjacent to *C. harlandii*, while Acritarch sp. C plots with *S. ludhamensis* at the positive end of the *Impagidinium* index. The peaks for both acritarch species occur during surface $\delta^{13}C$ peaks and coeval with peaks in the O/N signal, suggesting an oceanic source or rather intolerance of high nutrient levels.

As for the other more dispersed new species (i.e. Acritarch sp. B, *Impagidinium* sp. A and B, *Nematosphaeropsis* sp. A and Dinocyst sp. A), their distribution is located mostly in the lower half of the CCA graph, away from the P/D index and the dinocyst species *F. filifera*, *Impagidinium* sp. A and B plot unsurprisingly with other *Impagidinium* species. They are, however, concentrated around the more abundant of the *Impagidinium* species: *I. aculeatum*, *I. paradoxum*, *I. pallidum*, *I. strialatum* and *I. plicatum*. Of the last of the

new species, Acritarch sp. B plots quite separately from *Nematosphaeropsis* sp. B and Dinocyst sp. A. Acritarch sp. B is located almost 180° from the temperature (Mg/Ca) index, whereas *Nematosphaeropsis* sp. A and Dinocyst sp. A plot more towards the thermal end-member *P. zoharyi*. Dinocyst sp. A is immediately adjacent to *P. zoharyi*, and *Nematosphaeropsis* sp. A is predictably located close to *N. labyrinthus*. It is important to recognize that since these last new species are in fact not quite as abundant as Acritarch sp. A and C, the information revealed with CCA might therefore not adequately represent optimal paleoenvironmental conditions.

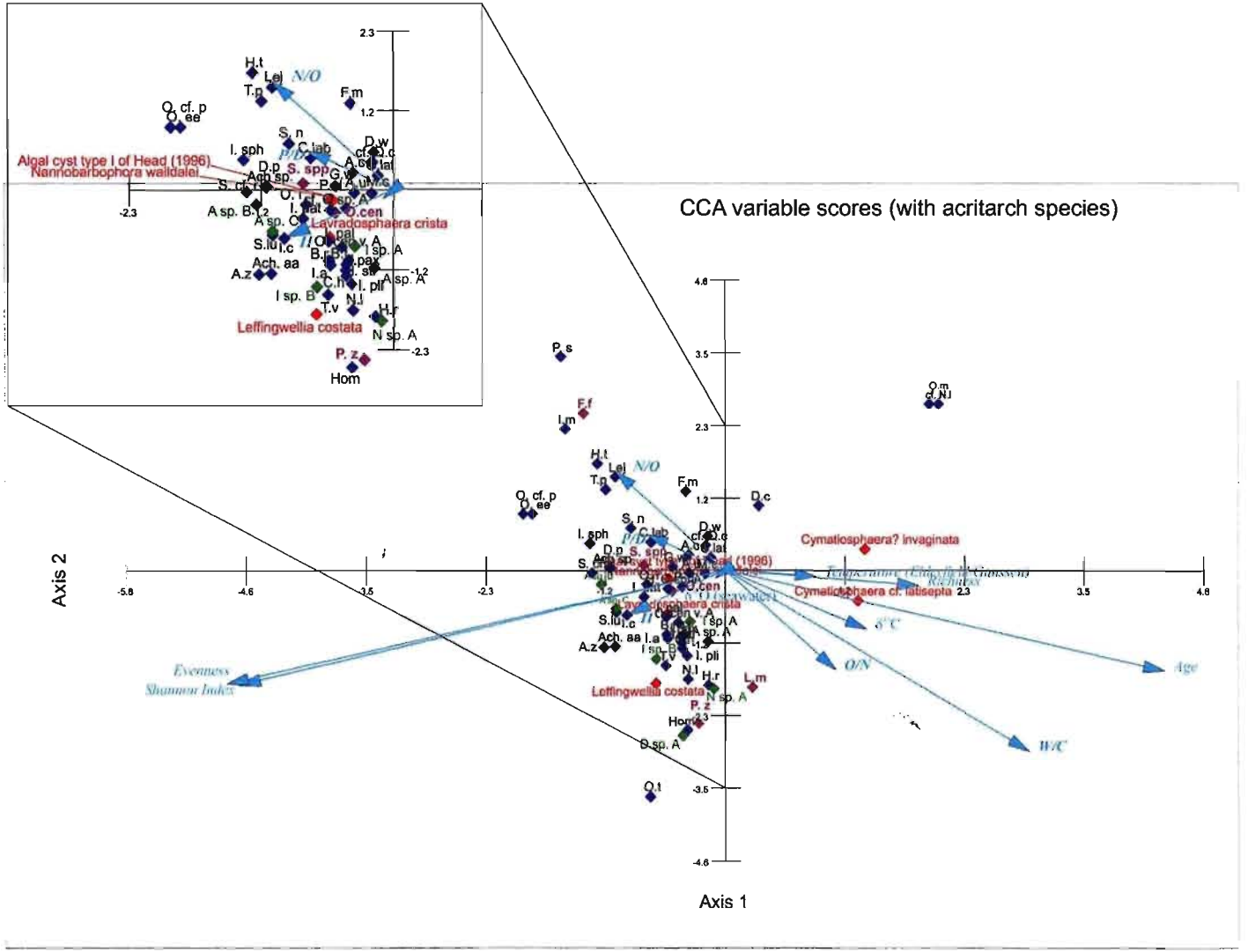

Figure 27. Species analysis obtained with Canonical Correspondence Analysis (including acritarch species) for new dinocyst and acritarch species plotted against their paleoenvironmental indices. Abbreviations for the paleoenvironmental indices are same as in Figure 25. Both the N/O (neritic/oceanic) and the O/N (oceanic/neritic) indices are plotted on this figure. Abbreviations for the dinocyst and acritarch taxa are listed in Table 11. Age is based on the model for this study. Acritarch taxa are colored in red. More abundant dinocyst taxa (*F. filifera*, *L. machaerophorum*, *P. zoharyi* and *Spiniferites* spp.) are colored in purple. New dinocyst taxa are colored in green.

7.3.5 Detrended canonical correspondence analysis

Graphical representation of sample DCCA (Figure 28) presents a similar picture to that represented with DCA. The W/C axis, with the two end-members *P. zoharyi* and *F. filifera*, is almost parallel to Axis 1. The samples with very high values for *F. filifera* plot towards the centre of the diagram and the samples with very high *P. zoharyi* values plot at the opposite end of Axis 1. Interestingly, the temperature (Mg/Ca) axis is at 32 degrees from the W/C axis. Given the overall decreasing trend in surface $\delta^{13}C$ values, it is not surprising that the $\delta^{13}C$ axis is almost parallel to the W/C axis. Most of the other samples are grouped together, although a few samples plot a little closer to the center than the *P. zoharyi* group. Within the largest group of samples, dispersion is parallel to the O/N axis, with samples rich in oligotropic/oceanic species plotting towards nul values for Axis 2 and samples rich in eutrophic/neritic species and a higher pollen to dinocyst ratio plotting towards highers values of Axis 2. The few samples clustered closer to the *P. zoharyi* group have higher W/C values, with an important component of *P. zoharyi*, and are also dispersed within the group according to the O/N index.

The placement of the other environmental axes within the sample plotting is also of interest and confirms what can be seen in the stratigraphic representation of the species and the environmental factors. While the N/O and P/D axes are almost parallel, the difference between the P/D axis and the W/C is 134 degrees. Although the temperature (Mg/Ca) values serve to produce the surface $\delta^{18}O$ values, some small differences can be seen in the stratigraphic representation of the two curves; these differences are reflected in the DCCA as the angle between the two axes is 107 degrees.

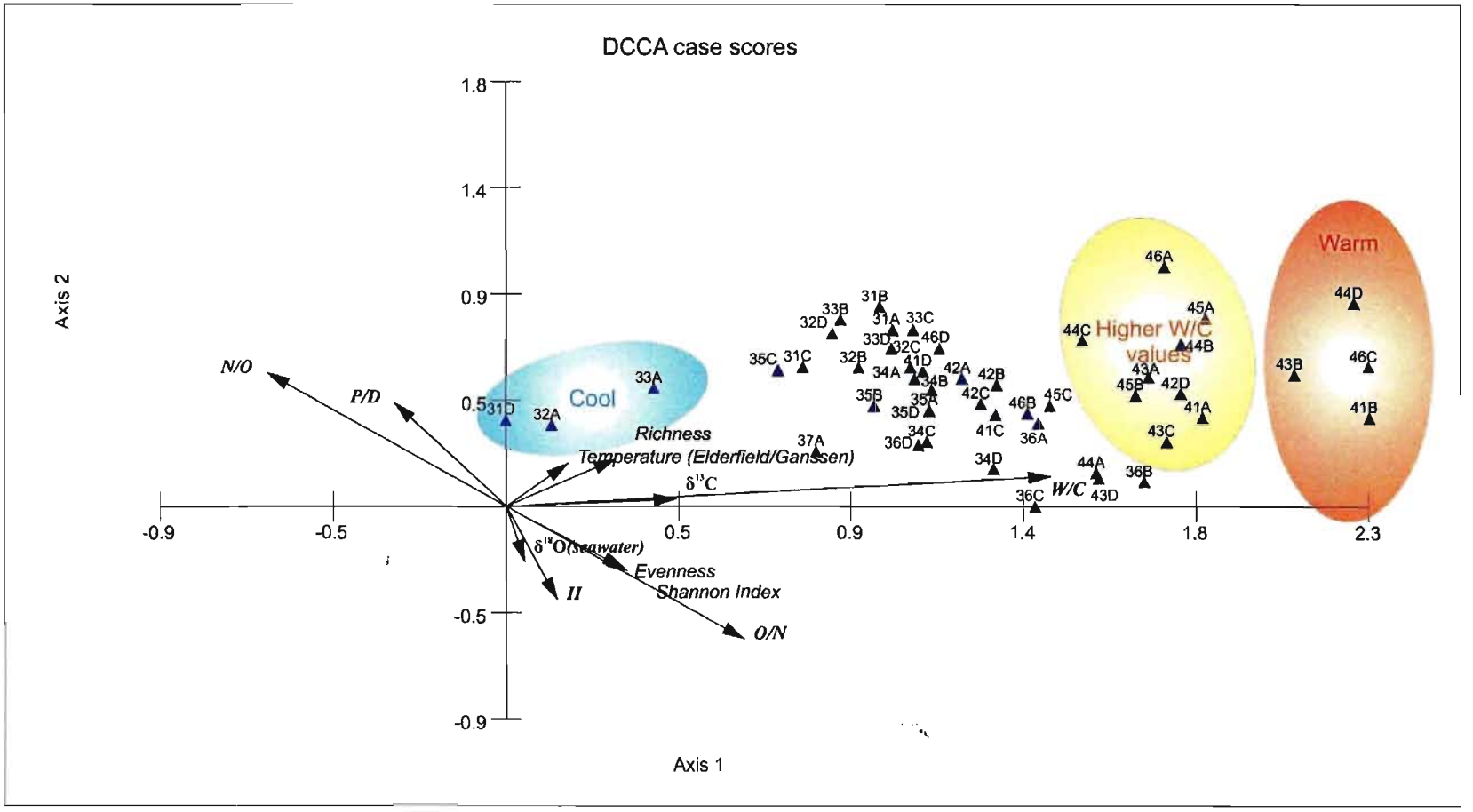

Figure 28. Graphical representation of samples analyzed with Detrended canonical correspondence analysis. Abbreviation for the paleoenvironmental indices are as in Figure 25.

7.3.6 Descriptive statistics

In addition to estimating the concentration of dinocysts per gram dry weight for each sample, Richness, the Shannon index, and the Evenness index were also calculated (Figure 15).

Sample 35B has the lowest richness value i.e. record of total dinocyst and acritarch species of this entire section of DSDP Hole 603C. It is also one of the only samples of the section with almost no counts for *C.? invaginata*. This sample is situated in the middle of AZ3, coeval with the point where the WSST decrease from a constant range of 10–13°C to an interval of variation between 6–10°C and 10–13°C. The second lowest richness value is located in the first half of AZ2, in sample 44B, and coincident with the second highest peak in P/D values and during a dip in the O/N index.

Both the oceanic and neritic concentrations mimic the curve of the total concentration for each sample, although the neritic component of the assemblage remains dominant throughout the section (Figure 29). The oceanic concentration essentially follows the major trends for both the neritic and the total dinocyst concentration. The easiest way to explain this situation is with the constant abundance of *Spiniferites* spp., only rarely replaced in dominance by other neritic species (e.g. *F. filifera* and *P. zoharyi*). The sample with the lowest value for all three concentrations (sample 32D) corresponds to the least abundant total estimates for dinocysts for the studied interval, due to the absence of *Lycopodium clavatum* spores.

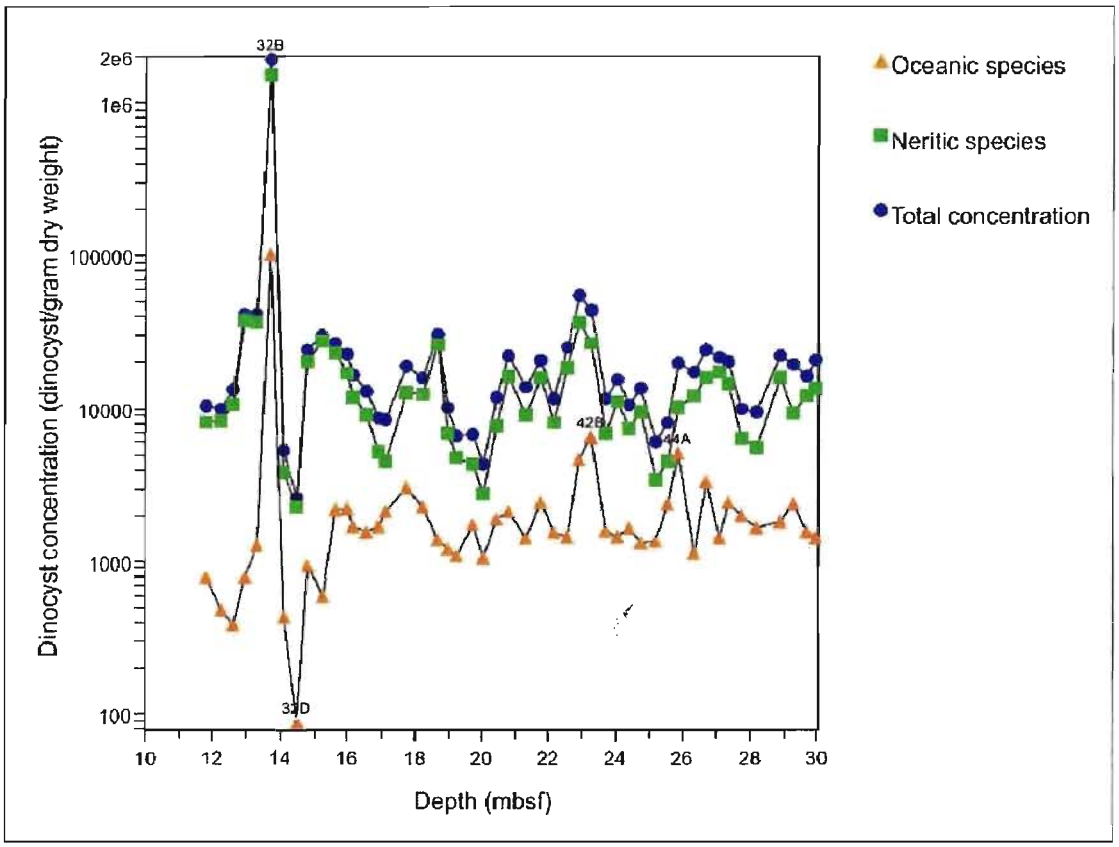

Figure 29. [10]Log plot of oceanic, neritic, and total dinocyst concentrations for DSDP Hole 603C.

The Shannon and Evenness indices show almost identical curves with three major dips (Figure 15; samples 35D, 42C and 46A) in the lower part of the interval studied and higher amplitude variation in the upper half of the interval. The fact that the dips are almost coeval indicates that these are periods of uneven species distribution rather than lower species diversity. The coincidence of these three events with the three major peaks for *C.? invaginata* is expected considering that both dinocysts and acritarchs were considered in the descriptive statistics. They can also be correlated with lower O/N and P/D values. A series of secondary dips can also be identified for both the Shannon and Evenness indices (samples 31D, 33B, 41B, 43C). The first two dips correspond to the highest values for the N/O index, corresponding respectively to peak intervals for *F. filifera* (66 %) with subdominant *T. pellitum* and *O. israelianum*. The third secondary dip in the Shannon and Evenness indices corresponds to the first important dip in the surface $\delta^{13}C$ signal and the highest count for *P. zoharyi* (52 %). The final secondary Shannon and

Evenness dip falls in the middle of an interval of low temperature estimates (Mg/Ca), on the downside of a major O/N peak.

Chapter 8 – Interpretations

8.1 Main paleoenvironmental events

When comparing the three paleo-temperature zones determined with Mg/Ca thermometry (Figure 9) with the assemblage zones from constrained cluster analysis (Figure 22), we see that AZ1 and AZ2 are grouped together and the upper part of AZ3 is grouped with AZ4 (Figure 30). The integration of these two proxies allows us to define our main paleoenvironmental zones (PEZ1 – 3). The boundaries between these paleoenvironemental events are not entirely reflected in the different statistical analyses; this section will be dedicated to determining why.

8.1.1 PEZ1

During PEZ1 (samples 46D to 41C) annual SST witnessed temperature amplitude variations of 6.2°C. The abundance (up to 30–40%) of *P. zoharyi* indicates that the spring–summer temperatures near the site were tropical to subtropical.

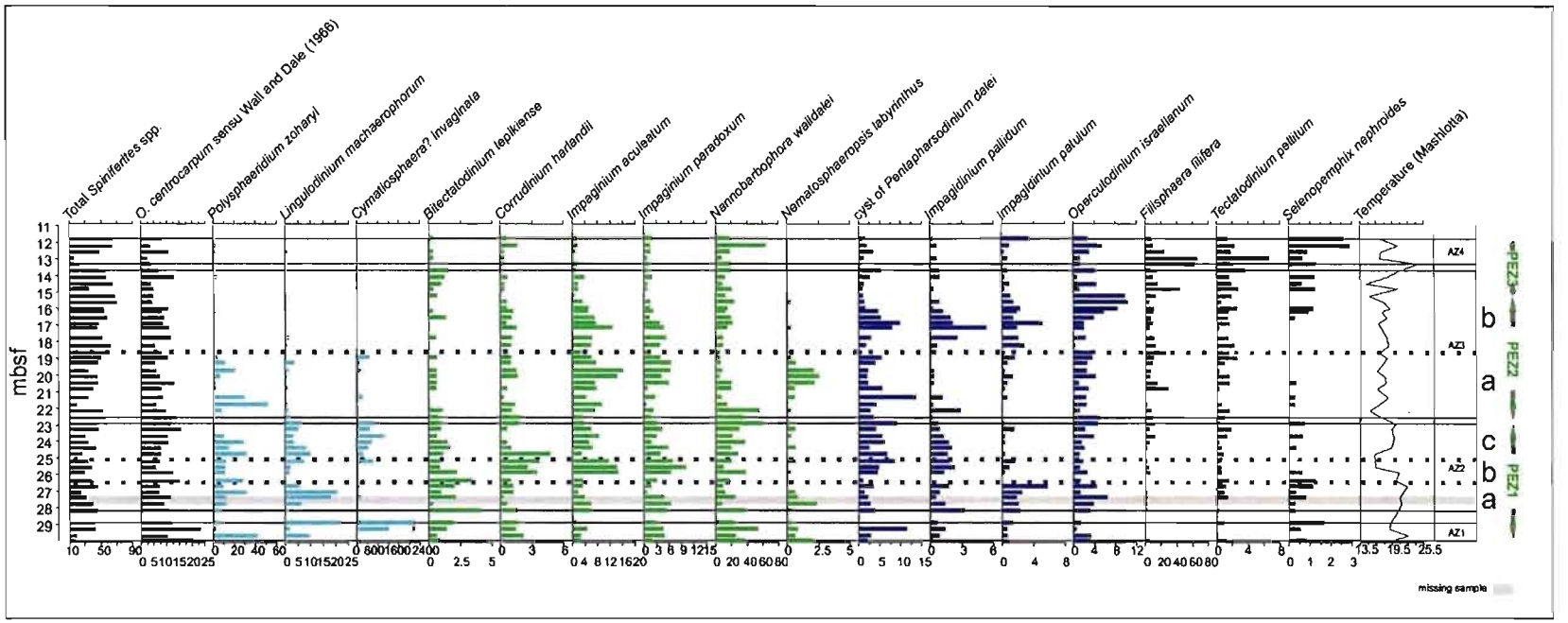

Figure 30. Main paleoenvironmental events as defined by the more abundant dinocyst and acritarch taxa as well as temperature (°C) estimated from the planktonic foraminiferal Mg/Ca ratios. All dinocyst species are in percentages. All the acritarch species are in raw counts. The color coding is the same as for Figure 8.

Constrained cluster analysis separates the last four samples (AZ1: samples 46D–46A) into a separate group. Evenness is highly variable in this zone due to the highest count for *C.? invaginata* in sample 46A. Richness, however, remains almost unchanged (39 to 40 species over 5 kyr). The separation between AZ1 and AZ2, as determined by the constrained cluster analysis, might be a result of the unusually large sampling distance. The missing sample indicated in Figure 30 is located between samples 45A (603C – 4 – 5; 17.5 – 19 cm at 27.375 mbsf) and 45B (4 – 5; 57.5 – 59 cm at 27.775 mbsf) at 27.69 mbsf (4 – 5; 49 – 51 cm). The distance between these two samples is smaller (40 cm) than the distance between the end of AZ1 (46A) and the beginning of AZ2 (45C) (71 cm), despite the missing sample between them. Furthermore, *C.? invaginata* values drop from over 2000 (sample 46A) counts to 12 (sample 45C). However, an additional sample between 46A and 45C might have shown a more gradual decline than observed and thus perhaps no statistical difference would then exist between AZ1 and AZ2.

AZ2 (samples 45C to 42A) represents all but the lower part of PEZ1 and contains long periods of stability with high amplitude variations which are identified by both the dinocysts (AZ2a – c) and the planktonic foraminifera (Figure 30).

In AZ2a (samples 45C to 44C), the combination of higher percentages of *P. zoharyi* (between 6 and 30%), higher P/D values, more reworked specimens and round brown cysts, suggest that this material was transported from a near-shore location with overall warm to tropical conditions. Surface $\delta^{13}C$ values remain stable, surface $\delta^{18}O$ values are slightly variable but remain above 0.5‰, and the species distribution for this subzone is relatively even.

P. zoharyi is an inner-neritic tropical to subtropical extant species, and one of the best indicators of very warm surface waters in the studied interval of Hole 603C. Highest abundances (>20%) occur today where summer sea-surface temperatures are above 25°C (Edwards and Andrle, 1992). This species has been found to tolerate high salinities, e.g. in lagoons on the Bahama Islands with salinities ranging from 37 to 42 psu, and in the Persian Gulf with salinities in excess of 40 psu (Head and Westphal, 1999 and references

therein), as well as elsewhere (Marret and Zonneveld, 2003 and references therein). However, it is also capable of tolerating subnormal salinities (Head and Westphal, 1999). The neritic affinity of this species implies that it has been transported to Site 603. This would explain the planktonic foraminiferal Mg/Ca temperatures of between 16 and 23°C in this interval of high *P. zoharyi* values. It might also be noted that paleotemperature proxies for the James City Formation of the Plio-Pleistocene of Atlantic Coastal Plain, which is just on-shore from Hole 603C, are at variance; with maximum temperatures of 25 to 27.5 °C for the ostracodes (Hazel, 1988) but only 20.7°C for the mollusks (Krantz, 1990). One of the possible explanations proposed was a situation of hypersalinity, which could produce the isotopic composition indicated by the ostracodes. This hypothesis was rejected for two reasons: firstly that the salinity would need to be ~40 psu, and secondly, sedimentological evidence indicated an open-shelf system with moderate to high wave and current enegy, arguing against restricted circulation and hence hypersalinity. However, the high abundance of *P. zoharyi*, in this and in subsequent zones of DSDP Hole 603C, up to 52%, perhaps allows for a situation of hypersalinity at least in inner neritic areas. The final conclusions drawn by Krantz (1990) from the discrepancy between the mollusks and ostracode temperatures was that the samples analyzed were collected from different horizons, thus representing different parts of the transgressive-regressive cycle. However, the presence of an additional tropical indicator (*P. zoharyi*) suggests that the shelf conditions for the James City Formation were perhaps quite complex.

Subzone AZ2b (samples 44C to 43B) shows a small drop in the annual SST based on Mg/Ca (down to 16°C from 20°C between samples 43D and 43B) coinciding with lower *P. zoharyi* values, higher values for oceanic/oligotrophic species (*I. aculeatum* and *I. paradoxum*), a first peak in surface $\delta^{13}C$ values and the highest values for the enigmatic *C. harlandii* (almost 5%). Offshore transport (pollen and reworked dinocysts) also drops, as do values for protoperidinioid species (round brown cysts and *S. nephroides*). The distribution of this subzone is a little offset in the CCA with sample 43B already plotting towards higher temperature values. Samples 44D to 43C plot quite clearly along the O/N axis, with samples 44A to 43C showing the highest percentages in oceanic/oligotrophic

species (20 to almost 30%). These high percentages of oceanic/oligotrophic species within samples 44A to 43C qualify them as the most oceanic of the studied interval of Hole 603C. This event also coincides with secondary dips for the Shannon and Evenness indices and a dip in the total concentration of dinocysts per sample.

Assuming that lower surface $\delta^{13}C$ values are an indication of nutrient-rich and hence $\delta^{12}C$-enhanced waters (Ahmad et al., 2009), then the opposite is plausible: $\delta^{12}C$-depleted, nutrient deficient waters would account for the more important presence of oligotrophic species, thus higher O/N values. The reduced amount of offshore transport suggests that $\delta^{12}C$-depleted, nutrient deficient waters were oceanic in origin, thus reducing transport to this site from the continental shelf. In addition, the similarity of the total *Impagidinium* species signal with the surface $\delta^{13}C$ signal, with almost identical peaks, leads credence to the hypothesis that the $\delta^{13}C$-rich intrusions were most likely oceanic in origin.

The extremely reduced values of round brown cysts (RBC) and *S. nephroides* are also significant, especially when combined with lower diversity values. The extremely reduced protoperidinioid values suggests taphonomic/preservational processes, but the reduced abundance of terrestrial material and the almost synchronous planktonic $\delta^{13}C$ peak implies that something more complicated might be at work.

Little is known about the paleoecological requirements for *C. harlandii*, although Versteegh (1995) suggested that these were not among the environmental factors considered in the Singa section (SST – based on planktonic foraminifera taxonomy, N/O, W/C, Age, $\delta^{18}O$ – based on *G. ruber* and sea-surface productivity – also based on planktonic foraminiferal taxonomy). Constraints determined from the present study tentatively suggest a preference for $\delta^{13}C$-enhanced surface currents with stable cooler conditions, since the subsequent surface $\delta^{13}C$ peak is coeval with high SST temperatures and does not record a similar *C. harlandii* peak. Furthermore *C. harlandii* is found to coexist with the cool tolerant *I. pallidum* which is also absent from the subsequent surface $\delta^{13}C$ peak.

The final subzone, AZ2c (samples 43A to 42A), represents a return to stable high annual SST values (19°C), lower O/N, and surface $\delta^{13}C$ values. The P/D ratio and protoperidinioid and reworked cyst values show a slight increase in number half way up this subzone and the richness index also increases. This subzone is also coeval with the second important peak in *C.? invaginata*. Other significant species of this subzone are *P. zoharyi* (almost 30%) and *F. filifera* (almost 10%). The more dominant oligotrophic species, i.e. *I. aculeatum* and *I. paradoxum*, as well as *C. harlandii*, are less abundant than during subzone AZ2b. The simultaneous occurrence of warm annual SST and the peak for *C.? invaginata* supports the notion that this is not a cold-water species, even though its geographical distribution in the Pliocene and lower Pleistocene was largely restricted to higher northern latitudes. Temperature is evidently not the only factor controlling its distribution.

Episodic occurrences of abundant *C.? invaginata* in southern Labrador Sea ODP Site 647 have been linked to inputs from intensified flow of the Labrador and East Greenland currents and possibly ice-rafted detritus (de Vernal and Mudie, 1992). However, at eastern Labrador Sea ODP Site 646, slightly to the northwest of ODP Site 647, *C.? invaginata* is regularly abundant through most of the Zanclean and throughout the Piacenzian except for the very top where abundance diminishes (de Vernal and Mudie, 1989; de Vernal and Mudie, 1992). The final disappearance of this species appears to be within the upper part of the Olduvai Subchron (De Schepper and Head, 2008, 2009), which corresponds to the interval of the present study. No distinct oceanic or climatic correlation could be linked to the significant numbers found in this study. However, considering the continued high counts down-core (M. J. Head, unpub. data), the extremely high but fluctuating numbers of *C.? invaginata* in the lower part of the studied interval seem to represent a series of pulses of favourable contitions before the overall changing conditions in the North Atlantic caused the final extinction. A similar single important pulse around the Olduvai Subchron is recorded by De Schepper and Head (2008, 2009) in DSDP Hole 610A. Lowering temperatures seem to be implicated in the extinction, particularly given that the decline following the last important peak of *C.? invaginata* in Hole 603C coincides with a drop in temperatures derived from Mg/Ca

analysis at the top of PEZ1. It should also be noted that the last important peak of *C.? invaginata* in Hole 603C is almost coeval with the last fairly abundant peak of *P. zoharyi* (21%). The cooling of the neritic environments, or the change in the source of the neritic signal, as indicated from the transition of the domimant neritic species from *P. zoharyi* to *F. filifera*, and thus enabling the dominance of the latter at DSDP Hole 603C, seem to have been detrimental to *C.? invaginata.*

8.1.2 PEZ2

During PEZ2 (samples 41C to 33B), low-amplitude annual temperature variations of up to 2.4°C occur. During this weakly variable annual SST zone, two significant O/N peaks can be seen, preceded by the juxtaposition of a $\delta^{13}C$-depleted and $\delta^{18}O$-depleted event. Furthermore, the previously abundant *P. zoharyi* (50%) is replaced by increasing numbers of *F. filifera* (5–30%).

This first $\delta^{13}C$-dip (samples 41D to 37A, at the bottom of AZ3) is juxtaposed against a small dip in $\delta^{18}O$. Events with this geochemical signature have been linked by Knies et al. (2007) to Arctic freshwater pulses in the northern North Atlantic at ODP Site 910 during the latest Pleistocene. Among the more significant dinocyst occurrences during this 9-kyr period, is an important peak in *P. zoharyi* (53% of the total assemblage) and the highest *Impagidinium* index values, at 51–87. The combination of abundant tropical to subtropical *P. zoharyi* and the high II values indicates warm winter and spring-summer conditions. This contrasts with the planktonic foraminiferal Mg/Ca signal, which registers among the lowest temperatures (15.29°C) for the studied interval of Hole 603C. Freshwater pulses from the Arctic Ocean would most likely have limited impact on a site as far south as Hole 603C, although these freshwater discharges have also been linked to decreases in NADW formation, which would most certainly have an impact on most of the Atlantic basin.

In addition, records for increased meltwater runoff from the Laurentide Ice Sheet are found in the Gulf of Mexico, starting at 2 Ma (Balco and Rovey II, 2010). Of two

possible sources of freshwater discharge provoking a simultaneous $\delta^{13}C$ and $\delta^{18}O$ decline, only a freshwater discharge originating from the Laurentide Ice Sheet involves the immediate vicinity of the western North Atlantic, as opposed to an Arctic discharge. The alternative hypothesis involves a much larger area of impact with these isotopic anomalies, corresponding Mg/Ca values and the dinocyst component not responding directly to the Arctic meltwater discharge but rather to a momentary interruption or slowing of the NADW. Benthic $\delta^{13}C$ and $\delta^{18}O$ from the eastern North Atlantic Feni and Gardar Drifts and the central North Atlantic ODP Site 607 have been interpreted by McIntyre et al. (1999) to reflect continued influence of overflow waters from the Nordic Seas, between 2.0 and 1.7 Ma, with circulation of the NADW present during the interglacial periods from 1.9 to 1.4 Ma from the western to eastern basin of the North Atlantic.

One additional possibility exists when we link the geochemical anomalies with the coeval dip in the Sr/Ca signal. Low Sr/Ca ratios have been linked to riverine fluxes, hydrothermal input and carbonate dissolution (Tripati et al., 2009). Although the absence of a correlation between the Sr/Ca and the reworked dinocyst and P/D signals might seem incongruous at first, as all three should demonstrate the occurrence of near-shore transport, a closer examination of the types of environments usually linked to the use of Sr/Ca reveals rather interesting information. Glacial/interglacial $(Sr/Ca)_{sw}$ in Quaternary sediments have been linked to the chemical weathering and recycling of shelf carbonates at low sea levels (Martin, 1999). If we consider the Sr/Ca in a localized context, there are no carbonate shelves in the vicinity of the New Jersey continental shelf to erode. However, the simultaneous presence of *P. zoharyi* with the largest trough in the Sr/Ca signal (1.317 mmol/mol, from an average of 1.418 mmol/mol) does allow for the situation of increased deposition of reef carbonates, which have also been linked to Sr/Ca decreases (Martin et al., 1999) somewhere nearby, despite the absence of evidence of more common vegetation related to reef deposition, such as mangroves, in sediments from the Atlantic Coastal Plains (Groot and Jordan, 1999).

The first O/N peak of AZ3 can be correlated to the second $\delta^{13}C$-rich event, which also coincides with an interval of high *N. labyrinthus* (samples 36D to 36B) and warm *Impagidinium* spp. counts, but is also almost devoid of protoperidinioids. This interval of 4 kyr plots at the lower end of axis 2 for DCCA. Once again, there is a slight offset in the CCA which is reflected in the constrained cluster analysis. In the CCA, samples 36C to 36A plot together along the O/N axis and are firmly centered at the II index, while in the constrained cluster analysis the three central samples, 36D to 36B, are clustered with the immediately neighboring samples, i.e. 37A and 36A. The most cool-water tolerant *Impagidinium* species, *I. pallidum*, is notably greatly reduced compared to the warm *Impagidinium* species during this interval.

In the context of the modern North Atlantic and adjacent seas (Rochon et al., 1999), *N. labyrinthus* has been linked to the mixing of cold Arctic waters from the East Greenland and Labrador currents with relatively warm North Atlantic waters, although Marret and Zonneveld (2003) offer a more cosmopolitan picture for this species. An increase in *N. labyrinthus* and warm *Impagidinium* species in the absence of the cool-tolerant *I. pallidum* may suggest that the $\delta^{13}C$-rich waters influencing Site 603 during these 4 kyr were possibly oceanic and tropical in origin, especially when compared to the previous $\delta^{13}C$-poor event that brought about abundances of *P. zoharyi*. Considering the modern context of Site 603, with the convergence of the Gulf Stream and the Slope Water, the intrusion of tropical waters would possibly not result in tropical conditions but rather, by the mixing with northern-sourced currents, in temperate conditions suitable for *N. labyrinthus* but unsuitable for *I. pallidum*.

Again, a taphonomic possibility must be considered. But, as was the case in AZ2, there are only small increases in the terrestrial indicators. Furthermore, here it is *N. labyrinthus* that emerges (2%), rather than *C. harlandii*, implying that the primary dinocyst signal is also at play here.

The end of the second O/N peak of AZ3 (samples 36A to 34B) is coeval with the moment when the terrestrial signal (P/D, reworked cysts, and RBC) starts to increase significantly,

as well as the Li/Ca signal. Subsequently, the oceanic component never reaches such high numbers. During the O/N peak, the protoperidinioids remain sparse and *N. labyrinthus* disappears once more. Both warm-water (*I. aculeatum* and *I. paradoxum*) and cool-water (*I. pallidum* and the cyst of *P. dalei*) species peak during this event. It is important to consider that the oceanic/oligotrophic species (e.g. *I. aculeatum*, *I, paradoxum*, *I. pallidum*) individually never reach more than 15%, in contrast with *P. zoharyi* (30%), *L. machaerophorum* (20%), or *F. filifera* (almost 70%), and hence they never represent the predominant signal for this site. However, the sum of the members of the genus *Impagidinium* during this peak do represent 24% of the assemblage, only second in magnitude to the surface $\delta^{13}C$-rich event during AZ3. Either of two questions is pertinent to this event: what was the reason for this resurgence in oceanic species; or why was there a momentary lull in the abundance of oceanic species between the two O/N peaks? The dip in the O/N signal corresponds to an interval of lowest values for Richness; it is also the last significant count for *C.? invaginata* (466 counts), which possibly correlates with other sites in the North Atlantic (ODP Sites 646 and 647). The lack of a distinct geochemical event occurring simultaneously to this O/N peak makes it more difficult to hypothesize the reason for its occurrence.

The possible correlation between DSDP Hole 603C and ODP Sites 646 and 647 introduces the defining factor for the end of AZ2 and the beginning of AZ1: the overabundant occurrence of *F. filifera*. The delay between the last important *C.? invaginata* event and the beginning of the abundant *F filifera* event can be estimated at 21 kyr, based on sedimentation rates. Similar delays can be observed between these two species at Labrador Sea ODP Sites 646 and 647 (de Vernal and Mudie, 1992) and in the central North Atlantic DSDP Sites 607 and 611 (Mudie, 1987), although the highest occurrence (HO) for *C.? invaginata* and the lowest occurrence (LO) for *F. filifera* are recorded for the Lower Pliocene at DSDP Site 611. Western North Atlantic ODP Hole 905A (de Verteuil, 1996) shows the records of the two species overlapping during the Pliocene, although de Verteuil recorded presence or absence, and not abundance. This delay between the disappearance of *C.? invaginata* and the beginning of *F. filifera* in

numerous North Atlantic and Labrador Sea sites, simultaneous with the O/N peak in Hole 603C, suggests a regional-scale significance for this event.

The difference in the position of the upper limit of PEZ2 and AZ3 seems to be controlled mainly by the abundance of *F. filifera*. At the bottom of PEZ3 *F. filifera* reaches an abundance of 44%, whereas at the bottom of AZ4 it reaches an abundance of 62%.

8.1.3 PEZ3

During PEZ3 (samples 33B to 31A), the higher occurrences for *F. filifera* (44%) begin when the temperature (Mg/Ca) amplitude begins to increase once again (sample 33A), with temperatures varying between 14.5 and 24.4 °C. The boundary between AZ3 and AZ4 is marked by a two-pronged dip in the surface $\delta^{13}C$ signal. The terrestrial signal remains mostly high during the period of high *F. filifera* values. The overabundance of this species limits the numbers of coexisting dinocysts in this period, making the presence of acritarch species all the more important and informative. *C.? invaginata* is significantly reduced from its previous high, only reaching 12 specimens. The only other significantly abundant acritarch species, *N. walldalei*, only reaches one-third of its highest values, at the AZ2 and AZ3 boundary (55 and 61 specimens) and in the sample immediately following the period of abundant *F. filifera* (63 specimens). Other species found with *F. filifera* are *O. centrocarpum* sensu Wall and Dale (1966), *O. israelianum*, *Spiniferites* spp., and the highest count for *T. pellitum* (up to 6%). *T. pellitum*, *L. machaerophorum*, and *P. zoharyi* have been used to track the retreat of late Cenozoic warm-waters into lower latitudes during glacial intervals (Dale and Dale, 1997; Head and Nøhr-Hansen, 1999). The abundance of *T. pellitum* in this interval of Hole 603C is usually not higher than one or two percent, and it is significant that during a period of extremely abundant *F. filifera* (68%) *T. pellitum* itself has relatively high abundance. The five dinocyst taxa that dominate PEZ3 are of neritic affinity, although the temperatures they imply are slightly different, especially *T. pellitum* and *F. filifera*. *F. filifera* is generally considered to be a cool-water or moderately cold-tolerant species (Matthiessen and Brenner, 1996; Head, 1996 and Mudie, 1987) since it is known mainly from the north

higher latitudes (Head, 1996 and references therein). *T. pellitum*, however, has a more south-temperate to sub-tropical distribution in the North Atlantic, Pacific, Mediterranean (Marret and Zonneveld, 2003; Wall et al. 1977). It seldom comprises more than 10% of the cyst assemblage (Edwards and Andrle, 1992; Head, 1997, Marret and Zonneveld, 2003), except in the Peruvian upwelling area where it represented 17% of the assemblage (Wall et al. 1977, appendix III). Marret and Zonneveld (2000) suggested that this high relative abundance could indicate an affinity for for mixed waters. The influence of neritic, estuarine-sourced waters, as suggested by a reduction in *Impagidinium* spp. values (11.8% from a previous high of 17.5%), is therefore supported within this zone by the Li/Ca signal and, possibly, by the absolute maximum values (6.5%), in this studied interval, for *T. pellitum*. Although specific applications of Li/Ca ratios with regards to planktonic foraminifera are not as widespread as Mg/Ca or Sr/Ca ratios, useful information can nonetheless be drawn from it. Li fluxes have been linked, in a study of Himalayan rivers (Kisakürek, 2005), to silicate weathering, and a similar linkage could well apply to the New Jersey continental shelf. The high values found during AZ4 for Li/Ca (0.323 mmol/mol from a mean value of 0.190 mmol/mol) as well as during short intervals coeval with high values for terrestrial proxies serves as support for the neritic or estuarine origin of the currents flowing over DSDP Site 603 during this time, and allowing these eutrophic/neritic species (*F. filifera*, *O. israelianum*, *T. pellitum*, and to a certain degree *P. zoharyi*) to thrive or perhaps simply to be carried to the site.

8.2 Glacial vs. interglacial taphonomy at Site 603

The age model used for Hole 603C is based on the position of the top of the Olduvai Subchron and the sedimentation rate determined from the duration of the Olduvai Subchron. When comparing the N/O signal of the present study with the Lisiecki and Raymo (2005) benthic stack, it is visually evident that these two curves fit geometrically (Figure 31), with troughs in the N/O signal (reduced values of neritic species) aligning well with global ice volume maxima (i.e., glacial episodes). Paradoxically, however, this relationship is opposite to that which might be expected. Rather, low global sea levels

(glacial episodes) would be expected to accelerate erosion on the shelf as well as bring the coastline towards the site of deposition, and thence deposit increasing quantities of shelf-derived sediment including neritic dinocysts (Figure 32).

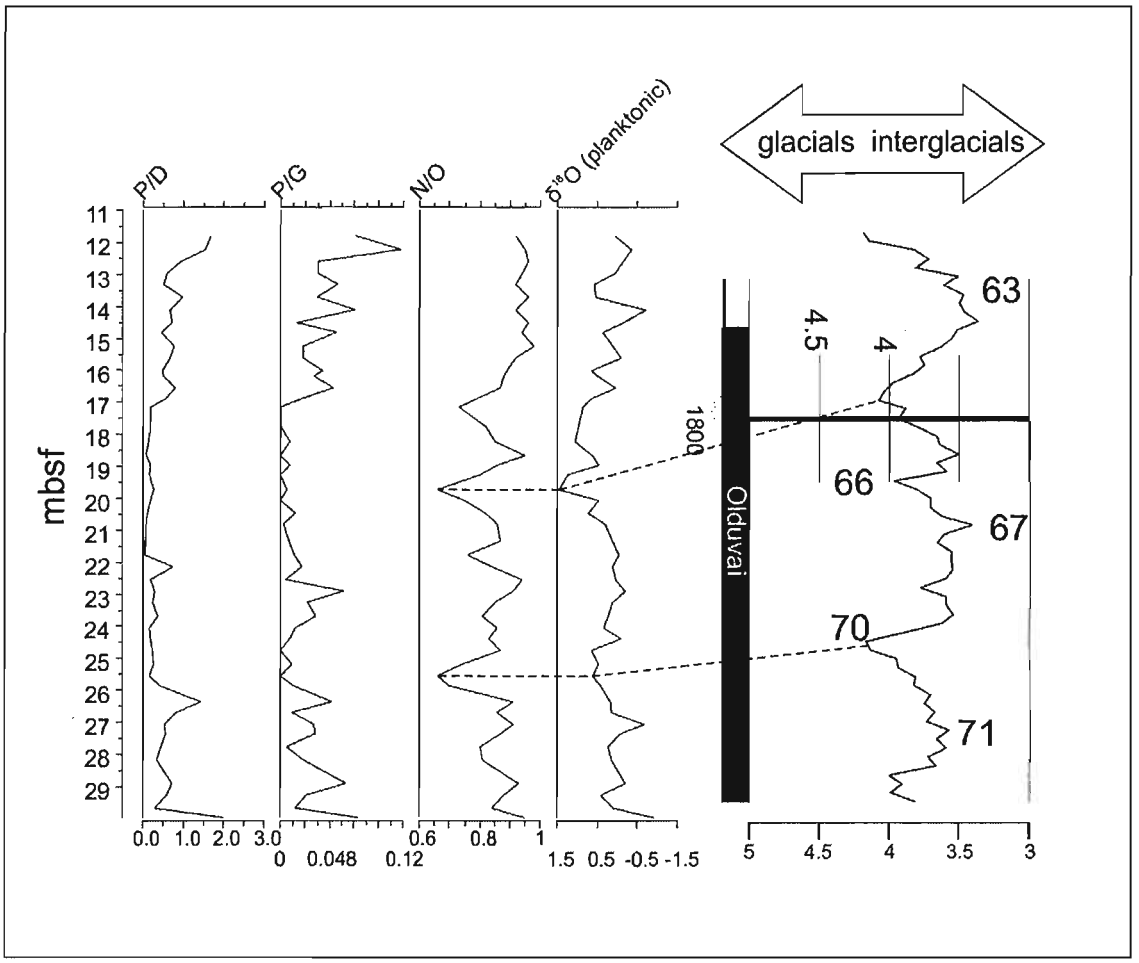

Figure 31. Correlation between the N/O (neritic/oceanic), P/G (protoperidinioid/gonyaulacoid) and P/D (pollen/dinocyst) signals and the Lisiecki and Raymo (2005) benthic stack, using the age model proposed for this study of DSDP Hole 603C.

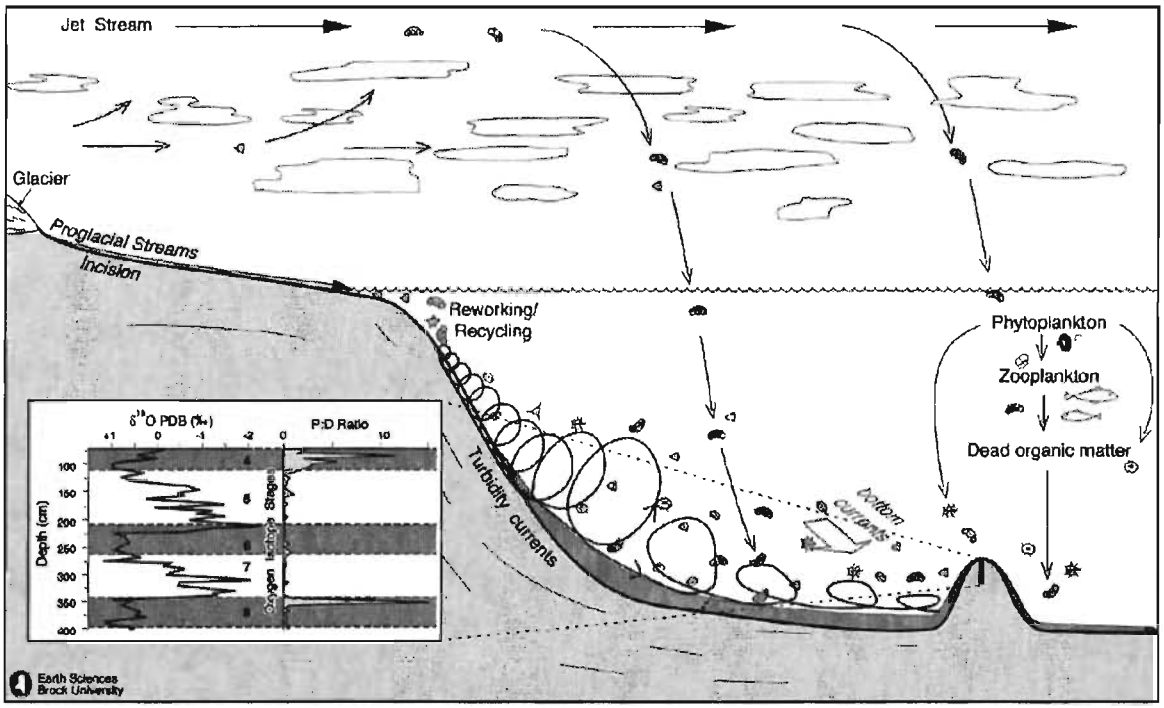

Figure 32. Idealized palynomorph behaviour for a passive margin during glacioeustatic lowstand. This example from McCarthy et al. (2004, fig. 1) illustrates the Early Wisconsin Stadial (MIS 4), with P/D peaks during the glacial events.

Downslope transport has been demonstrated by the combined presence of high P/D values and low P/G values (McCarthy et al., 2004). This situation is observed here with the strong positive correlation between the protoperidiniacean values (mainly represented by *S. nephroides* and *Lejeunecysta* spp.) and the P/D values, during neritic peaks. The periodic absence of protoperidinioids along with reduced P/D ratios during oceanic peaks, suggests that a factor additional to downslope transport-related oxidation has contributed to the taphonomic signal. In fact, the complete absence of protoperidinioids (including *S. nephroides*, Figure 31) combined with the lowering of the neritic component can be explained by the influence of the bottom-water DWBC, especially considering its role in the geological formation of the HOR, to which Site 603 is adjacent (Wise and van Hinte, 1987).

It is here postulated, therefore, that the neritic peaks aligned with peaks in terrestrial material, and partially-oxidized protoperidinioids are evidence of enhanced downslope transport to the site, as would be expected during a glacial interval. The oceanic peaks

(neritic troughs) aligned with extremely reduced P/D values and near absence of protoperidinioids are evidence of enhanced bottom-water oxidation brought on by the increased intensity of the DWBC, consistent with interglacial conditions. Thus sedimentation at Site 603 during the studied interval consists of an alternation of these two processes. Of course, slower sedimentation with reduced turbidite deposition is another obvious interpretation for enhanced oxidation (McCarthy et al., 2004).

The NADW is known to have a high oxygen content (Talley, 2002). Both it and the other components of the DWBC, which are carried from their source in the northern North Atlantic to the equatorial Atlantic, are more vigorous during interglacial than glacial intervals (Bhaumik and Giosan, 2007; Fagel et al., 1997; Chaisson et al., 2002). Indeed, this characteristic has been used to explain fluctuations in grain size in the lower Quaternary of Site 603 (Brew and Mayer, 1998). The near absence of protoperidinioids (and corresponding proportional increase in oxidation-resistant dinocysts; Zonneveld et al. 1997) during oceanic peaks are therefore consistent with both interglacial conditions and increased vigor of the NADW.

Given the internal consistency of data in the present study, its antiphase relationship with the global benthic stack of Lisiecki and Raymo (2005), namely that interglacials are aligning with glacials, suggests that a slight inaccuracy exists for the age model we have used based on the published position of the Olduvai Subchron.

Furthermore, we know that the HOR grew apace where the turbidity currents from the shelf were intercepted by the WBUC (Wise and van Hinte, 1987) during the Late Miocene. This situation is confirmed by the presence of a turbidite pond on the western side of the HOR (Wise and van Hinte, 1987; Figure 33) which was estimated to grow contemporaneously with the sediments from the HOR and at Site 603. It is therefore reasonable to assume that this current continued to have an influence even during the Quaternary, as with its impact on the western Atlantic BBOR and BR further south (Bhaumik and Gupta, 2007; Giosan et al., 2002; Chaisson et al., 2002; Franz and Tiedemann, 2002) which can be followed throughout the Quaternary. However, Brew

and Meyer (1998) using seismic data proposed that the turbidity currents did not spill over the HOR, and onto the lower continental rise and thus on DSDP Site 603, until the mid-Quaternary. With our data, we can propose that the palynomorph assemblages found in Hole 603C are evidence of deposition of fine sediment sourced by the shelf, at least as early as the Olduvai Subchron.

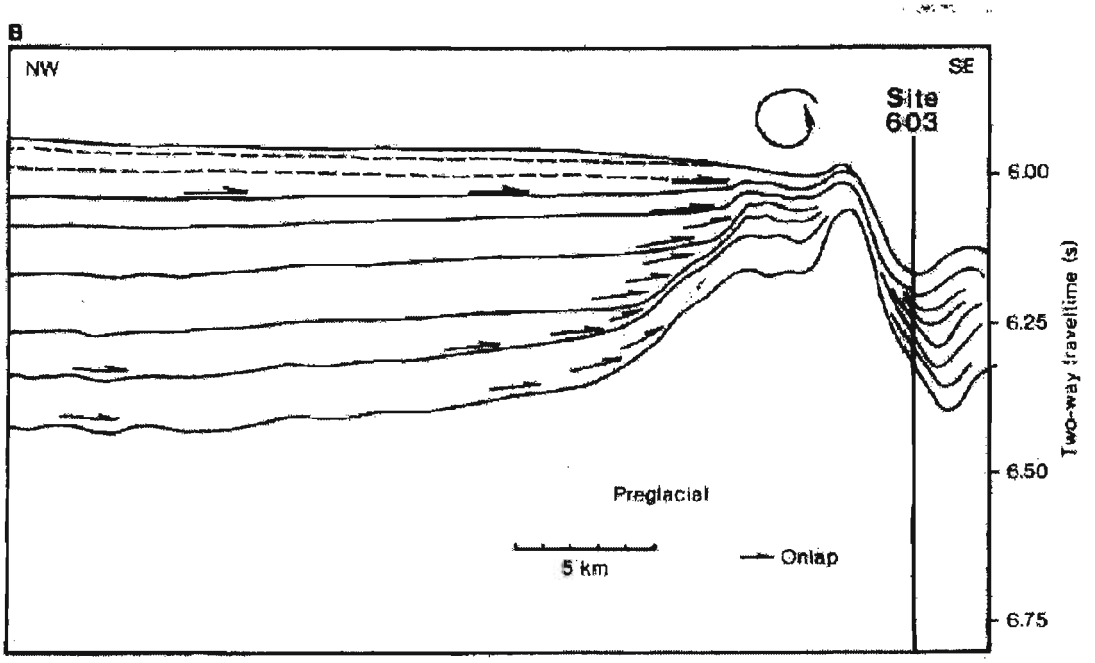

Figure 33 Interpretation based on the seismic reflection profile across Site 603 from DSDP Leg 93 showing the turbidite pond to the northwest and Site 603 to the southeast (from Wise and van Hinte, 1987, fig. 38). The coiled arrow indicates a side eddy that created the moat behind the ridge.

In this context of alternating down-slope deposition and bottom-water oxidation, the O/N peaks can indeed be qualified as oceanic events, in so much as the abundance of oxygen-resistant dinocysts reflects the augmented impact, or velocity (Brew and Meyer, 1998), of the WBUC (within the DWBC) on Site 603 and the remaining species distribution reflecting the more superficial current properties. Sedimentation rates during these O/N events must have been sufficiently low to ensure that all protoperidinioids were removed subsequently by the ongoing passage of the DWBC, as opposed to the partial removal from downslope transport during the N/O events.

8.3 Dinoflagellate cyst vs. foraminiferal occurrences

Ma'alouleh and Moullade (1987) noted an increase in the concentration of planktonic foraminifera (Ma'alouleh and Moullade, 1987, fig. 5) in zone PL6 sensu Berggren 1977 (ca. 2.05–1.9 Ma) of Hole 603C, which they attributed to a lowering of the carbonate compensation depth (CCD) at this time. Given the strong influence of downslope transport detected in the present study, this increase in concentration might instead be explained by the redeposition of sediments deposited higher on the shelf and thus above the CCD. If calcareous material is transported quickly through the CCD, for example by a turbidity current, it will not be as susceptible to dissolution as material settling through the water column. The top of the calcareous sequence might subsequently start to dissolve at the sea floor but as the water immediately above the sea floor becomes saturated any ensuing dissolution with be greatly decreased (Nichols, 2009). The foraminifera collected at Site 603 during the studied interval might therefore be, as is the case with the dinoflagellate cysts and acritarchs, of two sources. During the interglacial periods, the foraminifera would reflect in-situ conditions, while during glacial periods, the foraminifera along with the marine palynomorphs have been transported from the higher on the shelf.

Chapter 9 – Summary and Conclusions

A total of 48 samples mostly spanning the upper half of the Olduvai Subchron in DSDP Hole 603C were processed for benthic and planktonic foraminiferal geochemistry and marine palynomorphs, using a method that separates the two microfossil groups from the same sample (De Schepper et al., 2009). From these samples, 62 taxa of contemporary acritarchs and dinoflagellate cysts were found, including three species of undescribed acritarchs and four species of undescribed dinoflagellate cysts. These are documented in detail and named informally as Acritarch sp. A, B, and C, Dinocyst sp. A, *Impagidinium* sp. A, *Impagidinium* sp. B, and *Nematosphaeropsis* sp. A.

Elemental and isotopic analysis was performed on specimens of the planktonic foraminifera *G. bulloides* to produce annual sea-surface temperature estimates based on Mg/Ca ratios as well as surface $\delta^{18}O_{seawater}$ and $\delta^{13}C$ signals. Additional elemental analysis involving Li/Ca and Sr/Ca provided supplementary information of the paleoconditions of seawater at the time. Other less common isotopic and elemental analyses, such as surface $\delta^{13}C$, were used to determine paleoenvironmental controllers for fossil dinoflagellate cyst species such as *C. harlandii* and to expand the criteria used for paleoenvironmental analysis. Isotopic analysis was also conducted on benthic foraminifera but proved less effective due to the low abundance of specimens. This hindered one of this study's goals: to astronomically tune the studied interval by comparing it with the global benthic $\delta^{18}O$ Plio-Pleistocene stack of Lisiecki and Raymo (2005). The age model for this studied section was instead based on the sedimentation rate calculated from the positions of the top and base of the Olduvai Subchron as previously identified for Hole 603C (Canninga et al., 1987).

The dinoflagellate cyst assemblages of the studied interval comprise both neritic and oceanic species, including those of warm and cool-water affinities. Only a few taxa dominate the assemblages: *P. zoharyi*, *L. machaerophorum* and the acritarch *C.? invaginata* at the bottom of the section, and *F. filifera* at the top, with mostly constant percentages of *Spiniferites* spp. and *O. centrocarpum* sensu Wall and Dale (1966) throughout. *Impagidinium* spp. occupy at most 30% of the assemblage in different parts of the studied section. The assemblages have been analyzed statistically to reveal information about the paleoenvironments represented and the paleoecological affinities of individual dinoflagellate cyst species. Despite clear evidence of downslope transport at this site, especially in the lower and upper portions of the studied interval, information about sea-surface conditions was extracted from the samples. These appear to be consistent with other paleoenvironmental proxies. The palynological signals and geochemical proxies appear to show variability at the Milankovitch level of cyclicity but are difficult to reconcile with the global stack of Lisiecki and Raymo (2005), owing either to a strong taphonomic overprint or a problem with the age model.

9.1 Age model

A scarcity of specimens of the benthic foraminiferal species *U. peregrina* and *C. wuellerstorfi* (only 62.5% of the samples had sufficient specimens to produce a measurement) is consistent with the poor concentration of benthic foraminifera in Hole 603C as described by Blanc-Vernet and Moullade (1987). The age model proposed for the studied section is therefore based on the sedimentation rate calculated from the positions of the top and base of the Olduvai Subchron (Canninga et al., 1987). These positions are somewhat imprecise as they were recorded only graphically in the original publication (Canninga et al., 1987, fig. 6). Analyses are presently underway to re-measure the magnetic polarity of the studied interval in order to pinpoint the position of the top of the Olduvai Subchron. It should also be understood that while the age model assumes a constant sedimentation rate, the reality must have been different in detail, with higher sedimentation rates presumably occurring during glacial stages. Notwithstanding these limitations, our age model places the top of our studied interval at 1.771 Ma and the base at 1.866 Ma.

9.2 Geochemistry

Of the numerous isotopic and elemental analyses performed on the planktonic foraminifera, only Mg/Ca, Li/Ca, Sr/Ca, $\delta^{18}O$ and $\delta^{13}C$ were examined in detail in this study.

Paleothermometry from Mg/Ca was calculated using both the Mashiotta (1999) and Elderfield and Ganssen (2000) calibrations, yielding similar results, with maximum and minimum values for each calibration within ±1°C of each other. Three paleotemperature zones (PTZ 1–3) were visually estimated for the length of the studied interval. On either end, PTZ1 (samples 46D to 41C) and PTZ3 (samples 33B to 31A) show high temperature values (22.5° and 25°C) alternating with lower temperature values, for a total amplitude

of almost 10°C. In the middle, PTZ2 (samples 41C to 33B) shows an overall lower mean temperature and lower amplitude (one to two degrees).

By calculating the temperature using Mg/Ca, it was also possible to calculate planktonic $\delta^{18}O_{seawater}$, a proxy dependent partly upon global ice volume. The overall curve resembles that of the Mg/Ca-temperature values, although some differences can be distinguished. Two negative troughs (glacial) are interspaced with a shorter positive peak (interglacial) and followed by a period of high isotopic variability.

The planktonic $\delta^{13}C$ curve shows a distinct signal, different from both the Mg/Ca-temperature curve and the $\delta^{18}O_{seawater}$ curve. It presents an overall trend of upward decrease with two peaks and two troughs along the length of the studied interval.

Although neither the Li/Ca nor the Sr/Ca signals show high amplitude changes, their comparison with other proxies (abundance of certain dinocysts – *P. zoharyi* and reworked dinocysts) help to refine interpretations.

The location of the glacial and interglacial events as estimated by $\delta^{18}O_{seawater}$ supports the depositional hypothesis for the studied interval of Hole 603C, as do the higher values of Li/Ca. Although the $\delta^{13}C$ and Sr/Ca signals do not contribute considerably to the overall story, their inclusion in the present study provides interesting insight into the paleoenvironmental controllers for such species as *C. harlandii* and *P. zoharyi.*

9.3 Paleoclimatic events

Detailed statistical analyses of the palynological data enable the discrimination of four assemblage zones (AZ1–4; Figure 8). By integrating the geochemical data with these assemblage zones, three paleoenvironmental zones (PEZ1–3, Figure 30) are recognized. Based on this integration, a summary now follows.

A warm interval at the base of the studied interval (PEZ1 and the lower third of PEZ2; 1.862–1.819 Ma) is characterized by the presence of high numbers of the warm-water neritic *L. machaerophorum* alternating with the tropical–subtropical *P. zoharyi*. The simultaneous occurrence of moderately oxidized protoperidinioids and terrestrial material (pollen grains and reworked dinoflagellates cysts) indicates active downslope transport (presumably of turbiditic origin) for these neritic dinoflagellate cyst species (McCarthy et al., 2004) resulting in increased evidence of silicate weathering, as suggested by the higher Li/Ca values. During this period of strong tropical–subtropical neritic influence, two events can be distinguished from the planktonic geochemical signal. The first, at 1.836 Ma, is a cool oceanic-sourced event characterized by a peak in the surface $\delta^{13}C$ signal, up to almost 30% of *Impagidinium* species, and the highest abundance of *C. harlandii* in the entire studied interval. The significantly reduced ratio of protoperidinioids and terrestrial material during this event suggests an almost exclusively oceanic deposition with limited neritic influence. The second event, at 1.823 Ma, is defined by a simultaneous dip in the surface $\delta^{13}C$ and the Sr/Ca signals, accompanied by the highest peak for *P. zoharyi*. This second event, representing increased carbonate deposition as indicated by the strontium deficit, and most favorable for the growth of the tropical–subtropical *P. zoharyi*, was possibly linked to upwelling.

The upper half of the studied interval (the upper two-thirds of PEZ2 and PEZ3; 1.819–1.771 Ma) shows a transition from tropical–subtropical conditions on the shelf to cooler conditions, as shown by the disappearance of *P. zoharyi* in favor of the cool-tolerant *F. filifera*. These two species do not show a statistically significant overlap in the studied interval, unlike that observed subsequently on the New Jersey continental shelf (ODP 1072; McCarthy, pers. comm.). The dominance of *F. filifera* during the upper half of this interval is momentarily interrupted by two oceanic events. Although the first oceanic event can be linked to the second surface $\delta^{13}C$ peak as well as a peak for *N. labyrinthus*, the second cannot. Numbers of reworked cysts and for the P/D ratio remain low during both oceanic events; as does the lithium component, when compared to the *F. filifera*-rich zone during PEZ3, indicating reduced offshore or silicate fluvial transport. This interpretation fits well with the variable values for the protoperidinioid cysts and

terrestrial material. Increased numbers of these two proxies, as well as increased values for Li/Ca, during the *F. filifera*-rich periods suggests downslope transport, much like that associated with most of the *P. zoharyi* signal. The extremely reduced numbers of round brown cysts and terrestrial material during the oceanic events also suggests, as was the case in the lower half of PEZ2, a more bottom-water current controlled environment that will have facilitated the removal of sensitive cysts through oxidation. The first oceanic event, coeval with the surface $\delta^{13}C$ peak, was possibly warmer than the previous one, resulting in temperate mixed waters, due to the almost complete absence of the cold-water tolerant *I. pallidum*. The origin of the second oceanic event, which does not have a visible equivalent in the geochemical signals, is more difficult to hypothesize, but the highest count for *I. pallidum* (12%) suggests a cooler source.

9.4 The upper Olduvai Subchron of Site 603 within the western North Atlantic

Enhanced bottom-water circulation in the western North Atlantic is suggested by Giosan et al. (2002) as probable cause for the increase in hematite and sedimentation rates in the BBOR and BR between 1.8 and 1.6 Ma, despite previously suggested sluggish deep water circulation (Giosan et al., 2002; and references therein). Dinocyst assemblages at Site 603 suggest that these bottom-water events did not in fact occur as one, but rather as pulses.

The overall cooling trend observed in this studied interval from Site 603 fits well within the context of the North Atlantic and the coastal plains of eastern North America at the time. Pronounced cooling is suggested from the southern Norwegian-Greenland Sea ca. 1.7 Ma (Lawrence et al., 2009) and hiatuses related to cold climate periods are observed within the Gelasian Omar Formation in Delaware (Groot and Jordan, 1999) as well as between the lower James City and Waccamaw Formations in North and South Carolina and the upper James City and Waccamaw Formations (Ward et al., 1991). The dinocyst

assemblages at Site 603 suggest that the transition towards a cooler period, for the North Atlantic off the coast of New Jersey, started as early as 1.819 Ma.

9.5 Biostratigraphy

The following five dinoflagellate cyst taxa are reported from the mid-latitude western North Atlantic for the first time: *S. ludhamensis*, *O. eirikianum* var. *crebrum*, *A. zevenboomii*, *C. lata*, and the cyst of *P. stellatum*. The only other record of *S. ludhamensis* is from deposits of similar age from the North Sea basin (Head, 1996). Similarly, the only other record for *O. eirikianum* var. *cerebrum* is located in slightly older sediments from eastern North Atlantic DSDP Hole 610A (De Schepper and Head, 2008). The Atlantic Ocean fossil records for *C. lata* and *A. zevenboomii* are somewhat similar, as both species have been found in the tropics as well as in the North Sea Basin and in the eastern North Atlantic. The morphotype *Nematosphaeropsis* sp. cf. *N. labyrinthus* has so far been recorded only from Holocene sediments off Nova Scotia (Rochon et al., 1999). Cysts of *P. stellatum* are fairly widespread in the modern sediments, but have not been reported previously from deposits as old as the Olduvai Subchron. The presence of these two last species in Hole 603C therefore represent a downward extension of their stratigraphic range.

References

Full authorial citations of taxa mentioned in this paper are listed in the Appendix and follow De Schepper et al. (2004) and Fensome et al. (2004).

Ahmad, S. M., Babu, G. A., Padmakumari, V. M. and Raza, W., 2008. Surface and deep water changes in the northeast Indian Ocean during the last 60 ka inferred from carbon and oxygen isotopes of planktonic and benthic foraminifera. *Palaeogeography, Palaeoclimatology, Palaeoecology*, 262: 182–188.

Akers, W. H. 1972. Planktonic Foraminifera and biostratigraphy of some Neogene formations, northern Florida and Atlantic Coastal Plain. *Tulane Studies Geology and Paleontology*, 9(1–4): 139 p.

Antonov, J. I., Locarnini, R. A., Boyer, T. P., Mishonov, A. V. and Garcia, H. E. 2006. *World Ocean Atlas 2005, Volume 2: Salinity*. S. Levitus, Ed. NOAA Atlas NESDIS 62, U.S. Government Printing Office, Washington, D.C., 182 pp.

Aquirre, E., and Pasini, G. 1985. The Pliocene–Pleistocene boundary. *Episodes*, 8: 116–120.

Arthur, M., Srivastava, S. P., Kaminski, M., Jarrard, R. and Osler, J. 1989. Seismic stratigraphy and history of deep circulationand sediment drift development in the Baffin Bay and the Labrador Sea, p. 957–988. *In*: Srivastava, S.P., Arthur, M., Clement, B., et al. (Eds.), *Proceedings of the Ocean Drilling Program, Scientific Results*, 105, Ocean Drilling Program, College Station, TX.

Ashley, G. M., Dominguez-Rodrigo, M., Bunn, H. T., Mabulla, A. Z. P., and Baquedano, E. 2010. Sedimentary Geology and Human Origins: A Fresh Look at Olduvai Gorge, Tanzania. *Journal of Sedimentary Research*, 80(8): 703–709.

Balco, Greg, and Charles W. Rovey II. Absolute Chronology for Major Pleistocene Advances of the Laurentide Ice Sheet. *Geology* 38.9 (2010): 795-8.

Barker, S., Greaves, M. and Elderfield, H. 2003. A study of cleaning procedures used for foraminiferal Mg/Ca paleothermometry, *Geochemistry. Geophysics. Geosystems*, 4, 8407, doi:10.1029/2003GC000559.

Berggren, W. A. 1977. Late Neogene planktonic foraminiferal biostratigraphy of the Rio Grande Rise (South Atlantic). *Marine Micropaleontology*, 2: 265–313.

Bhaumik, A. K. and Gupta, A. K. 2007. Evidence of methane release from Blake Ridge ODP Hole 997A during the Plio-Pleistocene : Benthic foraminifer fauna and total organic carbon. *Current Science*, 92 (2): 192–199.

Blackwelder, B. W. 1981. Late Cenozoic Stages and Molluscan Zones of the U. S. Middle Atlantic Coastal Plain. *Memoir (The Paleontological Society)* 12, Supplement to Vol. 55, no. 5 of the Journal of Paleontology: 1–34.

Blanc-Vernet, L. and Moullade, M. 1987. Distribution of late Neogene and Quaternary benthic foraminifers in the northwest Atlantic, Deep Sea Drilling Project Leg 93, sites 603 and 604, p. 473–480. *In* VAN Hinte, J. E., Wise, Jr., S. W. et al. (Eds.), *Initial Reports of the Deep Sea Drilling Project*, 93 (2). U. S. Government Printing Office, Washington, D. C.

Bower, A. S., and Hunt, H.D. 2000. Lagrangian observations of the deep western boundary current in the North Atlantic ocean. Part I: large-scale pathways and spreading rates. *Journal of Physical Oceanography*, 30: 764–783.

Brew, D. S. and Mayer, L. A. 1998. Modelling of Pliocene–Pleistocene abyssal mudwaves using synthetic seismograms. *Marine Geology*, 149: 3–16.

Bujak, J.P. 1984. Cenozoic dinoflagellate cysts and acritarchs from the Beiring Sea and northern North Pacific, DSDP Leg 19. *Micropaleontology*, 30 (2): 180–212.

Bulfinch, D., and Ledbetter, M. 1984. Deep Western Boundary Undercurrent delineated by sediment texture at base of North American continental rise. *Geo-Marine Letters*, 3 (1): 1–36.

Canninga, G., Zijderveld, J. D. A. and VAN Hinte, J. E. 1987. Late Cenozoic magnetostratigraphy of Deep Sea Drilling Project Hole 603C, Leg 93, on the North American continental rise off Cape Hatteras, p. 839–848. *In* VAN Hinte, J. E., Wise, Jr., S. W. et al. (Eds.), *Initial Reports of the Deep Sea Drilling Project*, 93 (2). U. S. Government Printing Office, Washington, D. C.

Chaisson, W. P., Poli, M.- S. and Thunell, R. C. 2002. Gulf Stream and Western Boundary Undercurrent variations during MIS 10–12 at Site 1056, Blake-Bahama Outer Ridge. *Marine Geology*, 189: 79–105.

Chapman, M. R. 2000. The response of planktonic foraminifera to the Late Pliocene intensification of Northern Hemisphere Glaciation, p. 79–95. *In*: Culver, S. J. and Rawson, P. F. (Eds.), *Biotic Response to Global Change: The last 145 Million Years.* Cambridge University Press.

Chapman, P. 1999. Global ocean currents, p. 303–307. *McGraw-Hill Yearbook of Science and Technology,* 2000.

Chmura, G. L. Smirnov, A. and Campbell, I. D. 1999. Pollen transport through distributaries and depositional patterns in coastal waters. *Palaeogeography, Palaeoclimatology, Palaeoecology*, 149: 257–270.

Cronin, T. M., Bybell, L. M., Poore, R. Z., Blackwelder, B. W., Liddicoat, J. C. and Hazel, J. E. 1984. Age and correlation of emerged Pliocene and Pleistocene deposits,

U.S. Atlantic coastal plain. *Palaeogeography, Palaeoclimatology, Palaeoecology*, 47: 21–51.

Csanady, G. T., and Hamilton, P. 1988. Circulation of Slopewater. *Continental Shelf Research*, 8: 565–624.

Dale, B and Dale, A. 1997. *Environmental controls on the evolution of cyst-forming dinoflagellates*. American Assiciation of Stratigraphic Palynologists, 30th Annual Meeting, Woods Hole, MA (Abstract).

Dale, B. and Dale, A. 2002a. Application of ecologically based statistical treatments to micropaplaeontology, p. 259–286. *In*: S. K. Haslett (Editor), *Quaternary Environmental Micropalaeontology*, Arnold, London.

Dale, B. and Dale, A. 2002b. Environmental application of dinoflagellate cysts and acritarchs, p. 207–239. *In*: S. K. Haslett (Editor), *Quaternary Environmental Micropalaeontology*, Arnold, London.

Dale, B., Dale, A. and Jansen, J.H.F. 2002. Dinoflagellate cysts as environmental indicators in surface sediments from the Congo deep-sea fan and adjacent regions. *Palaeogeography, Palaeoclimatology, Palaeoecology*, 185: 309–338.

deMenocal, P. B. 2004. African climate change and faunal evolution during the Pliocene-Pleistocene. *Earth and Planetary Science Letters*, 220: 3–24.

De Schepper, S. 2006. *Plio-Pleistocene dinoflagellate cyst biostratigraphy and palaeoecology from the eastern North Atlantic and southern North Sea Basin.* Unpublished PhD thesis: University of Cambridge, 327 pp, 6 app. & 23 pls.

De Schepper, S., Head, M.J. and Louwye, S. 2004. New dinoflagellate cyst and incertae sedis taxa from the Pliocene of northern Belgium, southern North Sea Basin. *Journal of Paleontology*, 78 (4): 625–644.

De Schepper, S. and Head, M.J. 2008. New dinoflagellate cyst and acritarch taxa from the Pliocene and Pleistocene of the eastern North Atlantic (DSDP Site 610). *Journal of systematic Palaeontology*, 6 (1): 101–117.

De Schepper, S. and Head, M. J. 2009. Pliocene and Pleistocene Dinoflagellate Cyst and Acritarch Zonation of Dsdp Hole 610A, Eastern North Atlantic. *Palynology*, 33: 179–218.

De Schepper, S., Head, M. J. and Groeneveld, J. 2009. North Atlantic Current variability through marine isotope stage M2 (circa 3.3 Ma) during the mid-Pliocene, *Paleoceanography*, 24, PA4206, doi:10.1029/2008PA001725.

de Vernal, A and Marret, F. 2007. Organic-walled dinoflagellate cysts: tracers of sea-surface conditions, p.371–408. *In*: Hillaire-Marcel, C. and de Vernal, A. (Eds.), *Proxies in Late Cenozoic Paleoceanography*. Elsevier, University of Montréal, Montréal, Québec.

de Vernal, A and Mudie, P.J. 1989, Pliocene and Pleistocene palynostratigraphy at ODP sites 646 and 647, eastern and southern Labrador Sea, p.401–422. *In*: Srivastava, S.P., Arthur, M. A., Clement, B., et al. (Eds.), *Proceedings of the Ocean Drilling Program, Scientific Results*, 105: College Station, Texas (Ocean Drilling Program).

de Vernal, A. and Mudie, P.J. 1992. Pliocene and Quaternary dinoflagellate cyst stratigraphy in the Labrador Sea: paleoenvironmental implications, p.329–346. *In*: Head, M. J., and Wrenn, J. H. (Eds), 1992, *Neogene and Quaternary Dinoflagellate Cysts and Acritarchs*: American Association of Stratigraphic Palynologists Foundation, Dallas.

de Verteuil, L. 1996. Upper Cenozoic dinoflagellate cysts from the continental slope and rise off New Jersey, p. 439–454. *In*: Mountain, G. S., Miller, K. G. and Blum, P. et al (Eds.), *Proceedings of the Ocean Drilling Program, Scientific Results*, 150: College Station, Texas (Ocean Drilling Program).

Edwards, L. E., Mudie, P. J. and de Vernal, A. 1991. Pliocene paleoclimatic reconstruction using dinoflagellate cysts: comparison of methods. *Quaternary Science Reviews*, 10: 259–274.

Edwards, L. E. 1992. New semiquantitative (paleo)temperature estimates using dinoflagellate cysts, an example from the North Atlantic Ocean, p. 69–87. *In*: Head, M. J., and Wrenn, J. H. (Eds.), *Neogene and Quaternary Dinoflagellate Cysts and Acritarchs*: American Association of Stratigraphic Palynologists Foundation, Dallas.

Edwards, L. E. and Adrle, V. A. S. 1992. Distribution of selected dinoflagellate cysts in modern marine sediments, p. 259–288. *In*: Head, M. J., and Wrenn, J. H. (Eds.), 1992, *Neogene and Quaternary Dinoflagellate Cysts and Acritarchs*: American Association of Stratigraphic Palynologists Foundation, Dallas.

Elderfield, H. and Ganssen, G. 2000. Past temperature and $\delta^{18}O$ of surface ocean waters inferred from foraminiferal Mg/Ca ratios. *Nature*, 405: 442–445.

Fagel, N., Hillaire-Marcel, C. and Robert, C. 1997. Changes in the Western Boundary undercurrent outflow since the Last Glacial Maximum, from smectite/illite ratios in deep Lebrador Sea sediments. *Paleoceanography*, 12: 79–96.

Fensome, R. A. and Williams, G. L., 2004. *The Lentin and Williams Index of fossil dinoflagellates, 2004 edition.* American Association of Stratigraphic Palynologists, Contributions Series, 42: 1–909.

Ferretti, M. P. 2007. Evolution of bone-cracking adaptations in hyaenids (Mammalia, Carnivora). *Swiss Journal of Geoscience*, 100: 1–12.

Fischer, E. and Head, M.J. 2008. *Late Pliocene dinoflagellate cysts from the Chillesford Church Pit, Suffolk, Eastern England.* Eighth International Conference on Modern and Fossil Dinoflagellates, Dino 8, Montreal, 4–8th May. (Poster)

Franz, S. O. and Tiedemann, R. 2002. Depositional changes along the Blake-Bahama Outer Ridge deep water transect during marine isotope stages 8 to 10 – links to Deep Western Boundary Current. *Marine Geology*, 189: 107–122.

Ganssen, G. 1987. Late Cenozoic stable isotopic stratigraphy, Deep Sea Drilling Project Sites 603 and 604, Northeast American continental rise, p. 997–1002. *In* van Hinte, J. E., Wise, Jr., S. W. et al. (Eds.), *Initial Reports of the Deep Sea Drilling Project*, 93 (2). U. S. Government Printing Office, Washington, D. C.

Gibbard, P., and Head, M.J. 2009a. The definition of the Quaternary System/Era and the PleistoceneSeries/Epoch. *Quaternaire*, 20(2): 125–133.

Gibbard, P.L. and Head, M.J. 2009b. IUGS ratification of the Quaternary System/Period and the Pleistocene Series/Epoch with a base at 2.58 Ma. *Quaternaire*, 20(4): 411–412.

Gibbard, P.L., and Head, M.J. 2010. The newly-ratified definition of the Quaternary System/Period and redefinition of the Pleistocene Series/Epoch, and comparison of proposals advanced prior to formal ratification. *Episodes*, 33: 152–158.

Gibbard, P.L., Head, M.J., Walker, M.J.C. and The Subcommission on Quaternary Stratigraphy, 2010. Formal ratification of the Quaternary System/Period and the Pleistocene Series/Epoch with a base at 2.58 Ma. *Journal of Quaternary Science*, 25(2): 96–102.

Giosan, L. Flood, R. D., Grützner, J and Mudie, P. 2002. Paleoceanographic significance of sediment color on western North Atlantic Drifts: II. Late Pliocene–Pleistocene sedimentation. *Marine Geology*, 189: 43–61.

Groot, J.J., Jordan, R.R. 1999. *The Pliocene and Quaternary deposits of Delaware: Palynology, Ages, and Paleoenvironments*. Report of Investigations No. 58. Delaware Geological Survey, 36 pp.

Gyory, J., Mariano, A. J. and Ryan, E. H., 2009. "The Gulf Stream." Ocean Surface Currents. 2009. http://oceancurrents.rsmas.miami.edu/atlantic/gulf-stream.html.

Harland, R. 1979. Dinoflagellate biostratigraphy of Neogene and Quaternary sediments at holes 400/400A in the Bay of Biscay (Deep Sea Drilling Project Leg 48), p. 531–45. *In* Montadert, L. Roberts, D. G. et al. (Eds.) *Initial Reports of the Deep Sea Drilling Project*, 48. Washington D.C.: U.S. Government Printing Office.

Hazel, J.E. 1988. Determining late Neogene and Quaternary palaeoclimates and palaeotemperature regimes using ostracods, p. 89–101. *In*: De Deckker, P., Colin, J. -P., and Peypouquet, J.-P. (Eds.), *Ostracoda in the Earth Sciences*: Elsevier, Amsterdam.

Head, M. J. 1993. Dinoflagellate cysts, sporomorphs, and other palynomorphs from the upper Pliocene St. Erth Beds of Cornwall, southwestern England. *Paleontological Society Memoir 31* (*Journal of Paleontology*, 67 [3] Supplement), 62p.

Head, M. J. 1996. Late Cenozoic dinoflagellates from the Royal Society borehole at Ludham, Norfolk, Eastern England. *Journal of Paleontology*, 70 (4): 543–570.

Head, M. J. 1997. Thermophilic dinoflagellate assemblages from the mid Pliocene of Eastern England. *Journal of Paleontology*, 71 (2): 165–193.

Head, M. J. 1998. Marine environmental change in the Pliocene and early Pleistocene of eastern England: the dinoflagellate evidence reviewed. *In* The Dawn of the Quaternary (eds. T. Van Kolfschoten and P. L. Gibbard). *Mededelingen Nederlands Instituut voor Toegepaste Geowetenschappen TNO*, 60: 199–226.

Head, M. J. 2000. *Geonettia waltonensis*, a new goniodomacean dinoflagellate from the Pliocene of the North Atlantic region, and its evolutionary implications. *Journal of Paleontology*, 74 (5): 812–827.

Head, M. J. 2007. Last Interglacial (Eemian) hydrographic conditions in the southwestern Baltic Sea based on dinoflagellates cysts from Ristinge Klint, Denmark. *Geological Magazine*, 144 (6): 987–1013.

Head, M. J. and Nøhr-Hansen, H. 1999. The extant thermophilic dinoflagellate *Tectatodinium pellitum* (al. *Tectatodinium rugulatum*) from the Danian of Denmark. *Journal of Paleontology*, 73 (4): 577–579.

Head, M. J., Norris, G. and Mudie, P.J. 1989. Palynology and dinocyst stratigraphy of the upper Miocene and lowermost Pliocene, ODP Leg 105, Site 646, Labrador Sea, p. 423–451. *In* S. P. Srivastava, M. A. Arthur, B. Clement, et al. (Eds.), *Proceedings of the Ocean Drilling Program, Scientific Results*, 105. Ocean Drilling Program, College Station, Texas.

Head, M. J. and Norris, G. 2003. New species of dinoflagellate cysts and other palynomorphs from the latest Miocene and Pliocene of DSDP Hole 603C, western North Atlantic. *Journal of Paleontology*, 77 (1): 1–15.

Head, M.J. and Westphal, H. 1999. Palynology and paleoenvironments of a Pliocene carbonate platform: the Clino core, Bahamas. *Journal of Paleontology*, 73: 1–25.

Head, M.J., Gibbard, P.L., and Salvador, A. 2008a. The Quaternary: its character and definition. *Episodes*, 31(2): 234–238.

Head, M.J., Pillans, B., and Farquhar, S. 2008b. The Early–Middle Pleistocene Transition: characterization and proposed guide for the defining boundary. *Episodes*, 31(2): 255–259.

Henrich, R., Baumann, K.-H., Huber, R. and Meggers. H. 2002. Carbonate preservation records of the past 3 Myr in the Norwegian-Greenland Sea and the northern North Atlantic: implication for the history of NADW production. *Marine Geology*, 184: 17–39.

Hogg, N., and Huang, R.X, Eds., *Collected Works of Henry M. Stommel*, vol. 2 (American Meteorological Society, Boston, 1995), pp. 307–709.

Hopkins, J. A. and McCarthy, F. M. G. 2002. Post-depositional palynomorphs degradation in Quaternary shelf sediments: a laboratory experiment studying the effects of progressive oxidation. *Palynology*, 26: 167–184.

Iselin, C. O'D., 1936. A study of the circulation of the western North Atlantic. *Papers in Physical Oceanography and Meteorology* 4, No. 4, MIT-Woods Hole Oceanographic Institution, 101 pp.

Juggins. S. 2007 C2 Version 1.5 User guide. *Software for ecological and palaeoecological data analysis and visualisation.* Newcastle University, Newcastle upon Tyne, UK. 73 pp.

Kelch, Dean G. 1997. The phylogeny of the Podocarpaceae based on morphological evidence. *Systematic Botany*, 22 (1): 113–131.

King, W.B.R., and Oakley, K.P. 1949. Definition of the Pliocene–Pleistocene boundary: *Nature*, 163: 186–187.

Kisakürek, B., James, R. H. and Harris, N. B. W. 2005. Li and δ^{17}Li in Himalayan rivers: Proxies for silicate weathering? *Earth and Planetary Science Letters*, 237: 387–401

Kovach, W. L. 2007. *MVSP – A Multivariate Statistical Package for Windows, ver. 3.1.* Kovach Computing Services, Pentraeth, Wales, U.K.

Knies, J., Matthiessen, J., Mackensen, A., Stein, R., Vogt, C., Frederichs, T. and Nam, S.I. 2007. Effects of Arctic freshwater forcing on thermohaline circulation during the Pleistocene. *Geology*, 35 (12): 1075–1078.

Krantz, D. E. 1990. Mollusk-Isotope Records of Plio-Pleistocene Marine Paleoclimate, U.S. Middle Atlantic Coastal Plain. *Palaios*, 5 (4): 317–335.

Lawrence, K. T., Herbert, T. D., Brown, C. M., Raymo, M. E. and Haywood, A. M. 2009. High amplitude variations in North Atlantic sea surface temperature during the early Pliocene warm period, *Paleoceanography*, 24, PA2218, doi:10.1029/2008PA001669

Lear, C.H., Elderfield, H. and Wilson, P.A. 2000. Cenozoic deep-sea temperatures and global ice volumes from Mg/Ca in benthic foraminiferal calcite. *Science*, 287: 269–272.

Lewis, J., Dodge, J. D. and Powell, A. J. 1990. Quaternary dinoflagellates cysts from the upwelling system offshore Peru, Hole 686B, ODP Leg 112, p.323–327. *In*: Suess, E., von Huene, R., et al. (Eds), *Proceedings of the Ocean Drilling Program, Scientific Results*, 112: College Station, Texas (Ocean Drilling Program).

Lisiecki, L. E. and Raymo, M. E. 2005. A Pliocene–Pleistocene stack of 57 globally distributed benthic δ^{18}O records, *Paleoceanography*, 20, PA1003, doi:10.1029/2004PA001071.

Liu, L. Maiorano, P., and Zhao, X. 1996. Pliocene–Pleistocene calcareous nannofossils from the Iberia Abyssal Plain, p. 147–164. *In*: Whitmarsh, R. B., Sawyer, D. S., Klaus, A., and Mason, D. G., et al. (Eds.), *Proceedings of the Ocean Drilling Program, Scientific Results*, 149: College Station, Texas (Ocean Drilling Program).

Locarnini, R. A., Mishonov, A. V., Antonov, J. I., Boyer, T. P. and Garcia, H. E. 2006. *World Ocean Atlas 2005, Volume 1: Temperature*. S. Levitus, Ed. NOAA Atlas NESDIS 61, U.S. Government Printing Office, Washington, D.C., 182 pp.

Lourens, L., Hilgen, F., Shackleton, N. J., Laskar, J. and Wilson, D. 2004. The Neogene period, p. 409–440. *In*: F. Gradstein, J. Ogg and A. Smith, (Eds.), *A Geologic Time Scale*, Cambridge University Press.

Louwye, S., Head, M. J. and De Schepper, S. 2004. Dinoflagellate cyst stratigraphy and palaeoecology of the Pliocene in northern Belgium, southern North Sea Basin. *Geological Magazine*, 141 (3): 353–378.

Lozier, M S. 2010. Deconstructing the conveyor belt. *Science*, 328 (5985): 1507–1511.

Lynch-Stieglitz, J., Adkins, J. F., Curry, W. B., Dokken, T., Hall, I. R., Herguera, J. C., Hirschi, J. J.-M., Ivanova, E. V., et al. 2007. Atlantic Meridional Overturning During the Last Glacial Maximum. *Science*, 316 (5821): 66–69.

Ma'alouleh, K. and Moullade, M. 1987. Biostratigraphic and paleoenvironmental study of Neogene and Quaternary planktonic foraminifers from the lower continental rise of the New Jersey margin (western North Atlantic), Deep Sea Drilling Project Leg 93, Site 603, p. 481–491. *In* van Hinte, J. E., Wise, S. W., Jr., et al. (Eds.), *Initial Reports of the Deep Sea Drilling Project*, 93: Washington (U. S. Goverment Printing Office).

Magurrant, A. E. 2004. *Measuring biological diversity*. Blackwell Publishing, 256 pp.

Maher, Jr. L. J. 1981. Statistics for microfossil concentration measurements employing samples spiked with marker grains. *Review of Paleobotany and Palynology*, 32: 153–191.

Marret, F. and Zonneveld, K. A. F. 2003. Atlas of modern organic-walled dinoflagellate cyst distribution. *Review of Palaeobotany and Palynology*, 125 (1–2): 1–200.

Martin, P. A., Lea, D. W., Mashiotta, T. A., Papenfuss, T., and Sarnthein, M. 1999. Variation of foraminifera Sr/Ca over Quaternary glacial-interglacial cycles: Evidence for changes inmean ocean Sr/Ca? *Geochemistry, Geophysics, Geosystems*, 1. doi:10.1029/1999GC000006

Mashiotta, T.A., Lea, D. W and Howard, J. S. 1999. Glacial-interglacial changes in Subantartic sea surface temperature and δ^{18} O-water using foraminiferal Mg. *Earth and Planetary Science Letters*, 170: 417–432.

Matthiessen, J. and Brenner, W. 1996. Dinoflagellate cyst ecostratigraphy of Plio-Pleistocene sediments from the Yermak Plateau (Arctic Ocean, Hole 911A), p.243–253. *In*: Thiede, J., Myhre, A. M., Firth, J. V., Johndon, G. L. and Ruddiman, W. F. (Eds.) *Proceedings of the Ocean Drilling Program Scientific Results*, 151: College Station, Texas (Ocean Drilling Program).

McCarthy, F. M. G. 1992. *Quaternary climate change and the evolution of the mid-latitude western North Atlantic Ocean: palynological, foraminiferal, sedimentological, and stable isotope evidence from DSDP sites 604, 607 and 612,* unpub. PhD Thesis, Dept. Geology, Dalhousie U., Halifax, N.S., 269 pp.

McCarthy, F. M. G. and Mudie, P. J. 1996. Palynology and dinoflagellates biostratigraphy of upper Cenozoic sediments from sites 898 and 900, Iberia Abyssal Plain, p. 241–265. *In*: Whitmarsh, R. B., Saywyer, D. S., Klaus, A. and Masson, D. G. (Eds.) *Proceedings of the Ocean Drilliing Program, Scientific Results*, 149: College Station, Texas, (Ocean Drilling Program).

McCarthy, F. M. G. and Mudie, P. J. 1998. Oceanic pollen transport and pollen:dinocyst ratios as markers of late Cenozoic sea level change and sediment transport. *Palaeogeography, Palaeoclimatology, Palaeoecology*, 138: 187–206.

McCarthy, F. M. G., and Gostlin, K. E. 2000b. Correlating Pleistocene sequences across the New Jersey margin. *Sedimentary Geology*, 134: 181–196.

McCarthy, F. M. G., Gostlin, K. E., Mudie, P. J. and Scott, D. B. 2000a. Synchronous palynological changes in early Pleistocene sediments off New Jersey and Iberia, and a possible paleoceanographic explanation. *Palynology*, 24: 63–77.

McCarthy, F. M. G., Gostlin, K. E., Mudie, P. J. and Hopkins, J. A. 2003. Terrestrial and marine palynomorphs as sea-level proxies: an example from Quaternary sediments on the New Jersey margin, U.S.A, p. 119–129. *In* Olson, H. C. and Leckie, R. M. (Eds.). *Micropaleontologic proxies for sea-level change and stratigraphic discontinuities.* Society for Sedimentary Geology, Special Publication No. 75.Tulsa, Oklahama, U.S.A.

McCarthy, F. M. G., Gostlin, K. E., Mudie, P. J. and Pedersen, R. O. 2004. The palynological record of terrigenous flux to the deep sea: late Plioce-Recent examples from 41°N in the abyssal Atlantic and Pacific oceans. *Review of Palaeobotany and Palynology*, 128: 81–95.

McIntyre, K., Ravelo, A. C. and Delaney, M. L. 1999. North Atlantic Intermediate Waters in the late Pliocene to early Pleistocene. *Paleoceanography*, 14 (3): 342–335.

McMinn, A. 1992. Pliocene through Holocene dinoflagellates distribution cyst biostratigraphy of the Gippsland Basin, Australia, p. 147–161. *In* M. J. Head and J. H. Wrenn (Eds.), *Neogene and Quaternary Dinoflagellate Cysts and Acritarchs.* American Association of Stratigraphic Palynologists Foundation, Dallas, Texas.

Mertens, K.N., Verhoeven, K., Verleye, T., Louwye, S., Amorim, A., Ribeiro, S., Deaf A.S., Harding I. C., De Schepper S., González C., Kodrans-Nsiah M., De Vernal, A., Henry, M., Radi, T., Dybkjaer, K., Poulsen, N.E., Feist-Burkhardt, S., Chitolie, J., Heilmann-Clausen, C., et al. 2009. Determining the absolute abundance of dinoflagellate cysts in recent marine sediments: The *Lycopodium* marker-grain method put to the test. *Review of Palaeobotany and Palynology*, 157: 238–252.

Metzger, J. M, Flemings, P. B., Christie-BLick, N., Mountain, G. S., Austin Jr., J. A., and Hesselbo, S. P. 2000. Late Miocene to Pleistocene sequences at the New Jersey outer continental shelf (ODP leg 174A, sites 1071 and 1072). *Sedimentary Geology*, 134: 149–180.

Moullade, M. 1987. Deep Sea Drilling Project Leg 93: Biostratigraphic synthesis, p. 1271–1283. *In* J. E. van Hinte, S. W. Wise, Jr., et al. (Eds.), *Initial Reports of the Deep Sea Drilling Project*, 93(2). U.S. Government Printing Office, Washington, D.C.

Mudie, P. J. 1987. Palynology and dinoflagellates biostratigraphy of Deep Sea Drilling Project Leg 94, Sites 607 and 611, North Atlantic Ocean, p. 785–812. *In* Ruddiman, W. F., Kidd, R. B., Thomas, E., et al. *Initial Reports of the Deep Sea Drilling Project*, 94. Washington (U.S. Government Printing Office).

Nichols, Gary. 2009. *Sedimentology and Stratigraphy*, 2nd edition. Wiley-Blackwell. Chichester. UK. 419 pp.

Nikiforova, K. V. 1997. Foreword, *In* Van Couvering, J. A. (Editor). *The Pleistocene Boundary and the Beginning of the Quaternary*. World and Regional Geology Series; Cambridge University Press, U.K.

Nürnberg, D. and J. Groeneveld. 2006. Pleistocene variability of the Subtropical Convergence at East Tasman Plateau: Evidence from planktonic foraminiferal Mg/Ca

(ODP Site 1172A), *Geochemistry Geophysics Geosystems*, 7, Q04P11, doi:10.1029/2005GC000984.

Orsi, A. H., G. C. Johnson, and J. L. Bullister. 1999. Circulation, mixing, and production of Antarctic Bottom Water. *Progress in Oceanography*, 43 (1): 55–109.

Petuch, E. J. 2004. *Cenozoic Seas: The View for Eastern North America.* CRC Press, Boca Raton, Louisiana, USA, 308 pp.

Pickart, R. and Smethie Jr., W. M. 1993. How does the deep western boundary current cross the Gulf Stream? *Journal of Physical Oceanography,* 23: 2602–2616.

Pierrehumbert RT. 2000. Climate change and the tropical Pacific: the sleeping dragon wakes. *Proceedings of the National Academy of Sciences*, 97: 1355–1358.

Ravelo, A. C., Andreasen, D. H., Lyle, M., Lyle, A. O. and Wara, M. W. 2004. Regional climate shifts caused by gradual global cooling in the Pliocene epoch. *Nature*, 429: 263–267.

Ravelo, A.C. and Hillaire-Marcel, C. 2007, The Use of Oxygen and Carbon isotopes of foraminifera in paleoceanography, p. 735–765. *In.* Hillaire-Marcel, C. and de Vernal, A. (Eds.) *Proxies in Late Cenozoic Paleoceanography.* Elsevier, University of Montréal, Montréal, Québec.

Rio, D., Backman, J. and Raffi, I. 1996. Calcareous nannofossil Biochronology and the Pliocene–Pleistocene Boundary, p. 63–78. *In* Van Couvering, J. (editor) *The Pliocene-Pleistocene boundary: Definition and Worlwide Correlation*: Cambridge University Press.

Rochon, A. de Vernal, A., Turon, J.-L., Matthiessen, J. and Head, M. J. 1999. *Distribution of recent dinoflagellate cysts in surface sediments from the North Atlantic*

Ocean and adjacent seas in relation to sea-surface parameters. AASP Contributions series Number 35, American Association of Stratigraphic Palynologists Foundation. 152 pp.

Rook, L. and Martínez-Navarro, B. 2010. Villafranchian: The long story of a Plio-Pleistocene European large mammal biochronologic unit. *Quaternary International*, 219 (1–2): 134–144.

Sardella, R. and Palombo, M. R. 2007. The Pliocene-Pleistocene boundary: which significance for the so called "Wolf Event"? Evidences from Western Europe. *Quaternaire*, 18 (1): 65–71.

Schönfeld, J. 2006. Taxonomy and distribution of the *Uvigerina peregrina* plexus in the tropical to Northeastern Atlantic. *The Journal of Foraminiferal Research*, 36: 355–367.

Schweizer, M., Pawlowski, J., Kouwenhoven, T. and Van Der Zwaan, B. 2009. Molecular phylogeny of common cibicidids and related Rotaliida (Foraminifera) based on small subunit rDNA sequences. *The Journal of Foraminiferal Research*, 39: 300–315.

Sen Gupta, B. K. 1999. *Modern foraminifera.* Boston, Mass.: Kluwer Academic Publishers. 371 pp.

Stockmarr, J. 1971. Tablets with spores in absolute pollen analysis. *Pollen et Spores*, 13 (4): 615–621.

Stover, L.E. 1977. Oligocene and early Miocene dinoflagellates from Atlantic corehole 5/5B, Blake Plateau. *In*: Elsik, W.C. (Editor), *Contributions of Stratigraphic Palynology. 1: Cenozoic Palynology.* American Association of Stratigraphic Palynologists, Contributions Series 5A: 66–89.

Stommel, H. 1958. The abyssal circulation. *Deep-Sea Research Part I: Oceanographic Research Papers*, 5: 80.

Suc, J.-P., Bertini, A., Leroy, S.A.G. and Suballyova, D. 1997. Towards the lowering of the Pliocene/Pleistocene boundary to the Gauss–Matuyama reversal. *Quaternary International*, 40: 37–42.

Talley, L. D. 2002. Ocean Circulation. *In*: MacCracken, M. C. and Perry, J. S. (Eds.). *Encyclopedia of Global Environmental Change*. l., John Wiley and Sons, 23 pp.

Trauth, M. H., Maslin, M. A., Deino, A. L., Manfred, R. S., Bergner, A. G. N., and Dühnforth, M. 2007. High- and low-latitude forcing of Plio-Pleistocene East African climate and human evolution. *Journal of Human Evolution*, 53: 475–486.

Trauth, M. H., Larrasoaña, J. C. and Mudelsee, M. 2009. Trends, rhythms and events in Plio-Pleistocene African climate. *Quaternary Science Reviews*, 28: 399–411.

Tripati, A. K., Allmon, W. D. and Sampson, D. E. 2009. Possible evidence for a large decrease in seawater strontium/calcium ratios and strontium concentrations during the Cenozoic. *Earth and Planetary Science Letters*, 282: 122–130.

Turner, A., Antón, M. and Werdelin, L. 2008. Taxonomy and evolutionary patterns in the fossil Hyaenidae of Europe. *Geobios*, 41: 677–687.

United States.Forest Service, Burns, R. M., and Honkala, B. H. 1990. *Silvics of North America.* Washington, D.C.: Forest Service, United States Department of Agriculture. 877 pp.

van Aken, H. M. 2000. The hydrography of the mid-latitude Northeast Atlantic Ocean: II: The intermediate water masses. *Deep Sea Research Part I: Oceanographic Research Papers*, 47 (5): 789–824.

van Aken, H. M. 2007. *The oceanic thermohaline circulation: an introduction.* New York: Springer, 328 pp.

van der Made, J. 2010. Biogeography and climatic change as a context to human dispersal out of Africa and within Eurasia. *Quaternary Science Reviews*, Corrected Proof,

van Hinte, J. E., Wise Jr., S. W., Biart, B. N. M., Covington, J. M., Dunn, D. A., Haggerty, J. A., Johns, M. W., Meyers, P. A., Moullade, M. R., Muza, J. P., Ogg, J. G., Okamura, M., Sarti, M. and Von Rad, U. 1987. *Initial Reports of the Deep Sea Drilling Project*, 93(1). U.S. Government Printing Office, Washington, D.C., 469 pp.

Versteegh, G. J. M. 1995. *Palaeoenvironmental changes in the Mediterranean and North Atlantic in relation to the onset of northern hemisphere glaciations (2.5 Ma B. P.) – a palynological approach.* University of Utrecht, 134 pp.

Vink, A. Zonneveld, K. A. F. and Willems, H. 2000. Organic-walled dinoflagellate cysts in western equatorial Atlantic surface sediments: distributions and their relation to environment. *Review of Palaeobotany and Palynology*, 112: 247–286.

Wall, D., Dale, B., Lohmann, G. P. and Smith, W. K. 1977. The environmental and climatic distribution of dinoflagellates cysts in modern marine sediments from regions in the North and South Atlantic oceans and adjacent seas. *Marine Micropaleontology*, 2: 121–200.

Ward, L. W., Bailey, R. H. and Carter, J. G. 1991. Pliocene and Early Pleistocene Stratigraphy, Depositional History, and Molluscan Paleobiogepgraphy of the Coastal Plain, p. 274–289. *In* Wright Horton Jr., J. and Zullo, V. A. (Eds.), *The Geology of the Carolinas: Carolina Geological Society Fiftieth Anniversary Volume.* The University of Tennessee Press, Knoxville.

Warny, S. A. and Wrenn, J. H. 1997. New species of dinoflagellate cysts from the Bou Regreg Core: a Miocene–Pliocene boundary section on the Atlantic Coast of Morocco. *Review of Palaeobotany and Palynology*, 96: 281–304.

Weaver, A. J., Bitz, C. M., Fanning, A. F. and Holland, M. M. 1999. Thermohaline Circulation: High-Latitude Phenomena and the Difference Between the Pacific and Atlantic. *Annual Review of Earth Planetary Science*, 27: 231–285.

Wise, Jr., S. W. and van Hinte, J. E. 1987. Mesozoic-Cenozoic depositional environments revealed by deep sea drilling project Leg 93 drilling on the continental rise off the Eastern United States: cruise summary, p. 1387–1423. *In* van Hinte, J. E., Wise, S. W., Jr., et al. (Eds.), *Initial Reports of the Deep Sea Drilling Project*, 93: Washington. U. S. Goverment Printing Office.

Zonneveld, K. A. F. Versteegh, G. J. M. and de Lange, G. J. 1997. Preservation of organic-walled dinoflagellate cysts in different oxygen regimes: a 10,000 year natural experiment. *Marine Micropaleontology*, 29: 393–405.

Internet references

[1] "Antarctic Intermediate Water." *Encyclopædia Britannica*. 2010. Encyclopædia Britannica Online. 13 Jul. 2010 <http://www.britannica.com/EBchecked/topic/27016/Antarctic-Intermediate-Water>.

NetLibrary, Inc. 2003. *McGraw-Hill Dictionary of Earth Science*. 2nd ed. New York: McGraw-Hill.

"Cyrillaceae" *A Dictionary of Plant Sciences*. Michael Allaby. Oxford University Press, 2006. *Oxford Reference Online*. Oxford University Press. Brock University. 25 August

2010 <http://www.oxfordreference.com/views/ENTRY.html?subview=Main&entry=t7.e1881>

McGinley, Mark (Lead Author); J. Emmett Duffy (Topic Editor). 2008. "Species diversity." In: *Encyclopedia of Earth.* Eds. Cutler J. Cleveland (Washington, D.C.: Environmental Information Coalition, National Council for Science and the Environment). [First published in the Encyclopedia of Earth, February 8, 2007; Last revised July 22, 2008; Retrieved February 22, 2010]. <http://www.eoearth.org/article/Species_diversity>

"Shannon–Wiener index" *A Dictionary of Environment and Conservation.* Chris Park. Oxford University Press, 2007. *Oxford Reference Online.* Oxford University Press. Brock University. 22 February 2010.

APPENDIX 1 – Methodology

Benthic and planktonic foraminifera

- Each sample had an initial volume of about 20 ccs. The sample was cleaned of contaminants (from contact with the core liner, and any fungal growth on the open surface of the core) using a small stainless steel spatula, which was cleaned thoroughly with water between samples, before being weighed with an electronic balance. The balance has a precision of ± 0.02 g. All weights are provided in Table 8. Samples weighed between 22.31g (sample 36B) and 24.62 g (sample 35A).

- The samples, 12 at a time, were then disaggregated overnight in 250 mL Erlenmeyer flasks using an orbital shaker. To reduce disaggregation time, the samples were initially broken into pea-sized fragments in the flasks using a thin stainless steel spatula, and the Erlenmeyer flasks were filled with 100 to 150 mL of distilled water. The orbital shaker was set to a minimum of 80 rpm.

- Once the samples were disaggregated, each was passed through a 125 μm metal sieve assisted by a garden sprayer filled with distilled water and by the gentle use of an index finger. The sieve diameter fits exactly within the rim of a 1 L beaker, which was used to collect the filtrate. Most samples were sufficiently disaggregated to require only one 1 L beaker, although some samples (e.g. sample 43A) needed two. It is important to use a garden sprayer setting that is vigorous enough to break down larger pieces of clay without causing any particles to leave the containment of the sieve. It sometimes helped to place one's hand around the rim of the sieve, and to then clean that hand with the garden sprayer to prevent losses.

- The beakers were left to settle while the >125 μm fraction was allowed to dry in an oven overnight (15 hours) at approximately 60°C. To prevent contamination, pieces of paper were placed on top of the beakers and on the sieves placed in the oven.

- Once the sieves were dry, the content of each was then brushed gently into a 1 dram (⅛ fluid ounce) glass bottle, weighed (by subtracting the empty from full weight) and labeled. These weights are given in Table 8.

- After the sediment in the beakers had completely settled, the supernatant was siphoned off with a pipette attached to a venturi pump on a running tap, and the beakers were then placed in the oven to dry. Some samples that appeared to still have sediment in suspension (e.g. sample 41A) were left longer (24 to 48 hours) to settle. Any remaining small particles were considered too fine to be dinoflagellate cysts or acritarchs and removed during siphoning. The samples were dried to the point where desiccation cracks developed in the sample at the bottom of the beaker, and then transferred from the beakers into plastic sample bags. Although most of the sample at the bottom of the beakers was easy to remove, some remained attached to the lower sides of the beakers. It was removed using a small stainless steel spatula, taking care not to scratch the glass, and cleaning the spatula carefully between samples. These samples were weighed (Table 8), labeled, and set aside for palynological processing.

Geochemical analysis requires collecting 25 to 35 (40 if possible) planktonic specimens of one of the following species:

Globigerina bulloides (prefered)
Globigerinoides ruber
Neogloboquadrina pachyderma
Globorotalia truncatulinoides

Since the stable isotope analysis does not require as extensive cleaning as the elemental analysis, the foraminifera are split into two groups and cleaned separately (Groeneveld, pers. comm.). Stable isotopes analysis only require five to ten specimens per sample, whereas the elemental analysis requires, ideally, up to 30 specimens, due to 10-50% loss of the sample material during the excessive cleaning.

For benthic foraminifera, five specimens are sufficient owing to the relative stability of bottom waters and the fact that benthic foraminifera do not migrate through the water column. The following species were selected:

Cibicidoides wuellerstorfi
Uvigerina peregrina

It was decided to concentrate on the planktonic species *Globigerina bulloides* and the benthic species *Cibicidoides wuellerstorfi* and *Uvigerina peregrina*. Both benthic species were picked and identified due to the low abundance of benthic foraminifera in Hole 603C, and due to the uncertainty of proportions for each species. *C. wuellerstorfi* ultimately proved to be the more adundant and so was analyzed almost exclusively for benthic isotopic analysis. Two samples (31D and 33A) had enough specimens of *U. peregrina* to also provide benthic isotope values. These values also required adjusting to be compared with the *C. wuellerstorfi*. Optimal conditions for foraminiferal geochemical analysis require that all the specimens be of approximately the same size. For this reason both benthic and planktonic foraminifera were initially counted after passing the sample through a 350 μm sieve. When this method did not yield 40 *Globigerina bulloides* and five *Cibicidoides wuellerstorfi* or *Uvigerina peregrina* specimens, the smaller fraction was then added. Foraminifera were picked from a black picking tray using a light microscope. The picking itself used a small paint brush and a small flask with water. Species were identified by comparing with published illustrations (Chapman, 2000; McCarthy, 1992; Sen Gupta, 1999; Schönfeld, 2006; and Schweizer, 2009).

It was fairly easy to pick 40 specimens of *Globigerina bulloides* for most of the samples used in this study. The picking of benthic foraminifera proved more challenging. Not all samples yielded either *Cibicidoides wuellerstorfi* or *Uvigerina peregrina*, although one sample (sample 41B) produced as many as 12 specimens of *Cibicidoides wuellerstorfi* (Table 9).

Marine palynomorphs

- 200 mL of cold 20% of concentrated HCl was added incrementally to the dried <125 μm fraction in a 500 ml plastic beaker. The reaction was observed and noted as: none, slight, moderate, strong, or very strong, accordingly. Samples remained in acid for intervals of up to, but not exceeding, 24 hrs.

- The HCl was removed, without disturbing the sample, using a glass pipette attached to a venturi pump, and the beaker was then filled with distilled water (up to 400 mL). This was repeated about three times until the pH was approximately six (i.e. the pH of distilled water).

- Up to 200 mL of cold 48% HF was then added to each beaker, which was then swirled by hand to mix the sediment fully with the acid. Swirling two times a day, for one to two days, was sufficient to maintain the reaction. The HF was then decanted by pouring carefully so as not to disturb the residue, and replaced with 200 mL of new HF. After swirling as before, and again for one to two days, this HF was then decanted carefully without disturbing the sample.

- The remaining HF was diluted by adding 200 mL of 20% concentrated cold HCl to each beaker to remove any precipitates from the HF reaction. After standing for five to six hours, the beaker was swirled, topped off to 400 mL with additional HCl, and then allowed to stand for 12 to 15 hours.

- The mixture of HF and HCl was decanted again by careful pouring, and up to 400 mL of distilled water was added. Each beaker was allowed to stand for one day.

- The dilute acid was decanted, and the residue poured into 50 mL screw-topped disposable conical centrifuge tubes. The centrifuge was run for 4 minutes at 3500 rpm to concentrate the residue, and the supernatant liquid subsequently poured off. Two

Lycopodium clavatum spore tablets (batch number 006720) were then introduced to each centrifuge tube with a little HCl as necessary to dissolve the tablets.

- A small amount of distilled water was added (no more than five mL more than already in the centrifuge tube) and the contents mixed with a vortex mixer. The centrifuge tube was topped up with distilled water and put into the centrifuge again. This step was repeated until the pH of the supernatant water was again about six.

- Once all the samples had been neutralized in 50 mL centrifuge tubes, sieving of the residues commenced.

- A good portion of the supernatant water was removed from the centrifuge tube.

- All four components of the sieving set-up (sieve holder, retaining collar, sieve mesh, two watch glasses) were first washed with a soft cloth and warm soapy water, and then rinsed with distilled water.

- A small square of 10 μm nylon mesh was placed over the sieve holder, secured with the retaining collar, and rinsed with a distilled water jet from a squeeze bottle. The assembled sieve was placed on one watch glass, and another watch glass was placed temporarily on the open end of the sieve to prevent contamination.

- The centrifuge tube was mixed thoroughly with the vortex mixer to homogenize the residue, including any small accumulations of residue at the base of the conical centrifuge tube. A little water was added as necessary.

- A glass pipette, labeled with the sample number, was used to transfer a portion of the sample to the sieve.

- The residue was sieved using distilled water from a squeeze bottle until the filtrate was clear. Tapping the sieve holder with a fingernail accelerated this process

considerably. The thoroughness of the sieving process and the nature of the residue were evaluated by placing a small drop of the residue on a microscope slide and examining under a light microscope at low power. One sample (sample 32B) had a large amount of pyrite, which was reduced by swirling in a watch glass. The residue, once verified as being ready for slide making, was transferred from the sieve into a 15 mL centrifuge tube. No ultrasound treatment was used on any of the samples in the present study. This treatment is sometimes used to clean residues where unacceptable amounts of debris are adhering to the palynomorphs.

- The 15 mL centrifuge tubes were spun for about five minutes. While this happened, the sieve was rinsed with distilled water, the sieve mesh removed, rinsed with a squeeze bottle, and resealed into the sieve holder.

- A good portion of the supernatant water was removed from the centrifuge tube using a pipette. Two drops of stain (safranin-o) were added, and quickly mixed with the vortex mixer to insure that all the material was stained evenly.

- The stained residue was then sieved again, and after a finally checking of the wet preparation under the microscope, the residue if satisfactory was returned to the 15 mL tube for slide making.

The slide making process needs to be performed promptly after the residue has been sieved, so that it does not incur microbial growth. Ideally this should be done within a day or so.

- Glycerine jelly was heated in a 50 ml round-bottomed glass test tube placed in a water-filled glass beaker on a small hot plate.

- Pipettes were made ready for the residues to be mounted, and a small vial of distilled water was also placed at readiness near the slide warmer.

- The 15 mL tube containing the stained residue was spun down in the centrifuge and most of the supernatant was pipetted out of the tube with care to avoid disturbing the residue.

- The residue was homogenized with the pipette and verified with a wet preparation under the microscope to determine the density. More water was added if necessary. The amount of residue added to the slide depended also on the concentration of dinoflagellate cysts seen on the wet preparation, and not just on the general concentration of palynomorphs.

- On a clean cover-slip placed on a slide warmer, three drops of melted glycerine jelly and six drops of distilled water were added. The two were mixed together with a wooden cocktail stick and spread evenly and completely on the cover-slip, being careful to ensure that no bubbles were present.

- The residue was homogenized using its labeled pipette, and a number of drops was quickly (to preserve homogeneity) and evenly added to the cover-slip. Five to six drops of residue was the norm, but this varied depending on the concentration of palynomorphs seen in the wet preparation. It was essential to ensure that the residue did not overflow the coverslip.

- The cover-slip was left to dry covered on the slide warmer (usually one to two hours). To ensure it had dried, a microscope slide was held just above the dried cover-slip to check for any condensation.

- Ten drops of glycerine jelly (five per row in two rows) were placed in the central part of a microscope slide.

- The cover-slip was inverted residue-side down and carefully lowered onto the ten drops of glycerine jelly, ensuring that the glycerine jelly ran evenly and fully under

the cover-slip and being careful to ensure that no air bubbles were trapped under the coverslip.

- The mounted microscope slide was removed immediately from the slide warmer and placed on a cool surface to ensure rapid solidification. The microscope slide was then labeled with the sample number, slide number, and size of fraction.Three slides were made for sample 31A and 42D. For all other samples only two slides were made.

- The remaining residue was then placed in one or more vials, allowed to stand for a day, decanted with a pipette, filled with glycerine, and one drop of liquefied phenol added as a preservative. The vial was shaken to homogenize its contents, labeled and stored.

- The microscope slides, having been cleaned of superfluous glycerine jelly, were ready for observation under the microscope. Following microscopy at the end of this study, all microscope slides were re-cleaned to remove any immersion oil, and a narrow band of marine varnish (which is more durable than alternative sealants) was applied around the coverslip to seal the microscope slide for long-term storage.

The purpose of making microscope slides in the above manner (Evitt, 1984) was to ensure that: 1) all the palynomorphs were approximately in the same plane and immediately beneath the lower surface of the cover slip for ease of viewing, and 2) there was a sufficient quantity of glycerine jelly on the microscope slide to inhibit desiccation of the slide.

APPENDIX 2 – Tables

Table 8. Sample details (depth, weight, reaction to HCl) for the studied interval of DSDP Hole 603C

Core	Section	Top (cm)	Bottom (cm)	Sample Code	Depth (mbsf)	Wet weight (g)	Dry weight (>125 µm) (g)	Dry weight (<125 µm) (g)	Total dry weight (g)	% <125 µm	% >125 µm	Reaction to HCl
3	1	20	22	31A	11.8	24.04	0.23	17.31	17.54	0.987	0.013	Strong to very strong
3	1	64	66	31B	12.24	23.21	0.06	15.89	15.95	0.996	0.004	Moderate
3	1	102	104	31C	12.62	23.7	0.39	16.3	16.69	0.977	0.023	Strong
3	1	137	139	31D	12.97	23.85	0.19	16.51	16.7	0.989	0.011	Moderate to Strong
3	2	20	22	32A	13.3	23.8	0.03	17.38	17.41	0.998	0.002	Moderate
3	2	62	64	32B	13.72	24.27	0.35	18.17	18.52	0.981	0.019	Moderate to strong
3	2	100	102	32C	14.1	23.4	0.1	18	18.1	0.995	0.006	Moderate
3	2	140	141.5	32D	14.5	23.78	0.3	17.72	18.02	0.983	0.017	Slight to moderate
3	3	20	22	33A	14.8	23.05	0.48	15.89	16.37	0.971	0.029	Slight to moderate
3	3	64	66	33B	15.24	24.2	0.63	16.11	16.74	0.962	0.038	Moderate to slight
3	3	102	104	33C	15.62	23.4	0.1	14.9	15	0.993	0.007	Strong to very strong
3	3	140.5	142	33D	16.005	23.3	0.1	16.7	16.8	0.994	0.006	Strong to very strong
3	4	7.5	9	34A	16.175	23.25	0.09	16.8	16.89	0.995	0.005	Strong to very strong
3	4	46	47.5	34B	16.56	23.3	0.12	16.4	16.52	0.993	0.007	Strong to very strong
3	4	79.5	81	34C	16.895	22.7	0.12	16.23	16.35	0.993	0.007	Moderate to Strong
3	4	104.5	106	34D	17.145	23.05	0.28	16.29	16.57	0.983	0.017	Strong
3	5	17.5	19	35A	17.775	24.62	0.36	17.97	18.33	0.980	0.020	Very strong
3	5	62	63.5	35B	18.22	23.2	0.16	17.2	17.36	0.991	0.009	Moderate
3	5	106.5	108	35C	18.665	24.5	0.2	18.7	18.9	0.989	0.011	Moderate
3	5	138	139	35D	18.98	24.02	0.2	18.4	18.6	0.989	0.011	Very strong
3	6	16.5	18	36A	19.265	22.33	0.2	16.49	16.69	0.988	0.012	Very strong
3	6	64	65.5	36B	19.74	22.31	0.16	16.33	16.49	0.990	0.010	Very strong
3	6	95	97.5	36C	20.06	23.5	0.4	17.31	17.71	0.977	0.023	Strong to very strong
3	6	135.5	137	36D	20.445	23.52	0.22	18.19	18.41	0.988	0.012	Strong
3	7	20	21.5	37a	20.8	23.1	0.15	19.48	19.63	0.992	0.008	Moderate to strong
4	1	13.5	15	41A	21.335	22.8	0.2	17.4	17.24	0.988	0.012	Strong to moderate
4	1	56	57.5	41B	21.76	23.39	0.19	16.71	16.9	0.989	0.011	Moderate to strong
4	1	95	96.5	41C	22.15	23.68	0.06	16.56	16.62	0.996	0.004	Strong
4	1	135	137	41D	22.55	23	0.13	15.3	15.43	0.992	0.008	Moderate
4	2	20	21.5	42A	22.9	23.25	0.09	16.52	16.61	0.995	0.005	Moderate
4	2	56	57.5	42B	23.26	24	0.16	16.6	16.76	0.990	0.010	Moderate to strong
4	2	99	100	42C	23.69	23.39	0.15	15.95	16.1	0.991	0.009	Moderate to strong
4	2	136.5	138	42D	24.065	22.8	0.12	15.5	15.62	0.992	0.008	Moderate
4	3	20	21.5	43A	24.4	23.7	0.25	15.9	16.15	0.985	0.015	Moderate
4	3	56	57.5	43B	24.76	24.4	0.09	16.5	16.59	0.995	0.005	Moderate to strong
4	3	99	100	43C	25.19	23.15	0.23	15.9	16.13	0.986	0.014	Strong
4	3	136	137	43d	25.56	23.7	0.31	17.54	17.85	0.983	0.017	Very Strong
4	4	17.5	19	44A	25.875	23.05	0.2	16.55	16.75	0.988	0.012	Strong to very strong
4	4	66	67.5	44B	26.36	23.9	0.1	20.58	20.68	0.995	0.005	Strong
4	4	100	101	44C	26.7	24.55	0.19	19.33	19.52	0.990	0.010	Moderate to strong
4	4	137.5	139	44D	27.075	24.19	0.1	17.96	18.06	0.994	0.006	Moderate
4	5	17.5	19	45A	27.375	23.61	0.13	16.19	16.32	0.992	0.008	Moderate to strong
4	5	49	51		27.69	SAMPLE MISSING						
4	5	57.5	59	45B	27.775	24.05	0.13	16.19	16.32	0.992	0.008	Strong to very strong
4	5	98	99.5	45C	28.18	22.7	0.03	15.7	15.73	0.998	0.002	Moderate
4	6	19	20.5	46A	28.89	22.8	0.18	15.63	15.81	0.989	0.011	Moderate to strong
4	6	58	59.5	46B	29.28	24.13	0.08	16.7	16.78	0.995	0.005	Strong to moderate
4	6	98	99.5	46C	29.68	24.15	0.16	16.01	16.17	0.990	0.010	Very strong to strong
4	6	127.5	129	46D	29.975	23.51	0.05	16.29	16.34	0.997	0.003	Moderate

Table 9. Planktonic and benthic foraminifera data (number of specimens per sample) for the studied section of DSDP Hole 603C

Core	Sc	Top (cm)	Bottom (cm)	Sample code	Box number	*G. bulloides*	Box number	*C. wuellerstorfi*	*U. peregrina*
3	1	20	22	31A	31A	28	31E	0	0
3	1	64	66	31B	31B	33	31F	0	0
3	1	102	104	31C	31C	20	31G	1	0
3	1	137	139	31D	31D	27	31H	0	2
3	2	20	22	32A	32A	27	32E	3	0
3	2	62	64	32B	32B	23	32F	5	0
3	2	100	102	32C	32C	35	32G	3	0
3	2	140	141.5	32D	32D	24	32H	0	0
3	3	20	22	33A	33A	24	33E	2	0
3	3	64	66	33B	33B	30	33F	0	3
3	3	102	104	33C	33C	40	33G	1	0
3	3	140.5	142	33D	33D	35	33H	0	0
3	4	7.5	9	34A	34A	48	34E	1	0
3	4	46	47.5	34B	34B	40	34F	1	0
3	4	79.5	81	34C	34C	41	34G	1	0
3	4	104.5	106	34D	34D	36	34H	2	0
3	5	17.5	19	35A	35A	34	35E	0	0
3	5	62	63.5	35B	35B	40	35F	0	0
3	5	106.5	108	35C	35C	30	35G	2	0
3	5	138	139	35D	35D	43	35H	6	1
3	6	16.5	18	36A	36A	41	36E	2	0
3	6	64	65.5	36B	36B	36	36F	5	0
3	6	96	97.5	36C	36C	48	36G	10	0
3	6	135.5	137	36D	36D	40	36H	4	0
3	7	20	21.5	37A	37A	37	37B	0	0
4	1	13.5	15	41A	41A	44	41E	9	1
4	1	56	57.5	41B	41B	28	41F	12	0
4	1	95	96.5	41C	41C	40	41G	0	0
4	1	135	137	41D	41D	26	41H	5	0
4	2	20	21.5	42A	42A	39	42E	4	0
4	2	56	57.5	42B	42B	37	42F	3	0
4	2	99	100	42C	42C	40	42G	0	0
4	2	136.5	138	42D	42D	32	42H	9	0
4	3	20	21.5	43A	43A	35 and 33	43E	3	0
4	3	56	57.5	43B	43B	30	43F	0	0
4	3	99	100	43C	43C	39	43G	5	0
4	3	136	137	43D	43D	42	43H	0	0
4	4	17.5	19	44A	44A	42	44E	3	0
4	4	66	67.5	44B	44B	38	44F	8	0
4	4	100	101	44C	44C	38	44G	5	0
4	4	137.5	139	44D	44D	26	44H	6	0
4	5	17.5	19	45A	45A	30	45D	3	0
4	5	57.5	59	45B	45B	45	45E	3	0
4	5	98	99.5	45C	45C	37	45F	0	0
4	6	19	20.5	46A	46A	38	46E	0	0
4	6	58	59.5	46B	46B	26	46F	7	0
4	6	98	99.5	46C	46C	34	46G	1	0
4	6	127.5	129	46D	46D	26	46H	1	0

Table 10. Total concentration of dinoflagellate cysts per gram (dry weight) as estimated with the *Lycopodium clavatum* spores, with the equivalent error, as well as the number of bisaccate pollen grains counted for the studied section of DSDP Hole 603C

Code name	Bisaccates	Lycopodium spores	Total concentration of dinoflagellate cysts (cysts/gram)	Error for the concentration of dinoflagellate cysts calculated (%)	Estimated standard error (±)
31A	578	394	10376	7.75	804.17
31B	481	376	9801	8.03	786.85
31C	315	308	13158	8.21	1080.28
31D	183	91	41540	12.12	5035.36
32A	167	94	41097	11.95	4910.25
32B	315	2	1919700	70.97	1362386.78
32C	215	720	5349	7.10	379.57
32D	233	0 (on either slide)	min of 2568	N/A	N/A
33A	146	164	23917	9.84	2354.12
33B	236	121	30262	10.99	3324.70
33C	234	153	27185	9.98	2712.36
33D	164	185	22547	9.39	2117.02
34A	168	239	16412	8.82	1447.10
34B	292	340	12861	7.89	1014.36
34C	211	511	8673	7.21	625.45
34D	57	447	8510	7.70	654.87
35A	63	219	18992	8.94	1697.14
35B	42	241	15833	8.85	1400.52
35C	24	128	30921	10.67	3298.02
35D	60	374	10044	8.00	803.40
36A	50	553	6664	7.48	498.42
36B	86	583	6789	7.27	493.25
36C	55	864	4348	6.99	303.77
36D	35	329	11778	8.17	961.71
37A	31	189	22070	9.33	2058.73
41A	22	299	13713	8.25	1131.14
41B	15	207	20838	9.03	1880.92
41C	280	394	11489	7.57	869.35
41D	66	179	25289	9.37	2368.81
42A	117	86	54841	12.13	6651.38
42B	76	89	43938	12.18	5351.80
42C	117	321	11592	8.29	960.75
42D	51	263	15364	8.55	1313.15
43A	54	336	10545	8.30	875.33
43B	82	312	13635	8.10	1104.39
43C	88	642	6054	7.19	435.57
43D	58	522	8014	7.29	584.40
44A	136	189	19875	9.49	1887.15
44B	459	221	17266	9.06	1563.48
44C	282	172	23907	9.63	2301.20
44D	176	176	21815	9.66	2108.03
45A	207	219	20399	8.83	1800.28
45B	151	408	9962	7.70	767.55
45C	108	392	9401	7.96	748.35
46A	219	162	22018	10.03	2208.88
46B	204	218	19134	8.94	1711.15
46C	94	242	16159	8.79	1420.92
46D	697	199	20604	9.21	1897.87

Table 11. Dinoflagellate cyst and acritarch taxa used in Simple Correspondence Analysis, and their abbreviations for the studied interval of DSDP Hole 603C

Achomosphaera sp.	Ach.sp	*Impagidinium strialatum*	I.str
Achomosphaera andalousiensis andalousiensis	Ach.a.a	*Lavradosphaera crista*	L. cr
		Leffingwellia costata	L.co
Algal cyst type I of Head 1996	A.c.I	*Lejeunecysta* sp.	Lej
Amiculosphaera umbraculum	A.u	*Lingulodinium machaerophorum*	L.m
Ataxiodinium choane	A.c	*Melitasphaeridium choanophorum*	M.c
Ataxiodinium zevenboomii	A.z	*Nematosphaeropsis labyrinthus*	N.l
Bitectatodinium raedwaldii	B.r	*Nematosphaeropsis* sp. cf. *N. labyrinthus* of Rochon et al. (1999)	cf. N.l
Bitectatodinium tepikiense	B.t	*Nannobarbophora walldalei*	N.w
Capisocysta lata	C.lat	*O. centrocarpum* sensu Wall and Dale (1966)	O.cen
Corrudinium harlandii	C.h		
Corrudinium? labradori	C.lab	*Operculodinium israelianum*	O.i
Cymatiosphaera? invaginata	C.i	*O. centrocarpum* sensu Wall & Dale (1966) var. A [of whom ?]	O.cen.v.A
Cymatiosphaera cf. *latisepta*	C.cf.l		
Dalella chathamense	D.c	*Operculodinium? eirikianum eirikianum*	O.e.e
Dapsilidinium pseudocolligerum	D.p		
Desotodinium wrennii	D.w	*Operculodinium? megagranum*	O.m
Filisphaera filifera	F.f	*Operculodinium* cf. *psilatum*	O.cf.p
Filisphaera microornata	F.m	*Operculodinium tegillatum*	O.t
Geonettia waltonensis	G.w	*Operculodinium* sp. A of Vink et al. (2000)	O.sp.A
Habibacysta tectata	H.t	Cyst of *Pentapharsodinium dalei*	P.d
Homotryblium? sp.	Hom	*Polysphaeridium zoharyi*	P.z
Hystrichokolpoma rigaudiae	H.r	Cyst of *Protoperidinium stellatum*	P.s
Impagidinium aculeatum	I.a	cf. *Quinquecuspis concreta*	cf.Q.c
Impagidinium cantabrigiense	I.c	*Selenopemphix nephroides*	S.n
Impagidinium multiplexum	I.m	*Spiniferites* spp. undifferentiated	S.spp
Impagidinium pallidum	I.pal	*Spiniferites ludhamensis*	S.l
Impagidinium paradoxum	I.pax	*Spiniferites* cf. *rubinus*	S.cf.r
Impagidinium patulum	I.pat	*Tectatodinium pellitum*	T.p
Impagidinium plicatum	I.pl	*Tuberculodinium vancampoae*	T.v
Impagidinium sphaericum	I.sph		

Table 12. Benthic foraminifera $\delta^{13}C$ and $\delta^{18}O$ data

Sample code	Box number	Depth (mbsf)	$\delta^{13}C$	$\delta^{18}O$	$\delta^{18}O$_adjusted
31A	31E	11.8			
31B	31F	12.24			
31C	31G	12.62			
31D	31H	12.97	-1.08	4.05	4.05
32A	32E	13.3	0.98	3.81	4.45
32B	32F	13.72	-0.86	3.64	4.28
32C	32G	14.1	-2.63	3.98	4.62
32D	32H	14.5			
33A	33E	14.8			
33B	33F	15.24	-1.09	3.27	3.27
33C	33G	15.62	-0.05	1.46	2.10
33D	33H	16.005			
34A	34E	16.175	-0.01	2.22	2.86
34B	34F	16.56			
34C	34G	16.895	0.23	1.67	2.31
34D	34H	17.145	0.15	2.33	2.97
35A	35E	17.775			
35B	35F	18.22			
35C	35G	18.665	0.39	3.30	3.94
35D	35H	18.98	-0.18	3.03	3.67
36A	36E	19.265	-0.40	2.82	3.46
36B	36F	19.74	0.67	2.98	3.62
36C	36G	20.06	0.43	2.50	3.14
36D	36H	20.455	0.58	2.27	2.91
37A	37B	20.8			
41A	41E	21.335	0.62	-0.05	0.59
41B	41F	21.76	-0.46	2.66	3.30
41C	41G	22.15			
41D	41H	22.55	0.26	2.00	2.64
42A	42E	22.9			
42B	42F	23.26	0.45	2.71	3.35
42C	42G	23.69			
42D	42H	24.065	-0.35	3.03	3.67
43A	43E	24.4	0.36	3.12	3.76
43B	43F	24.76			
43C	43G	25.19	0.23	2.96	3.60
43D	43H	25.56			
44A	44E	25.875	0.16	3.28	3.92
44B	44F	26.36	0.22	2.60	3.24
44C	44G	26.7	0.45	1.51	2.15
44D	44H	27.075	0.03	2.95	3.59
45A	45D	27.375	0.88	1.55	2.19
45B	45E	27.775	0.27	2.68	3.32
45C	45F	28.18			
46A	46E	28.89			
46B	46F	29.28	0.30	2.84	3.48
46C	46G	29.68	1.29	1.88	2.52
46D	46H	29.975			

APPENDIX 3 – List of known acritarch and dinocyst taxa from DSDP Hole 603C

Achomosphaera andalousiensis Jan du Chêne 1977, emend. Jan du Chêne and Londeix, 1988 subsp. *andalousiensis* (autonym)

Acritarch sp. 1 of Head et al., 1989

Algal cyst type I of Head 1996

Amiculosphaera umbraculum Harland, 1979

Ataxiodinium choane Reid, 1974

Ataxiodinium zevenboomii Head, 1997

Bitectatodinium raedwaldii Head, 1997

Bitectatodinium tepikiense Wilson, 1973

Capisocysta lata Head, 1998

Corrudinium harlandii Matsuoka, 1983

Corrudinium? *labradori* Head et al., 1989

Cymatiosphaera? *invaginata* Head et al., 1989

Cymatiosphaera sp. cf. *C. latisepta* De Schepper and Head, 2008

Dalella chathamensis McMinn and Sun Xuekun, 1994

Dapsidinium pseudocolligerum (Stover, 1977) Bujak et al., 1980

Desotodinium wrennii De Schepper et al., 2004

Filisphaera filifera Bujak, 1984, emend. Head, 1994

Filisphaera microornata (Head et al., 1989) Head, 1994

Geonettia waltonensis Head, 2000

Habibacysta tectata Head et al., 1989

Hystrichokolpoma rigaudiae Deflandre and Cookson, 1955

Impagidinium aculeatum (Wall, 1967) Lentin and Williams, 1981

Impagidinium cantabrigiense De Schepper and Head, 2008

Impagidinium multiplexum (Wall and Dale, 1968) Lentin and Williams, 1981

Impagidinium pacificum Bujak, 1984

Impagidinium pallidum Bujak, 1984

Impagidinium paradoxum (Wall, 1967) Stover and Evitt, 1978

Impagidinium patulum (Wall, 1967) Stover and Evitt, 1978

Impagidinium plicatum Versteegh and Zevenboom in Versteegh, 1995

Impagidinium sphaericum (Wall, 1967) Lentin and Williams, 1981

Impagidinium strialatum (Wall, 1967) Stover and Evitt, 1978

Impagidinium velorum Bujak, 1984

Lavradosphaera crista De Schepper and Head, 2008

Leffingwellia costata Head and Norris, 2003

Lejeunecysta spp.

Lingulodinium machaerophorum (Deflandre and Cookson, 1955) Wall, 1967

Melitasphaeridium choanophorum (Deflandre and Cookson, 1955) Harland and Hill, 1979

Nannobarbophora walldalei Head, 1996

Nematosphaeropsis labyrinthus (Ostenfeld, 1903) Reid, 1974

Nematosphaeropsis sp. cf. *N. labyrinthus* Rochon et al. (1999)

Operculodinium centrocarpum sensu Wall and Dale (1966)

Operculodinium? *eirikianum* Head et al., 1989 emend. Head, 1997 var. *cerebrum* De Schepper and Head, 2008

Operculodinium? *eirikianum* var. *eirikianum* Head et al., 1989 emend. Head, 1997 (autonym)

Operculodinium giganteum Wall, 1967

Operculodinium israelianum (Rossignol, 1962) Wall, 1967

Operculodinium janduchenei Head et al., 1989

Operculodinium? *megagranum* Head in Head and Westphal, 1999

Operculodinium sp. A of Vink et al., 2000

Operculodinium tegillatum Head, 1997

Cyst of *Pentapharsodinium dalei* Indelicato & Loeblich III, 1986

Polysphaeridium zoharyi (Rossignol, 1962) Bujak et al., 1980

Cyst of *Protoperidinium stellatum* (Wall in Wall and Dale, 1968) Balech 1994

cf. *Quinquecupis concreta* (Reid, 1977) Harland 1977

Selenopemphix nephroides Benedek, 1972 emend. Bujak in Bujak et al., 1980

Spiniferites spp.

Spiniferites ludhamensis Head, 1996

Spiniferites sp. cf. *S. rubinus* (Rossignol, 1962) Sarjeant, 1970

Tectatodinium pellitum Wall, 1967 emend. Head, 1994

Tuberculodinium vancampoae (Rossignol, 1962) Wall, 1967

APPENDIX 4 – Taxonomy of new dinoflagellates cysts and acritarchs

This appendix informally describes four new species of dinoflagellate cyst and three new species of acritarch taxa encountered in the present study. Descriptions are based exclusively on light microscope observations. Measurements are usually given by their minimum, average (in parentheses) and maximum values.

Dinoflagellate cysts

***Impagidinium* sp. A** (Plate 4, figs. 18–20)

Description. A small to medium-sized species with a spherical central body bearing high sutural crests that incompletely reflect tabulation. The central body has a thin (less than 0.5 μm), unstratified wall and a smooth surface. Crests are thin (less than 0.5 μm), solid, have a smooth surface, arise from solid bases, and entire crest tops. Crests are of variable height over the cyst, shorter over the apex than on the antapex (e.g. Plate 4, fig. 18), although only two specimens present a clear ventro-dorsal view to verify this assertion. Crests reflect tabulation over large sections of the cyst: the posterior and anterior margins of the cingulum can be distinguished over most of the cyst (e.g. Plate 4, fig. 19), although separation between the plates is absent. However, tabulation is absent from the sulcal area. The archeopyle appears to be 1P, but was seldom observed owing to the thin wall and crumpling of cysts.

Dimensions. Central body equatorial diameter, 21 (26) 35 μm. Thirteen specimens were measured. Optimal dorso-ventral orientation of two specimens allowed for more precise measurements to be taken. Apical crest height: 5–7 μm. Antapical crest height: 8.5–9.0

μm. Cingular crest height: 6–9 μm. Central body height (excluding crests): 21–26 μm. Central body width (excluding crests): 25–26 μm.

Remarks. This species was found in low (<2%) but consistent numbers throughout the entire studied interval of Hole 603C. *Impagidinium* sp. A differs from *Impagidinium cantabrigiense* (Plate 2, fig. 11) by not having suturocavate crests with a shagreenate texture and by different tabulation representation in the ventral area. *Impagidinium pacificum* (Plate 2, figs. 13, 14) differs by having crests of equal height in the apical and antapical areas.

***Impagidinium* sp. B** (Plate 4, figs. 12, 13 and 16)

Description. A small to medium sized species with an ovoid central body bearing high sutural crests that incompletely reflect tabulation. The central body has a thin (0.5 μm) unstratified wall and smooth surface. Crest are thin (0.5 μm), solid and arise from solid bases. All crests have a smooth surface. The longitudinal crests, however, present a series of striations around the cingulum (e.g. Plate 4, fig. 16). Crests are of variable height around over the cyst: shorter in the polar areas and longer towards the cingulum. The archeopyle appears to be 1P (e.g. Plate 4, fig. 16).

Dimensions. Central body equatorial diameter, 17 (22) 29 μm. Central body length, 26 (30.5) 35 μm. Cingular crest height, 7 (9) 12 μm. Polar crest height. 4 (6) 11 μm. 9specimens were measured.

Remarks. This species was found in equally low (<1%) concentrations as *Impagidinium* sp. A throughout the interval. *Impagidinium strialatum* has similar demonstration of tabulation in the dorsal area, with the clear demarcation of a cingular plate (possibly the 4th cingular plate) as well as striae on the crests and is of similar size (28–33 μm, Jan du Chêne et al., 1986; Rochon et al., 1999). However, on *I. strialatum* the crests are thicker and more pronounced and striae are spread out uniformly on the crests. *Spiniferites*

rubinus, as documented by Harland (1979) from the Bay of Biscay, differs by its larger size (central body length, 46–54 μm; central body width, 38–46 μm) and by the presence of partial tabulation in the cingulum.

Dinocyst A (Plate 4, figs. 14, 15)

Description. Proximate cyst, broadly ovoidal, with entirely smooth surface. Cyst wall is unstratified and about 2 μm thick. A small apical (3 μm high) protuberance was observed on several specimens (e.g. Plate 4, fig. 14). The archeopyle is precingular, large, and has smooth margins and well defined angles. The operculum is free. There are no other indications of tabulation.

Dimensions. Equatorial diameter, 44 (48) 52 μm. Length including apical boss, 48 (53.5) 59 μm. Apical boss, 2 (3) 5 μm. Seven specimens were measured. Optimal orientation of two specimens allowed for measurements to be taken for the height of the archeopyle: 24 and 25 μm.

Remarks. *Operculodinium*? *megagranum*, described from the Lower Pleistocene (Gelasian) of the Bahamas (Head and Westphal, 1999), is similar in the shape and wall thickness but has coarse ornamentation. Genus and Species indeterminate, reported from the Upper Pliocene (Piacenzian) of Eastern North Atlantic DSDP Hole 610A by De Schepper and Head (2009), is possibly conspecific with Dinocyst sp. A. Low numbers of Dinocyst sp. A were reported throughout the length of the studied interval of DSDP Hole 603C, without any significant pattern.

***Nematosphaeropsis* sp. A** (Plate 5, figs. 11, 12).

Description. Trabeculate cyst with approximately spherical central body. Wall of central body thin (less than 0.5 μm), unstratified, and with a smooth surface. Processes are

mostly gonal, with hollow stems. Most processes are perforate at the base and occasionally higher in the stem. Processes are joined distally by pairs of threadlike trabeculae. Processes are also occasionally joined at the base and in the stem. There is no distinct reflection of tabulation on the central body surface, and no clear archeopyle was indentified.

Dimensions. Central body maximum diameter, 35 (41) 49 μm. Maximum process length, 11 (9) 15 μm. Seven specimens were measured.

Remarks. Very few complete specimens were found, limiting the number of measurements taken. This species is larger than the more common *Nematosphaeropsis labyrinthus* (Plate 3, fig. 3), and shares some features with *Nematosphaeropsis rigida* such as perforated process bases and solid trabeculae. *Nematosphaeropsis* sp. A is the least abundant of all the new species of dinoflagellate cysts found in the present study, and no specific pattern of occurrence can be determined.

Acritarchs

The following three species have not been reported previously in the literature.

Acritarch sp. A (Plate 4, figs. 8, 9)

Description. Central vesicle spherical to egg-shaped, and surrounded by an outer wall that curves towards, but doesn't always contact, the central vesicle in a series of invaginations. The outer wall appears to be supported by numerous solid, cylindrical rods. These rods can be seen when viewing the specimen in cross-section or at slightly higher or lower focus and seem to be connected to the invaginations. The outer wall is smooth. The inner wall is not clearly visible; it is therefore difficult to determine how the rods arise from it. Only one specimen showed a simple split.

Dimensions. Measurements were taken for five spherical and four egg-shaped specimens. Spherical specimens: central vesicle maximum diameter, 8 (9.6) 12 μm; overall maximum diameter, 12.5 (14.3) 16 μm. Egg-shaped specimens: central vesicle minimum width, 6 (8.6) 11 μm; central vesicle minimum length, 10 (10.8) 12 μm.

Remarks. This was the most abundant undescribed acritarch species found in the present study. Slightly higher numbers are found towards the lower part of the studied interval. Acritarch sp. A differs from *Ataxiodinium zevenboomii* (Plate 4, figs. 17 and 21) in having rods connecting the inner and outer walls, being significantly smaller in size and not showing any evidence of an archeopyle.

Acritarch sp. B (Plate 4, figs. 10, 11)

Description. Central vesicle approximately spherical, with a thin (< 1 μm) wall bearing narrow (< 0.5 μm), solid, erect, occasionally curved, hair-like processes. The distance between adjacent process bases is about < 1 μm. An opening was observed in the central vesicle wall of some specimens although its shape and size are mostly unclear.

Dimensions. Central vesicle maximum diameter, 25 (26. 5) 30 μm; maxumum length of processes, 2 (3.5) 6 μm. Six specimens were measured.

Remarks. This species shows some resemblance to Acritarch sp. C of Versteegh 1995, described from the Pliocene of southern Italy, but Versteegh did not report a pylome for his specimens. The dinoflagellate cyst *Batiacasphaera hirsuta* Stover, 1977, described from the Middle Oligocene of the Blake Plateau on the eastern Atlantic Shelf, is also similar although considerably larger (central body maximum diameter, 41–49 μm; Stover, 1977). Acritarch sp. B is the least abundant of the three new acritarch species described in the present study, and is present in low numbers distributed uniformly throughout the section.

Acritarch sp. C (Plate 4, figs. 5, 6)

Description. Central vesicle spherical, with a smooth, thin (1 μm) wall bearing interconnecting crests that form a regular reticulum. The crests (2.5 μm) occasionally present a serrated edge. The vesicle is composed of a series of similarly dimensioned four to six-sided plates. The pylome comprises six plates, fused together (e.g. Plate 4, fig. 6), which is free but often remains attached.

Dimensions. Central vesicle maximum diameter, 23 (25.4) 30 μm. Ten specimens were measured.

Remarks. Values for this species peak at around the middle of the studied section of DSDP Hole 603C with almost no occurrences in the upper or lower parts of the section. This peak is coincident with the second peak of the surface $\delta^{13}C$ signal, the second plateau for higher values for the $\delta^{18}O_{seawater}$ signal, and the peak in *N. labyrinthus* abundance.

APPENDIX 5 – Selected taxonomy

***Bitectatodinium tepikiense* Wilson 1973** (Plate 1, figs. 4–6)

Specifications of the wall structure for this species seem to vary depending on the temperature of the environment where the specimens are found. Specimens of *Bitectatodinium tepikiense* found in modern north-temperate or cold temperate environments show a vermiculate wall pattern, which differs slightly from that reported from the type material which is associated with mild to warm Middle Pleistocene paleoclimates of New Zealand (Wilson, 1973; Head and Westphal, 1999). De Vernal and Marret (2007) have found that today, while *B. tepikiense* tolerates freezing winter temperatures, this species actually requires high summer temperatures. In Hole 603C, *B. tepikiense* never exceeds 5% of the total dinocysts per sample. Most specimens have a vermiculate wall structure typical of modern specimens in the North Atlantic and adjacent seas, but a few specimens show a more complex and dense reticulation (Plate 1, Figure 6).

***Corrudinium harlandii* Matsuoka, 1983** (Plate 1, figs. 9–12)

There is no clear understanding of the paleoenvironmental conditions under which this species thrived; however De Schepper (2006) treated this species as neritic for his Neritic/Oceanic index. Most specimens in the present study were assigned to *C. harlandii* rather than *P. reticulata*, because the wall structure for most specimens could be placed between light and slightly denser ornamentation. Only two specimens showed a much denser ornamentation, with almost two degrees of reticulation (Plate 1, figs. 11, 12). This species is uncommon, never reaching more than 5% of the total dinoflagellate cyst assemblage. The only major abundance peak is located in the lower part of the section simultaneous with a rather important trough in the temperature estimates and a peak in surface $\delta^{13}C$. This peak is also coeval with a local maximum of warm species of the genus *Impagidinium*, suggesting that this species has in fact an oceanic or oligotrophic affinity rather than neritic as suggested by De Schepper (2006). Statistical analysis by Versteegh (1995) on the Singa section in Italy including, *C. harlandii*, which reaches

almost 30% of the non-reworked dinoflagellate cysts and acritarchs in that section, reveals similar trends to those seen in the present study. Versteegh found that, other than time controlled factors, *C. harlandii* doesn't respond to such usual environmental factors as sea-surface temperature, $\delta^{18}O_{seawater}$, W/C ratios or N/O ratios. This species appears to be subject to an unknown influence that is perhaps explained in the present study by the surface $\delta^{13}C$ signal.

***Impagidinium pacificum* Bujak, 1984** (Plate 2, figs. 13, 14)

This species is represented by a single specimen in the present study. Although it matches the description provided for the holotype by Bujak (1984), it does not resemble the holotype of *Impagidinium japonicum* Matsuoka, 1993 (Head, pers. comm.), suggesting that *Impagidinium pacificum* is not a synonym of *Impagidinium japonicum* as proposed by Bujak and Matsuoka (1986).

***Operculodinium* sp. A of Vink et al., 2000** (Plate 3, figs. 16, 20)

Operculodinium sp. A was first identified from modern sediments of the western Equatorial Atlantic, north of Brazil (Vink et al., 2000). Records and correspondence analysis for this area identify this species as having a generally offshore to oceanic distribution. *Operculodinium* sp. A was also found in DSDP Hole 610A (De Schepper, 2006), and is found infrequently but consistently throughout the present study. However, unlike the specimens observed by Vink et al. (2000), specimens in Hole 603C consistently show evidence of a 2P archeopyle. For those specimens showing a clear dorsal orientation, the archeopyle seems to represent the loss of the third and fourth precingular plates (Plate 3, Figure 16). The presence of this 2P archeopyle questions the assignation of this species to the genus *Operculodinium*, although the wall structure and presence of processes preclude its transfer to the genus *Bitectatodinium*.

APPENDIX 6 – Plates

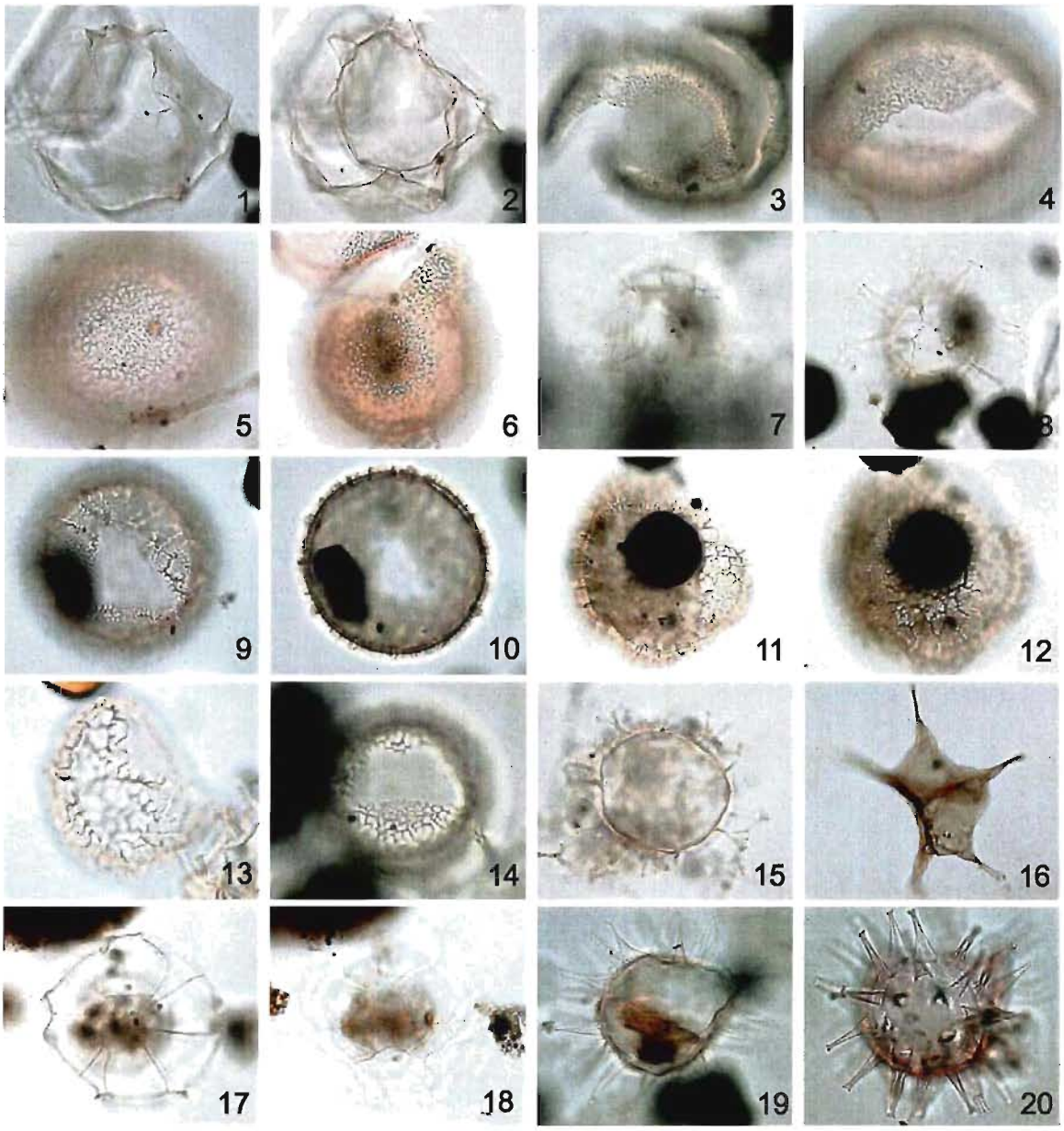

Plate 1. 1 - 2. *Amiculosphaera umbraculum* 3. *Bitectatodinium raedwaldii* 4 - 6. *Bitectatodinium tepikiense* 7 - 8. *Nematosphaeropsis* cf *Nematosphaeropsis labyrinthus* 9 - 10. *Corrudinium harlandii* 11 - 12. *Corrudinium harlandii* sensu stricto 13 - 14. *Corrudinium? labradori* 15. Cyst of *Pentapharsodinium dalei* 16. Cyst of *Protoperidinium stellatum* 17 - 18. *Dalella chathamensis* 19 - 20. *Dapsilidinium pseudocolligerum*

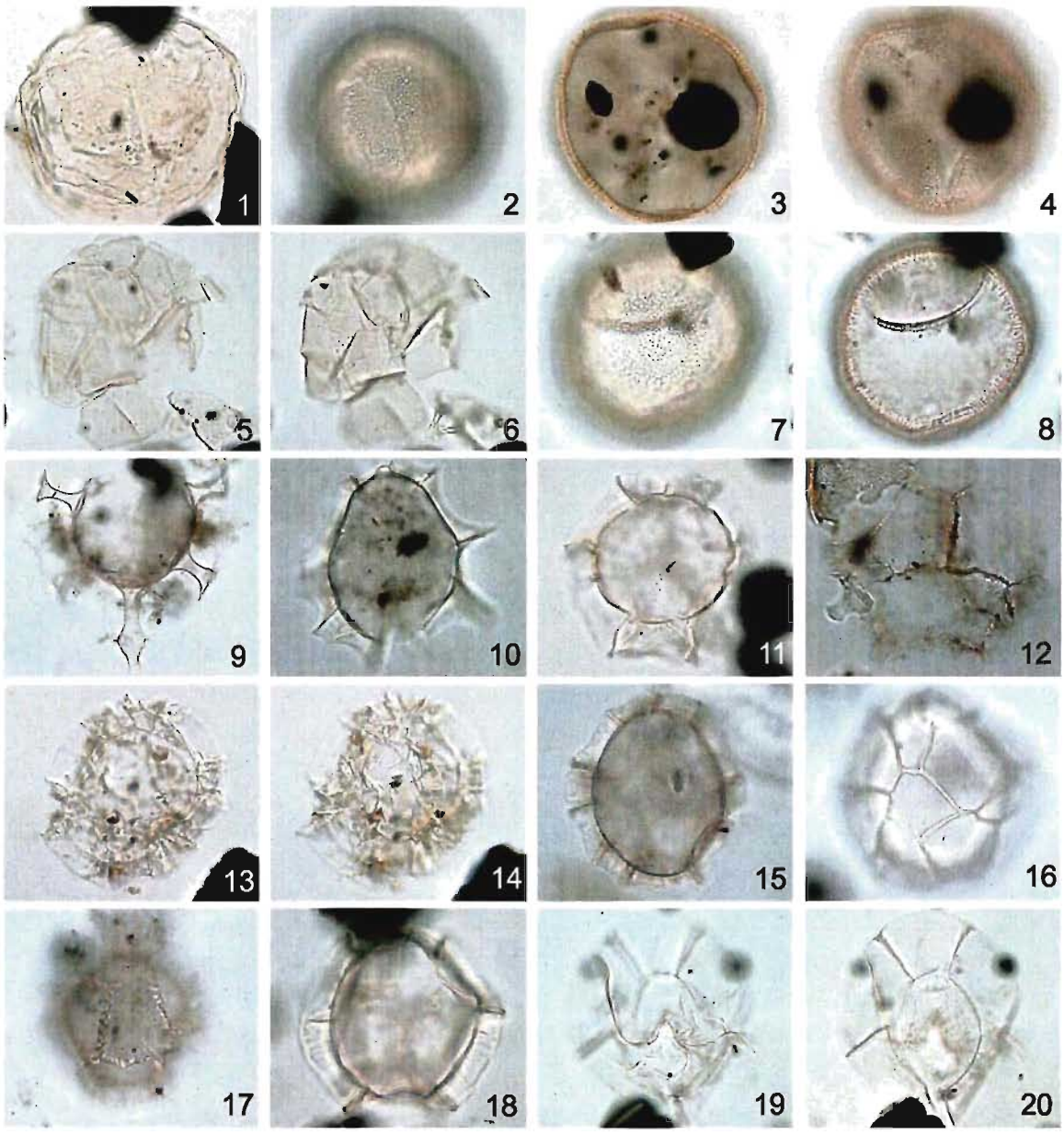

Plate 2. 1. *Desotodinium wrenii* 2. *Filisphaera filifera* 3 - 4. *Filisphaera microornata* 5 - 6. *Geonettia waltonensis* 7 - 8. *Habibacysta tectata* 9. *Hystrichokolpoma rigaudiae* 10. *Impagidinium aculeatum* 11. *Impagidinium cantabrigiense* 12. *Impagidinium pallidum* 13 - 14. *Impagidinium pacificum* 15. *Impagidinium paradoxum* 16. *Impagidinium patulum* 17. *Impagidinium plicatum* 18. *Impagidinium strialatum* 19 - 20. *Impagidinium velorum*

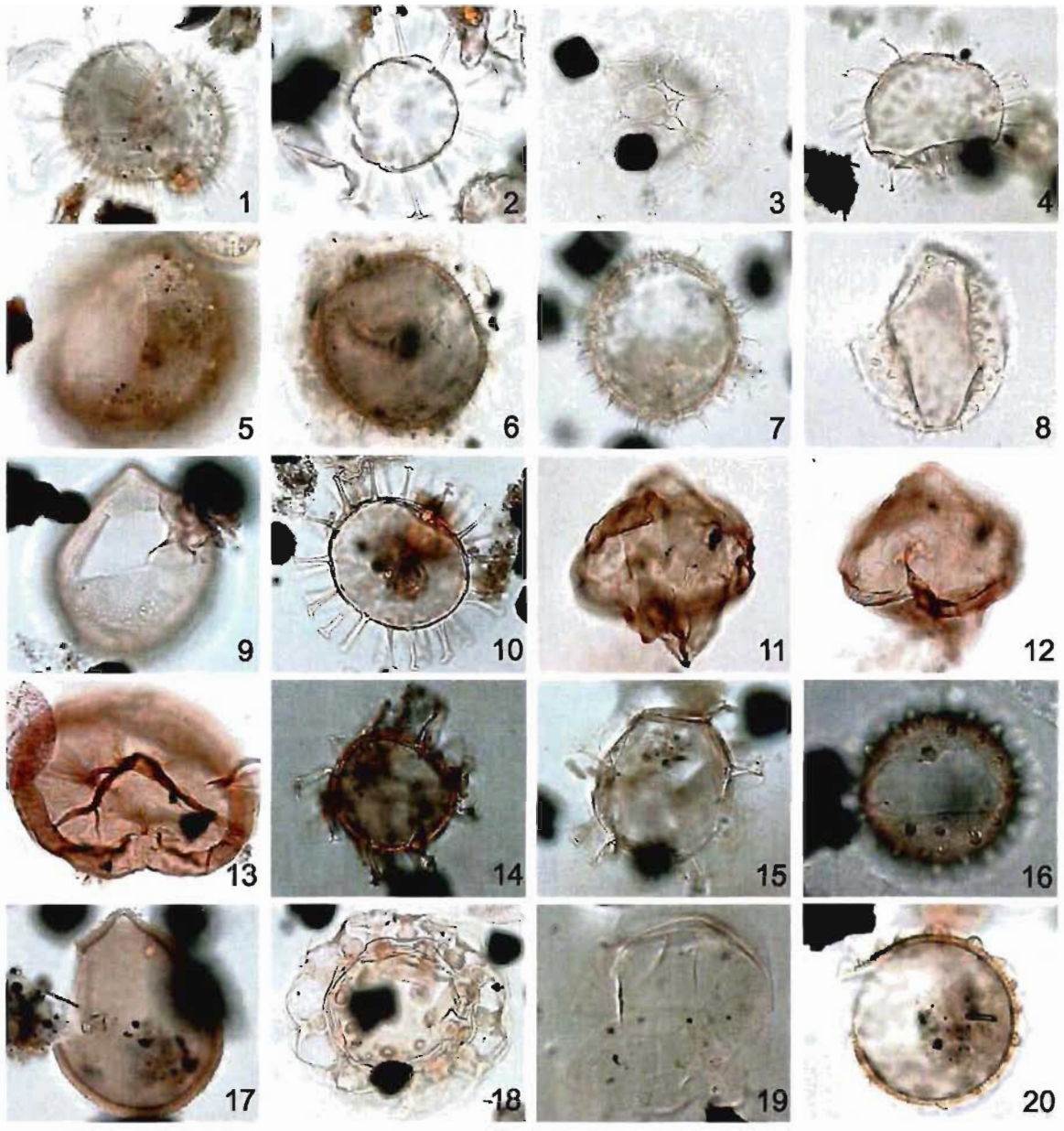

Plate 3 1. *Lingulodinium machaerophorum* 2. *Melitasphaeridium choanophorum* 3. *Nematosphaeropsis labyrinthus* 4. *Operculodinium centrocarpum* sensu Wall and Dale 1966 5. *Operculodinium*? *eirikianum* var. *crebrum* 6. *Operculodinium*? *eirikianum* var. *eirikianum* 7. *Operculodinium israelianum* 8. *Operculodinium janduchenei* 9. *Operculodinium*? *megagranum* 10. *Polysphaeridium zoharyi* 11 - 12. cf. *Quinquecuspis concreta* 13. *Selenopemphix nephroides* 14. *Spiniferites ludhamensis*15. *Spiniferites* cf. *rubinus*16 and 20. *Operculodinium* sp. A of Vink et al., 2000 17. *Tectatodinium pellitum*18. *Tuberculodinium vancampoae* 19. *Capisocysta lata*

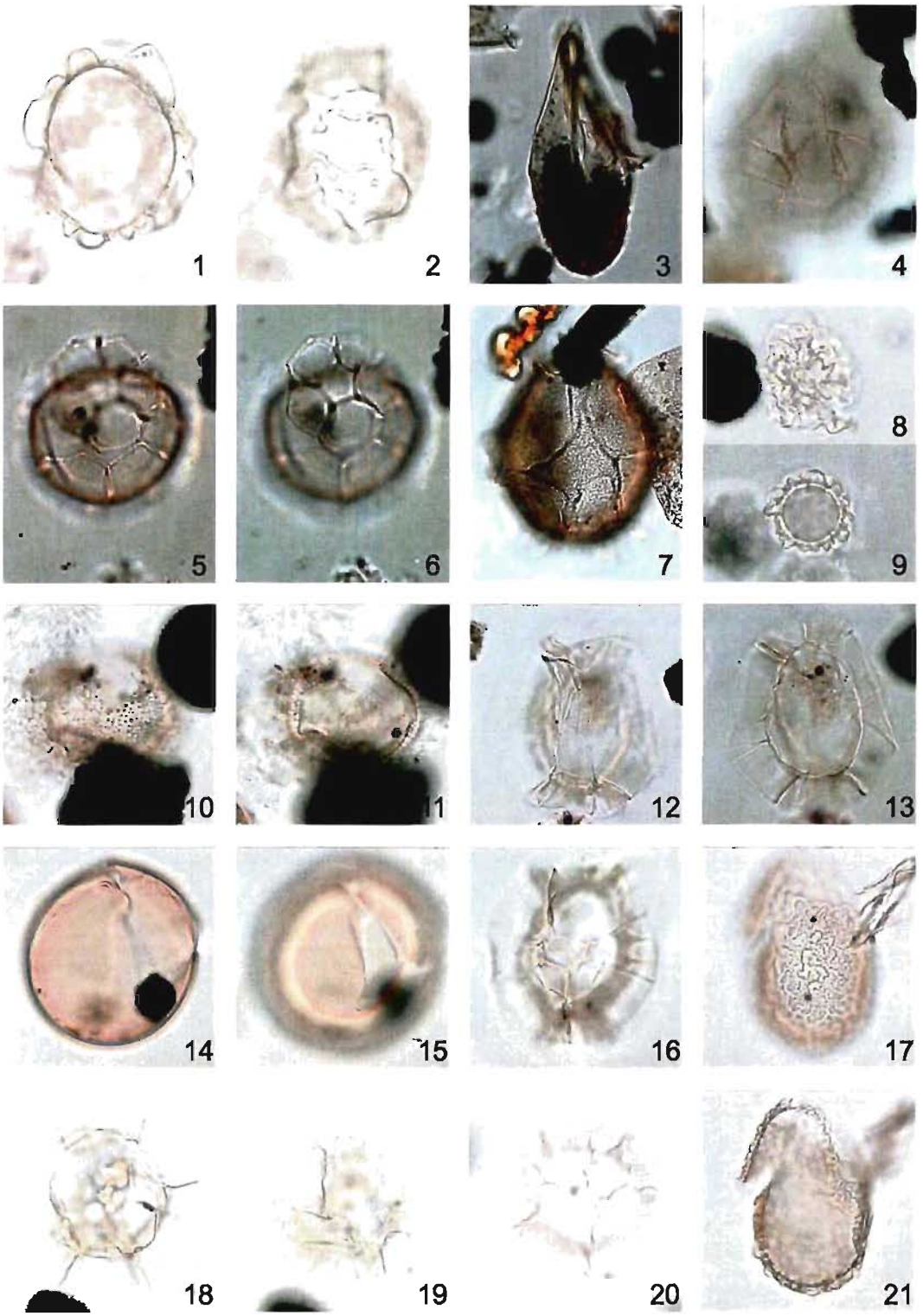

Plate 4. 1 - 2. *Ataxiodinium choane* 3. *Leffingwellia costata* 4. *Impagidinium sphaericum* 5 - 6. Acritarch sp. C 7. *Impagidinium multiplexum* 8 - 9. Acritarch sp. A 10 - 11. Acritarch sp. B 12, 13 and 16. *Impagidinium* sp. B 14 - 15. Dinocyst sp. A 17 and 21. *Ataxiodinium zevenboomii* 18, 19 and 20. *Impagidinium* sp. A

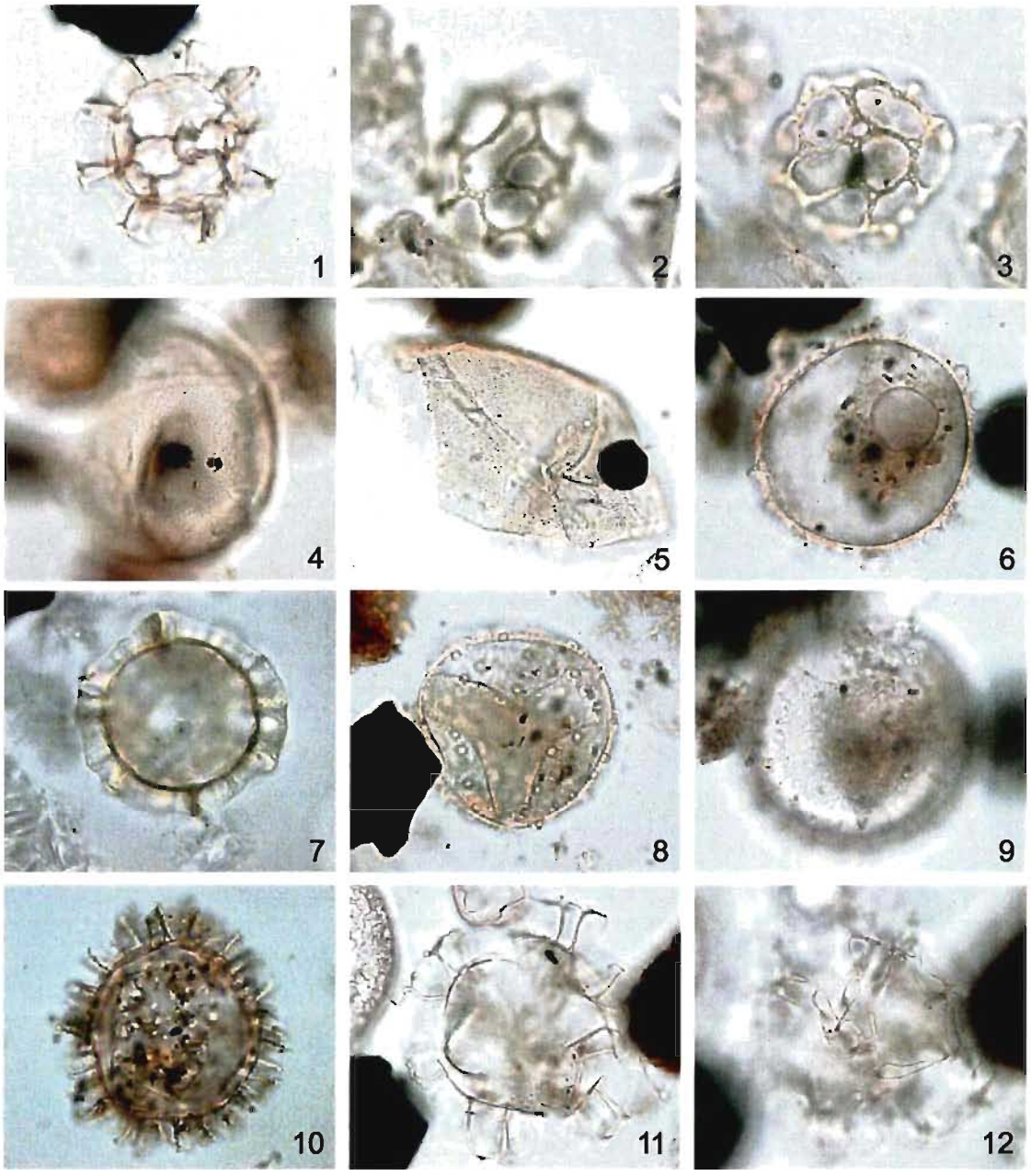

Plate 5. 1. *Cymatiosphaera*? *invaginata* 2 - 3. *Cymatiosphaera* cf. *latisepta* 4. cf. *Operculodinium psilatum* 5. *Operculodinium giganteum* 6 and 9. *Operculodinium tegillatum* 7. *Lavradosphaera crista* 8. var. A of *Operculodinium centrocarpum* sensu Wall and Dale (1966) 10. *Nannobarbophora walldalei* 11 - 12. *Nematosphaeropsis* sp. A